FR 2.4 - Experimental and Clinical Pharmacology and Toxicology

Faculty II – Medicine: Theoretical Medicine and Biosciences Universität des Saarlandes, Homburg / Saar

Expression and function of TRPM3 proteins in the pituitary gland of the mouse

Dissertation submitted to fulfill the requirements for the degree of

Doctor rerum naturalium at

UNIVERSITÄT DES SAARLANDES

2014

Submitted by: Nouma Hasan

Born on: 08.3.1983 in Latakia, Syria

First referee   PD. Dr. Stephan Philipp

Second referee   Univ. Prof. Dr. Peter Lipp

Homburg, August 2014

To my husband,

my son

my parents

and beloved sister and brothers

Acknowledgments

Table of content

List of Figures

List of Tables

List of Abbreviations

Units and sizes

bp	base pair
g	bram
x g	multiplied by gravity force
kb	kilobasepairs
kD	kilodalton
kg	kilogramm
l	liter
mA	milliampere
mM	millimolar
M	molar
µg	microgram
µl	microlitre
µm	micrometer
min	minute
pmol	picomole
rpm	rotations per minute
RT	room temperature
s	second
SEM	standard error of the mean
Tm	average melting temperature
UV	ultraviolet
(v/v)	volume percent (ml/100ml)
(w/v)	weight percent (g/100 ml)

Chemical and biochemical compounds

aa	amino acids
AM	acetoxymethylester
ATP	adenosine-5'-triphosphate
BSA	bovine-serum-albumin
BCA	bicinchoninic acid assay
cAMP	cyclic adenosine monophosphate
Ca^{2+}	calcium ion
DAG	diacylglycerol
DDT	dithiothreitol
DEPC	diethylpyrocarbonate
DMEM	dulbecco's modified Eagle's medium
DMSO	dimethylsulfoxide
DNA	deoxyribonucleic acid
dNTP	deoxynucleotide triphosphates
EDTA	ethylene diaminetetraacetic acid
EGTA	ethylene glycol tetraacetic acid
FCS	fetal calf serum
HBSS	Hank's Balanced Salt Solution
HEPES	4-(2-hydroxyethyl)-1-piperazineethanesulfonic acid
HRP	Horseradish peroxidase
IP3	inositol-1,4,5-trisphosphate
IPTG	isopropylthio-β-galactoside
Na^{+}	sodium ion
NMDG	N-Methyl-D-glucamin
PBS	phosphate-buffered saline

PBST   phosphate buffered saline containing 10 % tween 20
PFA   paraformaldehyde
PIP_2 phosphatidylinositol-4,5-bisphosphate
P-L-L   poly-L-lysine
PregS   pregnenolone sulfate
RNA   ribonucleic acid
SDS   sodium dodecyl sulfate
TBE   Tris-borate EDTA
TBS   Tris buffered saline
X-gal   5-bromo-4-chloro-3-indolyl-β-D-galactopyranoside

Proteins and peptides
ACTH   adrenocorticotropic hormone
CRH   corticotropin-releasing hormone
FSH   follicle-stimulating hormone
GFAP   glial fibrillary acidic protein
GFP   green fluorescent protein
GH   growth hormone
GHRH   growth-hormone-releasing hormone
GLAST   glutamate aspartate transporter
GnRH   gonadotropin-releasing hormone
GPCR   G protein-coupled receptor
LH   luteinizing hormone
OXT   oxytocin
PKA   protein kinase A
PKC   protein kinase C
PLC   phospholipase C
POMC   pro-opiomelanocortin
PRL   prolactin
S100B   calcium binding protein B
TRH   thyrotropin-releasing hormone
TRP   transient receptor potential
TRPA   Transient Receptor Potential Ankyrin
TRPC   Transient Receptor Potential Canonical
TRPM   Transient Receptor Potential Melastatin
TRPML   Transient Receptor Potential Mucolipin
TRPP   Transient Receptor Potential Polycystin
TRPV   Transient Receptor Potential Vanilloid
TSH   thyroid-stimulating hormone
VP   arginine vasopressin
α-MSH   alpha melanocyte-stimulating hormone

Other abbreviations
AL   anterior lobe
$[Ca^{2+}]_i$ intracellular calcium concentration
CP   choroid plexus
DRG   dorsal root ganglion
EC_{50} half-maximal effective concentration
ER   endoplasmic reticulum
FS   folliculostellate cell
h   human
HEK   human embryonic kidney cells
IC_{50} half-maximal inhibitory concentration

ICF	indispensable for channel function
IL	intermediate lobe
GFP-Ki	green fluorescent protein-knock in
KO	knock out
m	mouse
NaV	voltage-activated sodium current
NCX	Na^+/Ca^{2+} exchanger
PCR	polymerase chain reaction
PL	posterior lobe
PMCA	plasma-membrane Ca^{2+}-ATPase
PVN	paraventricular nucleus
RT-PCR	reverse transcription-polymerase chain reaction
SERCA	endoplasmic reticulum Ca^{2+}-ATPase
SON	supraoptic nucleus
TG	trigeminal Gganglion
TM	transmembrane
VGCC	voltage-gated calcium channel
WT	wild type

1   Summary

TRPM3 proteins belong to the large family of Transient receptor potential (TRP) proteins, which are involved of a wide variety of physiological functions. TRPM3 as well as other members of TRP proteins are thought to assemble into homo- or hetero-tetrameric complexes to build ion-conducting channels in the plasma membrane. TRPM3 build ionotropic steroid receptors that are activated by the neurosteroid pregnenolone sulfate (PregS) and efficiently blocked by flavanones like Hesperetin. TRPM3 channels are expressed in pancreatic β-cells and dorsal root ganglion neurons where they are involved in insulin secretion and pain perception, respectively. TRPM3 transcripts are also expressed in the pituitary gland and a plethora of other cells and tissues. However, their function in these tissues is still unknown.

Cloning of 98 cDNAs from mouse pituitaries identified 12 different variants that differed in exon 8, 13, 15, 17 and 20 but not in the pore-coding exon 24. Western blots and RT-PCR analysis confirmed expression of TRPM3 transcripts and proteins in the pituitary gland of the mouse and indicated TRPM3 expression in both neuro- and adeno-pituitary. Accordingly, knock-in mice expressing the green fluorescent protein under the control of the TRPM3 promoter displayed prominent GFP-expression in the posterior lobe (PL), weaker expression in the intermediate lobe (IL) as well as expression in single cells of the anterior lobe (AL). Detailed immunohistochemical analysis indicated TRPM3 expression in folliculostellate cells (FS) of the AL, pituicytes of the PL and finally in melanocyte-stimulating hormone (α-MSH) releasing cells (melanotrophs) of the IL.

Fura-2 imaging experiments uncovered PregS-induced Ca^{2+} entry in both AL- and IL/PL cells that was blocked in the presence of Hesperetin. Consistently, we detected PregS/Hesperetin-sensitive currents in melanotrophs that largely resembled currents through recombinant TRPM3 channels and that were not detectable in melanotrophs from TRPM3-deficient mice. The data demonstrate expression of functional TRPM3 channels in α-MSH secreting cells and provide the basis for a deeper understanding of their biological role in the pituitary gland.

Zusammenfassung

TRPM3 Proteine zählen zur großen Familie der Transient Rezeptor Potential (TRP)-Proteine, die eine Vielzahl unterschiedlicher physiologischer Funktionen besitzen. TRPM3-Proteine lagern sich vermutlich zu homo-oder hetero-tetrameren Kanalkomplexen zusammen und

bilden auf diese Weise ionenleitende Poren in der Plasmamembran. TRPM3 bildet ionotrope Steroidrezeptoren, die durch das Neurosteroid Pregnenolonsulfat (PregS) aktiviert und umgekehrt effizient durch Flavanone wie Hesperetin blockiert werden. TRPM3-Kanäle werden in pankreatischen β-Zellen und Neuronen der Hinterwurzelganglien exprimiert, wo sie an der Insulinsekretion bzw- Schmerzwahrnehmung beteiligt sind. TRPM3-Transkripte werden auch in der menschlichen Hypophyse und einer Vielzahl von anderen Zellen und Geweben exprimiert. Allerdings ist ihre Funktion in diesen Geweben noch unbekannt.

Die Klonierung von 98 unterschiedlichen cDNA-Transkripten aus der Maushypophyse identifizierte 12 unterschiedliche Spleißvarianten die sich in Exon 8, 13, 15, 17 und 20 nicht jedoch im porencodierenden Exon 24 unterschieden. Western Blots und RT-PCR-Analysen bestätigten die Expression von TRPM3-Transkripten und Proteinen in der Hypophyse der Maus sowohl in der Neuro- als auch in der Adenohypophyse. Im Übereinstimmung mit diesen Ergebnissen zeigten Knock-in Mäuse, die das grün-fluoreszierende Protein (GFP) unter der Kontrolle des TRPM3-Promoters exprimierten, starke GFP-Expression im Hypophysenhinterlappen (HHL) sowie schwächere Expression im Hypophysenzwischenlappen (HZL) und Hypophysenvorderlappen (HVL). Detaillierte immunohistochemische Analysen zeigten TRPM3-Expression in follikulostellaren (FS) Zellen des HVLs, in Pituizyten des HHLs und in Melanozyten-stimulierendes Hormon (α-MSH)-sekretierenden Zellen (melanotrope) des HZLs. Ca^{2+}-Imaging Experimente mit Fura-2 zeigten einen PregS-induzierten Ca^{2+}-Einstrom in Zellpräparaten des HVLs- und aus HZL/HHLs, der in Gegenwart von Hesperetin gehemmt war. Dem entsprechend zeigten Patch-Clamp-Messungen PregS/Hesperetin-sensitive Ströme in melanotropen Zellen. Die biophysikalischen Charakteristika dieser Ströme entsprachen dem Strom durch rekombinante TRPM3-Kanäle. Solche Ströme waren in melanotropen Zellen aus TRPM3-defizienten Mäusen nicht nachweisbar.

Die Ergebnisse demonstrieren die Expression von funktionstüchtigen TRPM3-Kanälen in α-MSH- sekretierenden Zellen und bilden die Grundlage zur Untersuchung der biologischen Rolle von TRPM3-Ionenkanälen in der Hypophyse.

2 Introduction

2.1 The pituitary gland

The pituitary gland is a central endocrine gland that plays a key role in the maintenance of body homeostasis and regulates basic physiological functions including growth and reproduction. The functions of the gland itself are regulated by hypothalamic hormones synthesized in the cell bodies of the hypothalamic neurons.

2.1.1 Anatomy and histology of the pituitary gland

The pituitary gland or *hypophysis* is a small gland located at the basis of the brain in a tiny bony cavity of the sphenoid bone of the skull called *sella turcica* [1]. The pituitary gland is anatomically and functionally connected to the hypothalamus by the median eminence via the infundibular stalk (Figure 2-1). Structurally, the pituitary gland comprises two morphologically, embryologically and functionally distinct lobes, namely the adenohypophysis (or anterior lobe) and the neurohypophysis (or the posterior lobe). The adenohypophysis is pinkish in color and built up of soft, friable granular tissue, whereas the neurohypophysis is white, firmer and more fibrous. The adenohypophysis is composed of two parts: pars tuberalis and pars distalis (Figure 2-1). The pars tuberalis forms a collar of cells surrounding the external region of the lower hypophysial stalk. The pars distalis or anterior lobe is the largest part and comprises 80 % of the gland [1]. Five types of endocrine cells that can be stained by acidic or basic chromophors can be distinguished in the anterior pituitary depending on the hormones that they release. Corticotrophs comprise 15-20 % of the anterior lobe cells and produce adrenocorticotropic hormone (ACTH) by the cleavage of the precursor polypeptide pro-opiomelanocortin (POMC). Gonadotrophs comprise 10-15 % of all anterior pituitary cells and release luteinizing hormone (LH) or follicle stimulating hormone (FSH) or both. Thyrotrophs comprise 10 % of the anterior pituitary all population and release thyroid stimulating hormone (TSH). Somatotrophs or growth hormone (GH) releasing cells comprise 30-50 % of all anterior pituitary cells and finally, lactotrophs or prolactin (PRL) releasing cells comprise 15-20 % of the anterior pituitary cells [2,3].

In addition to endocrine cells, the anterior pituitary contains chromophobic, non-endocrine cells. Folliculostellate cells (FS cells) comprise 5-10 % of anterior pituitary cell population [1]. FS cells were first described 60 years ago by Rinehart and Farquhar [4] and were thought to be derived from the neuroectoderm [5]. As the name indicates, FS cells have star-shaped morphology and express the protein S100B, a glial-specific intracellular calcium binding

protein which is primarily expressed in astrocytes [6]. FS-cells were also described to express other astrocytic proteins like the glial fibrillary acidic protein (GFAP) [7] and the glutamate aspartate transporter (GLAST) [8]. FS cells are organized in a three dimensional network capable to perform intercellular communication between endocrine cells via gap junction-mediated signals [9].

The pars intermedia or the intermediate lobe is located in the marginal area between anterior and posterior pituitary and has been considered to be part of the adenohypophysis in humans due to its rudimentary structure. In vertebrates other than human, the pars intermedia contains a single endocrine cell type, the melanotrophs, which are also POMC-producing cells that release alpha-melanocyte-stimulating hormone (α-MSH) and β-endorphin. In addition, two non-endocrine glial cell types, the marginal cells and the astrocyte-like cells, are also localized in the pars intermedia [1].

The neurohypophysis is composed of the median eminence of the hypothalamus, the infundibular stem which forms the inner part of the stalk and the infundibular process or the posterior lobe. The posterior lobe is composed mainly of the axonal terminals of the magnocellular neurosecretory cells (MNCs) originating from the hypothalamic supraoptic (SON) and paraventrical (PVN) nuclei. The axons of these neurons project caudally and medially to collect in the hypothalamo-neurohypophysial tract passing the median eminence to reach the neurohypophysis. The axons ramify into branches and these branches are divided to give rise to nerve terminals of 3 μm diameter. In addition to the small nerve terminals, neuro-secretory axonal swellings (Herring bodies) of 6-8 μm in diameter are formed due to the accumulation of hormones and their carrier molecules in dense vesicles [10]. Vasopressin (VP) and its carrier molecule neurophysin II as well as oxytocin (OXT) and its carrier molecule neurophysin I are released from the nerve endings to the systemic circulation. Pituicytes, a special type of glial cells, are the only resident cell type in the posterior lobe and they are normally found around axonal terminals. Like the FS cells, pituicytes express S100b, GFAP and GLAST [8,11]. In addition to the neurosecretory nerve terminals, a smaller number of non-neurosecretory axons terminate in the posterior lobe. Both types of axons were shown to terminate in a synaptoid contact with pituicytes [10].
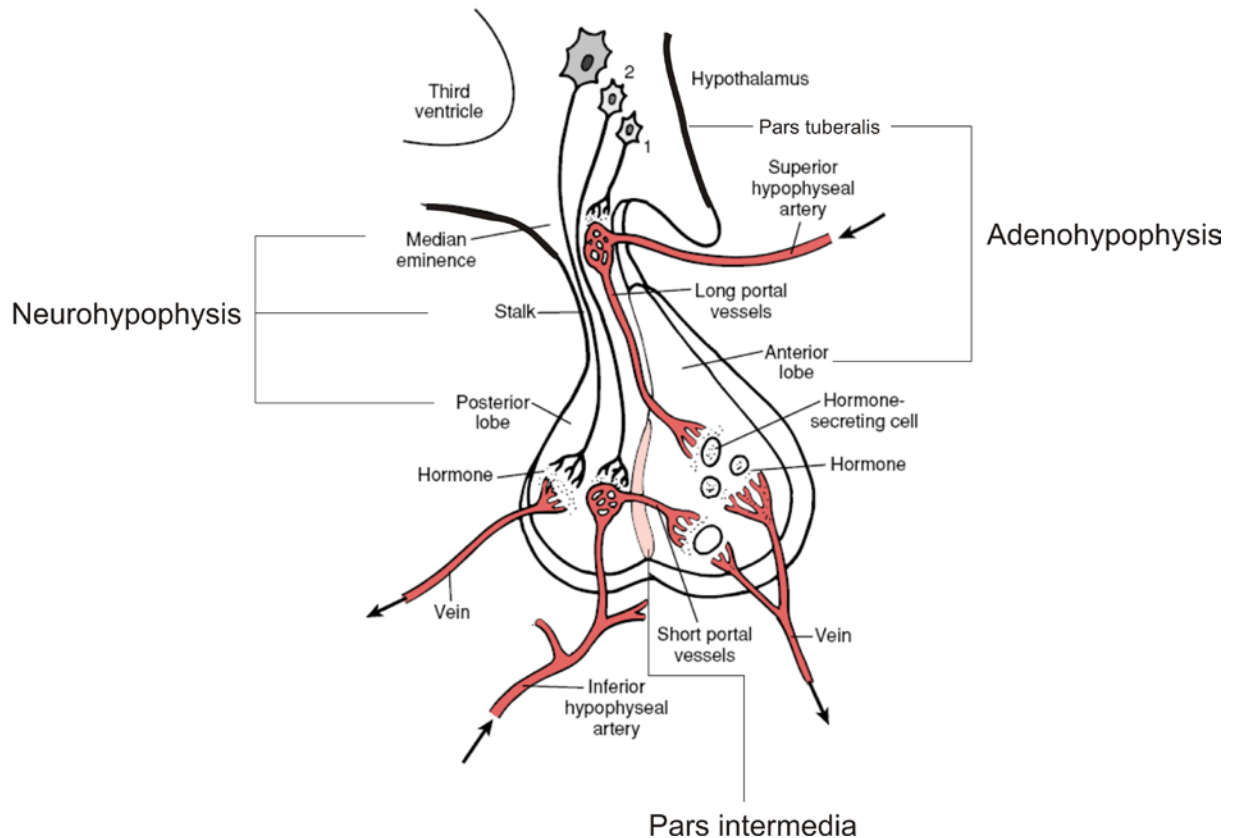
Figure 2-1: Scheme of a midsagittal section of the human pituitary gland [12].
The main parts of the pituitary gland are illustrated as well as the blood supply to the pituitary. Hypothalamic neuron indicated by its gray soma represents a magnocellular neuron releasing vasopressin which ends in the posterior lobe. Neurons 1 and 2 are secreting releasing factors into capillary networks that give rise to the long and short hypophyseal portal vessels, respectively. Releasing hormones are shown reaching the hormone-secreting cells of the anterior lobe via the portal vessels.

2.1.2 Regulation and function of hormone-releasing pituitary cells

Due to its central role in hormone regulation of the body, the primary functions of the pituitary cells are defined by the hormones that they secrete. In addition, a number of non-secreting cells exist in the pituitary that play important but sometimes neglected and indirect roles in hormone secretion.

2.1.2.1 Somatotrophs

Somatotrophs release GH which is essential for growth during the first few months after birth and for the maintenance of normal growth rate during childhood. GH exerts its function by stimulation of Insulin-Like Growth Factor-I (IGF-1) synthesis in the liver and other tissues [13]. Following early childhood and prior to adolescence, IGF-1 mediates longitudinal bone

growth, skeletal maturation, and acquisition of bone mass, whereas in adults it is important in the maintenance of bone mass [14]. In addition, GH plays an important role in fat and carbohydrates metabolism [15]. GH release is regulated by two different hypothalamic regulators; growth hormone-releasing hormone (GHRH) which increases GH release and somatotropin-releasing inhibitory factor (SRIF) or somatostatin which decreases GH release. The signaling cascade of GHRH is initiated by binding to the G_s-protein coupled GHRH receptor in the plasma membrane of the somatotrophs. The binding activates adenylyl cyclase leading to an increase in the cyclic adenosine monophosphate (cAMP) concentration [16]. cAMP increases the activity of protein kinase A (PKA) to phosphorylate proteins responsible to increase GH secretion and GH gene expression [17,18]. In addition, stimulation of GHRH receptors leads to an elevated $[Ca^{2+}]_i$. Somatostatin decreases GH release by binding to inhibitory G_i-proteins coupled to adenylyl cyclase and decreases the intracellular calcium concentrations $[Ca^{2+}]_i$. Furthermore, GH release is also regulated by peripheral regulators including IGF-1 and ghrelin via Ca^{2+}-dependent mechanisms [19-21].

2.1.2.2 Lactrotrophs

Lactotrophs release prolactin (PRL) that regulates the lactation process and milk synthesis in all mammals. PRL induces the growth of mammary glands and their differentiation (mammogenesis), milk production by alveolar cells (lactogenesis) and the maintenance of lactation (galactopoiesis) [22]. PRL release is mainly regulated by hypothalamic dopamine. Dopamine binds to D2 receptors in lactotrophs, inhibits cAMP and Ca^{2+} signaling pathways and thereby inhibiting PRL release [2,23]. Other different inhibitory factors including gamma amino butyric acid and gonadotropin-associated peptide have been proposed to inhibit PRL release [2]. Thyrotropin-releasing hormone (TRH) is also identified as a PRL-releasing factor with unclear stimulation mechanism [24]. Many other peptides were suggested to promote PRL release such as oxytocin, hypothalamic vasoactive intestinal peptide (VIP) and endothelin [25].

2.1.2.3 Gonadotrophs

Gonadotrophs release LH and FSH which are the main regulators of the reproductive system including sperm/ova production and sexual hormone release. In males, LH controls the synthesis and the release of testosterone via binding to G-protein coupled receptors on testicular Leydig cells and activating cAMP signaling pathway [26]. The role of FSH in males is not well defined, however it is well documented that FSH binds to its receptors in Sertoli cells and increases the production of androgen binding proteins which may support spermatogenesis [27]. In females, FSH stimulates the growth of ovarian follicles, whereas LH induces ovulation and regulates the secretion of progesterone from the corpus luteum. Both

LH and FSH regulate follicular steroidogenesis and androgen and estradiol secretion [12]. The two major regulators of the release of gonadotropins are the hypothalamic gonadotropin-releasing hormones (GnRH) and the feedback of the gonadal factors. GnRH reaches the anterior lobe through the hypophysial portal system and promotes a Ca^{2+}-dependent pulsatile secretion of gonadotropines. GnRH binds to its receptors on gonadotrophs and activates a cascade of intracellular signaling pathways including activation of phospholipase C that leads to Ca^{2+} release and activation of protein kinase C [28].

2.1.2.4 Thyrotrophs

Thyrotrophs release TSH which mainly regulates the synthesis and the release of triiodothyronine (T3) and thyroxine (T4) by the thyroid gland. TSH binds to G_s-coupled receptors of the thyrocytes and activates cAMP signaling pathways. This leads to an increase in iodine transport and expression of thyroglobulin and thyroperoxidase resulting in increased thyroid hormones release [29]. T3 and T4 have an important effect on body growth, metabolism and differentiation of the central nervous system (CNS). TSH secretion is regulated by the hypothalamic thyrotropin- releasing hormone (TRH). TRH binds to G_q-coupled receptors on thyrotrophs and leads to a PLC-dependent increase of the intracellular Ca^{2+} concentration which stimulates TSH secretion. DAG promotes the activity of PKC enhancing TSH release [30]. T3 and T4 exert a negative feedback effect on TSH release on both the pituitary and hypothalamic level [12].

2.1.2.5 Corticotrophs

The major function of corticotrophs is the synthesis and release of ACTH which is the major regulator of glucocorticoids synthesis in the zona fasciculate of the adrenal gland. ACTH binds to melanocortin-2 receptors (MC_2R) that activate cAMP signaling pathways (Figure 2-2). ACTH is produced in the corticotrophs from its precursor POMC (Figure 2-2). POMC is cleaved by the activity of prohormone convertase PC1 to give rise to six different peptides including a N-terminal peptide, the joining peptide (JP), ACTH, β-lipotropin (β-LPH), γ-lipotropin (γ-LPH) and β-endorphin (β-end) [31].
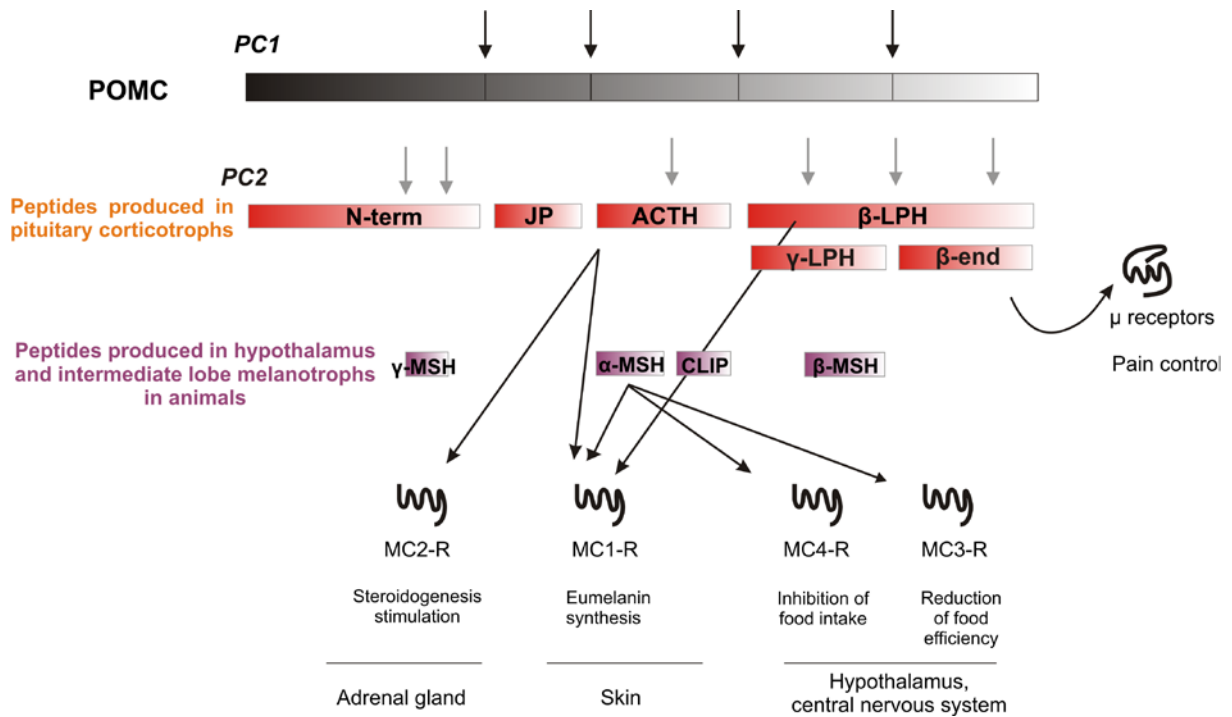
Figure 2-2: POMC processing by PC1 and PC2.
The physiological roles of its derivate peptides are also shown, modified from [31].

2.1.2.6 Melanotrophs

Melanotropic cells (Melanotrophs) of the intermediate lobe produces α-MSH that is also produced from POMC (Figure 2-2). In humans, this is done in the so-called POMC neurons of the hypothalamus [32]. A well-known physiological function of α-MSH is to stimulate the melanogenesis after binding to melanocortin 1 receptors (MC1R) in melanocytes [33,34]. This leads to an increase of cAMP which in turn regulates the transcription and the function of tyrosinase, tyrosine hydroxylase and phenylalanine hydroxylase [35,36]. α-MSH also acts in a receptor-independent manner to directly regulate the tyrosinase activity [35]. Furthermore, α-MSH was shown to play a significant role in controlling inflammation and immunomodulation in the skin by inhibiting the production of proinflammatory cytokines such as interleukin-1 (IL-1), IL-6 and tumor necrosis factor-α (TNF-α), and by upregulation of immunosuppressive cytokines such as IL-10 [37]. α-MSH is suggested to be involved in energy homeostasis, appetite regulation and inhibition of food intake by binding to MC3R and MC4R in the hypothalamus ([32,38,39], Figure 2-2). Recently, α-MSH was also shown to modulate the activity of basophilic granulocytes by binding to MC1R causing significant suppression of the secretion of the proallergic cytokines IL-4, IL-6, and IL-13 [40]. The secretion of α-MSH from the intermediate lobe is controlled by γ-amino butyric acid (GABA) and neuropeptide Y (NPY) as well as dopamine (DA) released by subpopulations of

hypothalamic neurons (tubero-hypophyseal neurons) that directly terminate in the intermediate lobe [41,42]. Dopamine binds to D2-receptors in the plasma membrane of the melanotrophs and reduces their synthesis of POMC and the release of POMC-cleavage products [43] via a cAMP-dependent pathway [44].

2.1.2.7 Oxytocin-releasing hypothalamic nerve terminals

Nerve terminals of the MNCs of the hypothalamus release OXT that is synthetized as a pro-hormone in their cell bodies. OXT release is associated with neurophysin I release, a carrier protein which is transported in vesicles with OXT to the posterior lobe [12]. OXT is essential for parturition and lactation. Suckling stimulates sensory nerves in the nipple of the mamma which in turn stimulates oxytocin-releasing MNCs. Released OXT stimulates the contraction of myoepithelial cells which surround the milk-laden alveoli resulting in milk ejection. During childbirth pain, afferent nerve impulses stimulate OXT release leading to strong contractions of the uterus supporting delivery of the newborn and the placenta [2,11].

2.1.2.8 Vasopressin-releasing hypothalamic nerve terminals

Similar to OXT, vasopressin (VP) or anti-diuretic hormone (ADH) is synthetized as a pro-hormone in the cell bodies of MNCs and packed in dense-core neurosecretory vesicles. The pro-hormones are cleaved by the activity of proteolytic enzymes to produce VP and its associated peptide neurophysin II. This cleavage takes place during the passage of vesicles from the Golgi apparatus to the terminals and swellings of the MNCs in the posterior lobe [12]. VP-release via exocytosis is stimulated in response to action potentials initiated in the plasma membrane of the MNCs. VP diffuses to the blood stream through fenestrated capillaries of the posterior lobe. Dehydration is the major physiological signal that stimulates VP release. VP plays an important role in the maintenance of body fluids and the regulation of blood osmolality. VP binds to V2 receptors in the plasma membrane of the epithelium of the collecting duct of the kidney and increases water reabsorption by increased integration of water channels (aquaporins) into the epithelial membrane [2,11]. In addition, parvocellular neurons of the PVN and SON terminate in the median eminence and release VP into the hypophyseal portal system. VP then stimulates corticotrophs synergistically with CRH to produce ACTH [45].

2.1.3 Function and regulation of non-endocrine pituitary cells

2.1.3.1 Pituicytes

Notwithstanding that pituicytes, the astroglial cells of the posterior lobe, do not secret any hormone they are suggested to play an important role in the regulation of neurohypophysal

hormone output. Pituicytes undergo a remarkable structural reorganization during increased demand of hormone release. Under resting conditions, the axonal terminals and swellings are laden with dense core neurosecretory vesicles (filled with hormones and their carrier proteins) and are completely engulfed by the processes and membranes of pituicytes. Neurosecretory swellings and terminals appear to form a synaptoid contact with the pituicytes in which the intermembrane distances are small (15-20 nm). The basal lamina, the barrier which separates neurohypophysial parenchyma from the fenestrated blood capillaries, is more than 60 % occupied with pituicytes limiting hormone availability to the blood stream [10,46]. Under stress conditions, such as dehydration, lactation and parturition, pituicytes tend to retract from the blood vessels resulting in a reduction of the number of terminals engulfed by pituicytes and a significant increase in neurovascular contact followed by a remarkable decrease of the amount of neurosecretory granules in the nerve terminals (Figure 2-3). Thus, pituicyte retraction allows more hormones to be released into the blood stream. When the demand of hormone release returns to its basal level, pituicytes recover to the resting morphology thereby limiting hormone availability. Released VP can act on the V1a receptors in the pituicytes and increase $[Ca^{2+}]_i$ via the IP_3 pathway [47]. Activation of V1a receptors induces taurine release from pituicytes. Taurine can act at the nerve terminal as a negative feedback inhibitor that inhibits hormone output [48]. Pituicytes release taurine selectively in response to hypoosmotic stimulation [46].
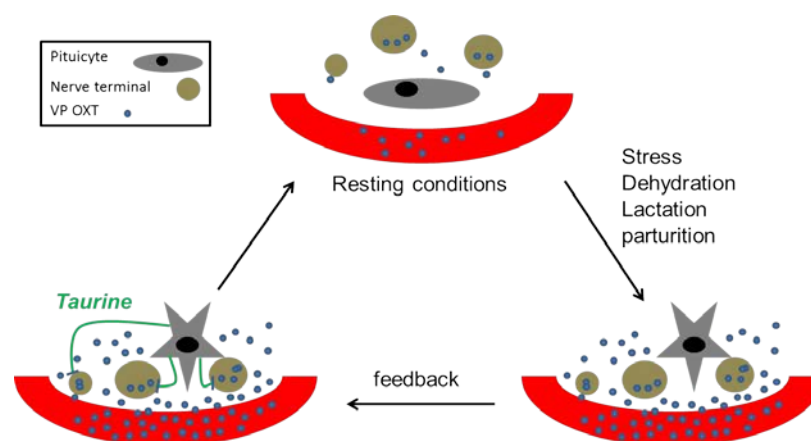
Figure 2-3: Postulated scheme for the modulation of neurohypophysal hormone secretion by V1a receptor activation of pituicytes, modified from [49].

2.1.3.2 Folliculostellate cells

Folliculostellate cells of the adenohypophysis are described to form a three dimensional cell network, in the meshes of which the endocrine cells reside [5,9,50]. The cells are connected by gap junctions and transfer informations such as Ca^{2+} signals and small diffusible

molecules over a long distance in the anterior pituitary providing an efficient communication system [9]. Additionally, folliculostellate cells display phagocytotic activity and function as scavenger cells [1,51]. A study of Shirasawa and Yamanouchi suggested that FS cells might be involved in controlling glutamate level and scavenging toxic ammonia [52]. FS cells modulate the function of endocrine cells by producing compounds such as lipocortin-1, which play an inhibitory effect on CRH and corticotropin secretion, and follistatin, which regulates in a paracrinic manner the production and secretion of FSH from gonadotrophs [53-55]. FS cells produce many other bioactive peptides like basic fibroblast growth factor which stimulates the growth of lactotrophs [56], and nitric oxide (NO) which might regulate LH secretion [57,58]. Recently, FS cells were shown to have the potency to differentiate into skeletal muscle cells [50] supporting an old hypothesis that these cells are suspected to act as stem cells in the pituitary gland [58].

2.2 Calcium signaling in pituitary cells and regulation of hormone release

Ca^{2+} plays a crucial role as a second messenger in a variety of cellular processes such as proliferation, migration, apoptosis, neuronal excitability, exocytosis and gene expression. The Ca^{2+} concentration inside the cell is 20000-fold lower than its concentration in the extracellular space. Since Ca^{2+} ions don't bind water tightly and precipitate phosphates, cells exclude Ca^{2+} ions from the cytoplasm to maintain the concentration at ~ 100 nM. Ca^{2+} signals in response to external stimuli, range from Ca^{2+} spikes which transfer fast responses to Ca^{2+} transients or Ca^{2+} waves which control slower responses. In principle Ca^{2+} signals are created by two types of reactions: calcium 'On' reactions including Ca^{2+} influx from the extracellular space through plasma membrane ion channels and Ca^{2+} release from the endoplasmic reticulum (ER) via Inositol trisphosphate (IP3) receptors while calcium 'Off' reactions include Ca^{2+} removal from the cytosol by different pumps and exchangers such as the Na^+/Ca^{2+} exchanger (NCX), the plasma-membrane Ca^{2+}-ATPase (PMCA) which extrudes Ca^{2+} to the outside and the endoplasmic reticulum Ca^{2+}-ATPase (SERCA) which pumps Ca^{2+} back into the ER [59,60].

In endocrine pituitary cells, an increase in the intracellular Ca^{2+} concentration above the threshold of stimulus-transcription or stimulus-secretion coupling leads to calcium-dependent hormone production and/or release [3,61,62]. As endocrine pituitary cells are similar to neuronal cells in the expression of different voltage-gated calcium, sodium, potassium and chloride channels, they are spontaneously able to fire action potentials which are normally associated with an increase at the intracellular calcium concentrations [3]. The electrical

activity can be modulated by the stimulation of G protein-coupled receptors (GPCRs). Stimulative G-proteins (G_s) stimulate the production of c-AMP by adenylcyclase which in turn increases the electrical activity and facilitates Ca^{2+} entry through voltage-gated channels directly or indirectly by c-AMP-dependent kinase activity. Activation of inhibitory (G_i)-coupled receptors in endocrine pituitary cells leads to the inhibition of electrical activity and hormone release. G_q-coupled receptors or calcium-mobilizing receptors are also expressed in pituitary cells and their activation leads to the production of diacylglycerol (DAG) and 1,4,5-trisphosphate (IP3) which induces Ca^{2+} release from the ER and subsequently increases hormone release. In addition to the voltage-gated channels mentioned above, transcripts of many members of transient receptor potential channels (TRP channels) like TRPM3, TRPC1, TRPC3, TRPC5 and TRPC7 were shown to be expressed in the pituitary gland [63,64]. Signaling through TRP channels may account for hormones production and/or release in a direct or an indirect way.

2.3 TRP ion channels

Transient receptor potential (TRP) channels are a superfamily of cation channels which display, apart from their sequence homology and basic channel architecture, distinct features regarding the activation mechanisms, ion selectivity and physiological functions [65]. A number of these channels play important roles in sensory physiology ranging from thermosensation to osmosensation, mechanosensation, vision, olfaction and audition [66]. The *trp* gene was first characterized in a *Drosophila melanogaster* mutant with impaired phototransduction. A prolonged light stimulation of *Drosophila* wildtype photoreceptors induced a sustained response characterized by an initial and an adaptive phase of the receptor potential, while *trp*-mutated photoreceptors showed only a transient response with a quick decay to a basal line [67]. In 1989, the *trp* gene was cloned by Montell and Rubin [68]. The idea that the encoded TRP proteins may build membrane channels was initiated by Minke and Selinger [69] and in parallel, Hardie and Minke were able to show that the light-induced Ca^{2+} influx is reduced up to 10 fold in *trp*-mutant flies supporting the idea that TRP proteins function as a calcium permeable ion channel [70].

Trp genes have been identified in different organisms ranging from worms (*C.elegans*) to men [71]. In mammals, 28 TRP proteins have been identified and were classified based on their topological similarities [72]. The mammalian superfamily of TRP channels is divided into six subfamilies, the canonical (TRPC), vanilloid (TRPV), melastatin (TRPM), ankyrin (TRPA), Mucolipin (TRPML) and polycystin (TRPP) channels (Figure 2-4). The TRPC, TRPV, TRPM, TRPA and TRPN subfamilies are classified as Group 1 of TRP channels as they show the

highest degree of sequence homology to the founding member Drosophila TRP, while the TRPP and TRPML subfamilies are classified as Group 2 of TRP channels as they display a large extracellular loop between transmembrane domains 1 and 2 and are weakly related to group 1 [66,71].
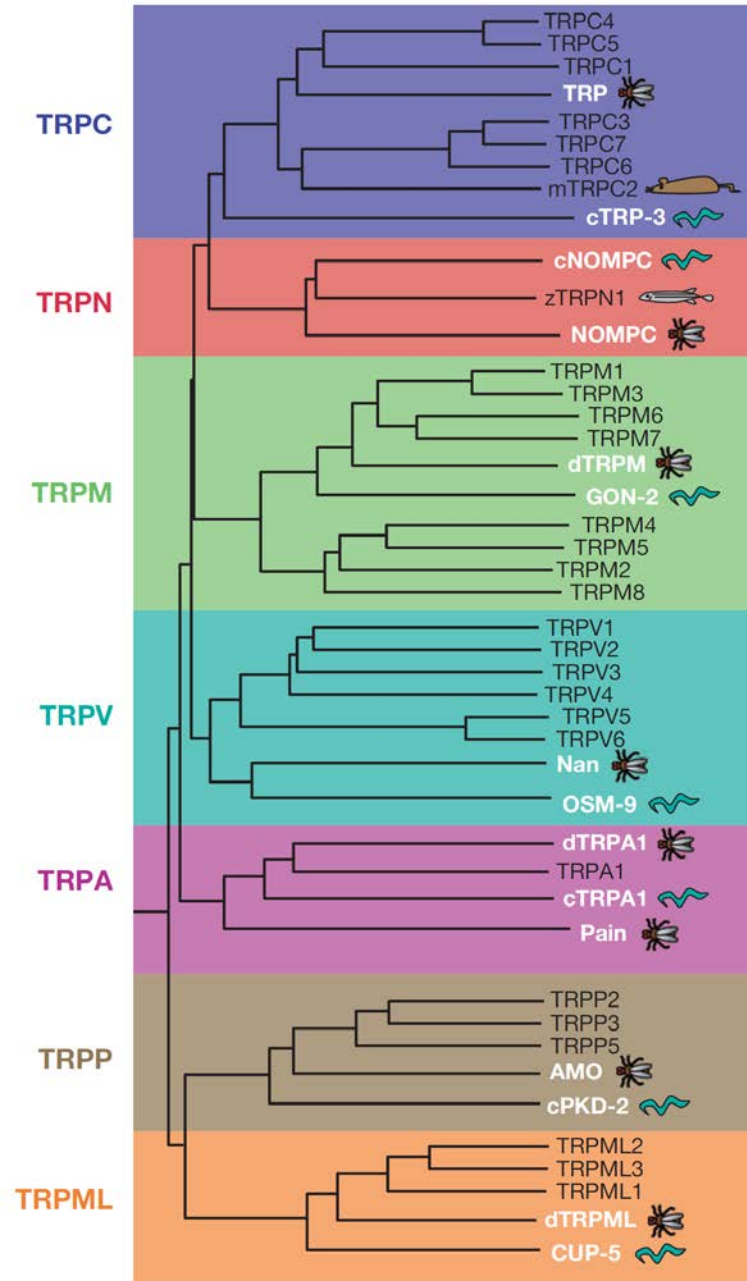
Figure 2-4: Phylogenetic tree of TRP proteins.
The dendrogram of vertebrate TRPs includes mostly human TRPs, except for mouse TRPC2 which is a pseudo gene in man and zebrafish TRPN1 which has no orthologue in mammals. White text and cartoons highlight the TRP proteins from worms and flies. One *C.elegans* and one *Drosophila* member of each subfamily are included [71].

The TRPC subfamily is composed of seven members sharing up to 40 % amino acid identity with each other and with the *Drosophila* TRP protein [73]. TRPV channels display only ~25 % sequence homology to the members of TRPC subfamily [66]. The name vanilloid was used since the first known member TRPV1 was identified as ligand-gated ion channel that is activated by vanilloids like capsaicin [74]. The TRPM subfamily, which shares ~20 % amino acid sequence identity to TRPC proteins, consists of eight members. The first member TRPM1 was initially named Melastatin because its expression appeared to be inversely correlated with the metastatic potential of melanoma cells [75]. TRPA1 is the only member of its subfamily and was identified in an oncogenic screen of down-regulated genes from fibroblasts [76]. The TRPP and TRPML proteins have very low sequence similarity with other TRP members and were discovered as mutant genes in autosomal dominant polycystic kidney disease (ADPKD) and mucolipidosis type IV (MLIV), respectively [71,77].

2.3.1 Structure of TRP channel complexes

TRP proteins contain six transmembrane spanning domains (S1-S6) and a pore forming region that is located between S5 and S6 (Figure 2-5). The amino (N) and carboxy (C)-termini are located in the cytosol and comprise most of the protein.
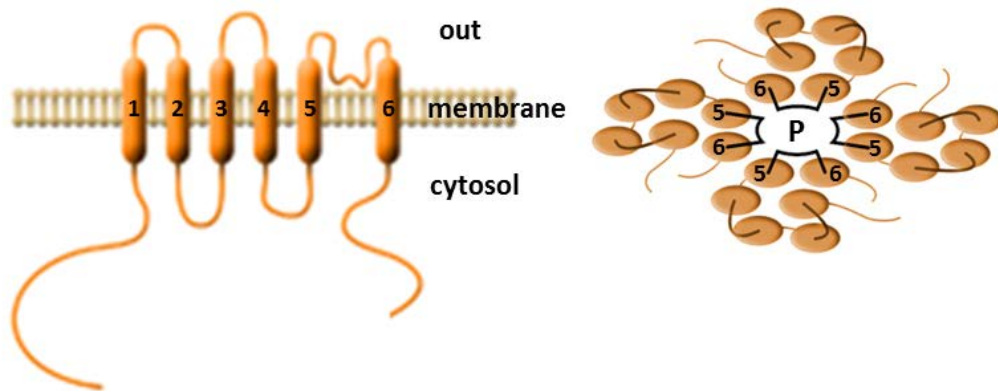
Figure 2-5: The predicted protein structure of TRP proteins.
The predicted membrane topology of monomeric TRP polypeptides (left) and the tetrameric channel complex (right) are shown. Transmembrane spanning domains that flank the ion conducting pore (P) are numbered. (Modified from [78]).

Other structural features of TRP proteins are illustrated in Figure 2-6. The N-terminal domains of TRPC, TRPV and TRPA contain up to 3, 6 and 15, ankyrin (ANK) repeats respectively. An ANK repeat domain is a ~33 residue motif consisting of two α-helices separated by loops [79]. ANK repeats have been proposed to bind to regulatory molecules

like calmodulin and ATP [80]. TRPM channels lack ANK repeats but instead contain a TRPM homology region of unknown function. A well conserved block of ~25 residues C-terminal to the sixth transmembrane domain, called the TRP domain or TRP box, is present in TRPC, TRPM and TRPV proteins [71,81]. TRP domains were shown to be required for phosphatidylinositol 4,5-bisphosphate (PIP_2) binding and the regulation of channel gating of TRPM8 and TRPV5 channels [82]. Heptead repeat structures called coiled-coil domains, are present in some members of TRP channel family [83]. They belong to the best defined protein-protein interaction domains with a conserved alpha-helical structure. A coiled-coil domain in TRPP2 was suggested to link the protein to PKD1 [84,85]. Coiled-coil domains also seem to play a role in the multimerization of TRPM channels [86-88]. The C-terminal domains of some TRPM channels (M2, M6 and M7) possess enzyme activity and thus the proteins were termed chanzymes [71]. The kinase activity of TRPM7 was thought to modulate the channel sensitivity for intracellular cAMP regulation and Mg^{2+} inhibition [89,90], whereas in TRPM6 the function of the kinase domain is still unknown. TRPM2 channels are linked to a nucleoside diphosphate pyrophosphatase (NUDIX) domain that possess adenosine diphosphate (ADP)-ribose hydrolase activity [81].
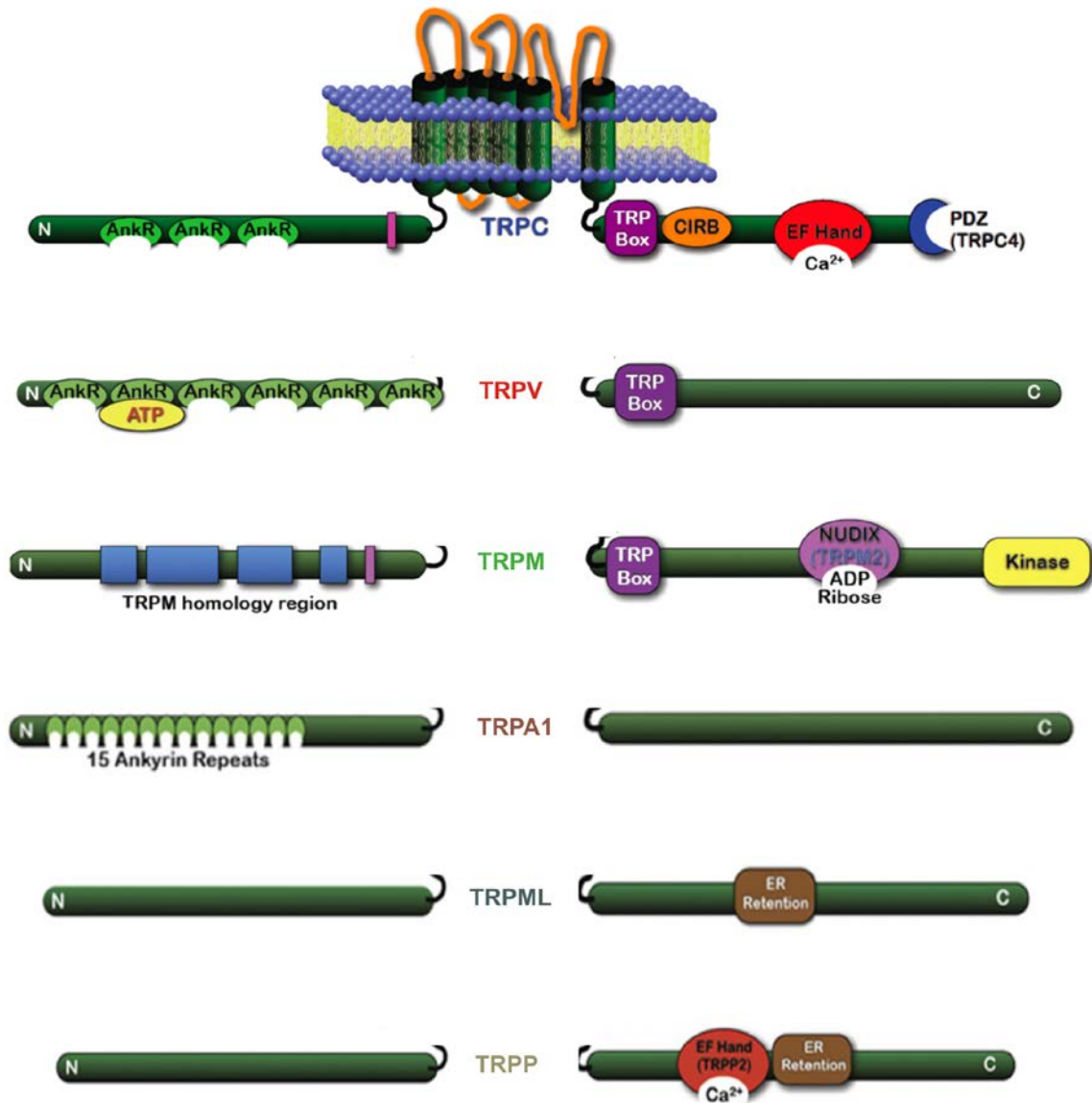
Figure 2-6: Structure of TRP channels.
In TRPC and TRPP, the C-terminus contain the EF hand domain which is found in a large family of calcium-binding proteins and PDZ (postsynaptic density 95/disc-large/zona occludens) which is a common protein interaction motif that joins proteins in signaling complexes. In TRPML and TRPP, the ER retention signal is a small domain that has been proposed to maintain the channel in the endoplasmic reticulum. The other domains indicated are described in the text. (Modified from [81]).

Similar to other six transmembrane domain channels, TRP proteins form a tetrameric quaternary structure in which the S5 and the S6 domains from each subunit contribute to a shared selectivity filter and ion-conducting pore ([71], Figure 2-5). Recently, detailed informations about the TRPV1 channel structure has been achieved by cryo-electron microscopy of the protein at a resolution close to 3 Å. These data confirmed the predicted information about the tetrameric structure of TRP channels and ion conducting pore [91,92].

TRP proteins form channels that control the flux of cations along their electrochemical gradients. Cation entry through the channel is regulated by the upper gate or the selectivity filter of the channel and the lower gate which is formed by the cytoplasmic end of the S6 helix [81,93]. Most TRP channels form non-selective ion pores with similar ion permeability for Ca^{2+} and Na^+ (permeability ratio $P_{Ca}/P_{Na} \leq 10$). However, TRPM4, TRPM5 and the TRPM3α1-variant are almost impermeable for divalent cations, whereas TRPV5 and TRPV6 are highly selective for Ca^{2+} ($P_{Ca}/P_{Na} \geq 100$) [94]

2.3.2 Activation and functional properties of TRP channels

TRP channels are widely expressed in large number of tissues and cell types. Since TRP channels allow the flux of cations through the plasma membrane, they play important roles in regulating the intracellular Na^+ and Ca^{2+} concentrations ($[Na^+]_i$, $[Ca^{2+}]_i$) and the membrane potentials in both excitable and nonexcitable cells [95]. TRP channels are sensitive to a wide range of activators and activation mechanisms including changes in temperature, pH, osmolality and intracellular second messenger (Table 2-1).Therefore, TRP channels play important roles in a plethora of physiological functions including vision, taste, smell, hearing, and touch. Table 2-1 shows modes of activation for each individual TRP channel. TRPC channels are modulated via a GPCR-mediated pathway including PIP_2 hydrolysis and the production of DAG and IP3. IP3 binds the IP3 receptors resulting in Ca^{2+} release from intracellular stores which in turn activates cation entry through TRP channels. Other TRP channels can be activated from outside by a plethora of agonists. For example, plant secondary compounds like capsaicin and icilin activate TRPV1 and TRPM8, respectively. Most of these channels also belong to the group of the so-called thermo-TRPs (TRPV1-4, TRPA1, TRPM3 and TRPM8) since they are also sensitive to changes of the ambient temperature [65]. Finally, a number of channels already display constitutive activity that is modulated by a variety of intracellular second messenger.

Most of the TRP channels are nonselective for mono and divalent cations. However, TRPV1 and TRPM8 show increased selectivity for divalent cations with a fractional Ca^{2+} current under physiological conditions of 3-5 % [96], others like TRPA1 and TRPM3 display even higher fractional Ca^{2+} currents of about 25 % and finally TRPV5 and TRPV6 are extraordinary Ca^{2+}-selective with fractional Ca^{2+} current close to 100 % [95,97]. The activation of TRP channels may trigger gating of voltage-gated Ca^{2+} channels and/or induce Ca^{2+}-dependent channel inactivation. This indicates that the electrogenic effect of TRP channel activation might be as important as its contribution to Ca^{2+} changes by mediating Ca^{2+} entry. Members of the TRPC subfamily are reported to have a significant importance in

the regulation of firing pattern of neurons [98]. In non-excitable cells, TRP channels activation regulates the driving forces for Ca^{2+} entry [95]. Finally, TRP proteins like TRPML are also located in the intracellular organelles like the ER, endosomes and lysosomes and serve as intracellular Ca^{2+} release channels [95,99].

Table 2-1: Properties of channels formed by mammalian TRP proteins. Modified from [71,100].

Subtype	Selectivity P_{Ca}/P_{Na}	Activation/ modulation of activity	Function/ Associated diseases	Consequences of TRP-deletion in mice
TRPC1	~1	PLC activation, store depletion, conformational coupling, mechanical stretch	Required for EPSC in Purkinje cells	Elevated body weight, impaired salivary gland fluid secretion
TRPC2	~1-3	PLC activation, diacylglycerol (DAG)	Acrosome reaction, Pheromone perception	Abnormal sexual and mating behavior
TRPC3	~1.5	PLC activation, store depletion, conformational coupling, DAG, exocytosis	Modulating neuritis extension	Defects in motor coordination and walking behavior
TRPC4	~1-8	PLC activation, store depletion (?), PIP_2 breakdown, exocytosis	Vasorelaxation, neurotransmitter release	Impaired vascular function, altered 5-HT-mediated GABA release, defects in intestinal motility
TRPC5	~2-9	PLC activation, store depletion (?), sphingosine-1-phosphate, exocytosis	Modulating neuritis extension	Decreased anxiety-like behavior
TRPC6	~5	PLC activation, conformational coupling , DAG, PIP_3	platelet aggregation	Grossly normal, increased artery contractility, impaired light response in intrinsically photosensitive retinal ganglion cells in TRPC6/TRPC7 compound KO mice
TRPC7	~1-5	PLC activation, store depletion, DAG	?	impaired light response in intrinsically photosensitive retinal ganglion cells in TRPC6/TRPC7 compound KO mice
TRPV1	~4-10	Heat (43˚C), vanilloids, proinflammatory cytokines, protons, PIP_2	Hot pain sensor 43°C	Reduced inflammatory hyperalgesia, impaired bladder function
TRPV2	~1-3	Heat (52˚C), osmotic cell swelling, exocytosis	Very hot pain sensor 52°C	Accelerated mortality in bacterial infection
TRPV3	~1-10	Warm (33–39˚C); PUFAs; menthol; compounds from oregano, cloves, and thymes	Warm temperature sensor (30°-39°C)	Impaired thermosensation, skin barrier effects, curved whiskers, and hair
TRPV4	~6	Warm (27–34˚C), osmotic cell swelling, 5'6'-EET, anandamide, 4αPDD, exocytosis	Osmosensor, warm sensor (27°C) in keratinocytes	Altered body osmolarity; increased bone mass; impaired bladder function; reduced inflammatory hyperalgesia
TRPV5	>100	Constitutively active[1], exocytosis (?)	Ca^{2+} reabsorption in kidneys	Impaired renal Ca^{2+} reabsorption; decreased bone thickness
TRPV6	>100	Constitutively active[1], store depletion (?), exocytosis (?)	Ca^{2+} - homeostasis, differentiation keratinocytes	Impaired epididymal Ca^{2+} absorption, male hypofertility, impaired Ca^{2+} absorption
TRPM1	<1	Translocation (?)	Visual perception?	impaired ON bipolar cell function and vision
TRPM2	~0.3-2	ADP-ribose, cADP-ribose, pyrimidine	Redox sensor	Impaired neutrophilin filtration in inflammation, increased ROS production in

		nucleotides, arachidonic acid, NAD, H_2O_2, Ca^{2+}		phagocytes, higher basal glucose level and impaired glucose tolerance
TRPM3	~1-10 [2]	Constitutively active[1], osmotic cells welling, store depletion (?), pregnenolone sulfate, d-erythro-sphingosine (?), heat (33-40°C)	Insulin secretion Pain sensation	Impaired noxious heat perception
TRPM4	Monovalent selective	Ca^{2+}, voltage modulated, PIP_2	Allergy, immune response	Increased release of inflammatory mediators from mast cell and cutaneous anaphylaxis; impaired dendritic cell migration; reduced secondary hemorrhage and lesions after spinal cord injury, hypertension associated with increased catecholamine release from chromaffin cells
TRPM5	Monovalent selective	Taste receptor activation (T1R,T2R), Ca^{2+}, Voltage modulated, PIP2, heat (15–35˚C)	Taste	Impaired sweet, umami, and bitter taste reception; deflects in glucose-induced insulin release
TRPM6	<10[3]	Mg^{2+} inhibited, translocation	hypomagnesemia, hypocalcemia	Embryonic lethality, neural tube defects in development
TRPM7	~0.2-2[3]	Activation mode of native channels unclear, Mg^{2+} inhibited, ATP, protons, phosphorylation, PIP_2	Cell viability	Embryonic lethality; conditional TRPM7 deletion in T cells causes abnormal thymocyte development
TRPM8	~0.3-4	Cool (23–28°C), menthol, icilin, pH modulated, PIP2	Cool temperature sensor (23°–28°C)	Deficiencies in response to cold
TRPA1	~0.8-5	Cold (17˚C) (?), icilin, isothiocyanates, allicin (garlic), cannabinoids, bradykinin, PLC activation, DAG, PUFAs	Cold pain sensor (17°C), hearing	Reduced response to noxious cold and intestine mechanical force
TRPML1	[4]	Activation mode of native channels unclear, potentiation by low pH	Lysosomal trafficking?, mucolipidosis type IV	Motor deficits, retinal degeneration, decreased life span
TRPML2	[4]	Activation mode of native channels unclear, potentiation by low pH	-	-
TRPML3	[5]	Activation mode of native channels unclear, removal and readdition of extracellular Na^+	Hearing	Varitint-waddler (Va) mice with a TRPML3 (A419P) gain of function mutation exhibit deafness, circling behavior, and pigmentation defects
TRPP2	Non-selective	Translocation with TRPP1, fluid flow, mechanical gating (?)	Polycystic kidney disease	Lethal E13; embryonic cysts and extrarenal abnormalities including left-right asymmetry of visceral organs
TRPP3	~1-10	Ca^{2+}, voltage modulated	-	-
TRPP5	Non-selective	?	-	-

[1] Not yet measured in primary cells; [2] significant differences in individual splice variants; [3] divalent cation selective (Ca^{2+} and Mg^{2+}); [4] localization primarily intracellularly in endolysosomes, permeability for Na^+, K^+, Ca^{2+}, Fe^{2+}; [5] localization primarily intracellularly in endolysosomes, permeability fo Na^+, Ca^{2+}, K^+.

2.4 Transient receptor potential Melastatin 3 (TRPM3)

TRPM3 is the last identified member of the TRPM subfamily [101-104]. TRPM3 is most closely related to TRPM1, the founding member of the subfamily. It differs from TRPM2, TRPM6 and TRPM7 by the lack of enzymatic activity and from TRPM4 and TRPM5 by its permeability for Ca^{2+} ions. Similar to TRPM8, TRPM3 is activated by changes of temperature [105].

2.4.1 The *Trpm3* gene encodes a variety of different TRPM3 proteins

Trpm3 genes display a highly conserved configuration in mouse, rat and human. In the mouse, the gene is located on the chromosome 19b spanning more than 850 kb and comprising 28 exons (Figure 2-7). The human and rat genes are located on chromosome 9 (9q21.11-q21.12) and chromosome 1q5, respectively [106]. *Trpm3* genes encode a large number of variants due to alternative splicing of their primary transcript (Figure 2-7). Furthermore, the variability of TRPM3 transcripts is increased by the presence of at least three promoters that give rise to three alternative transcription start sites encoding three different amino termini of the protein. The different promoters were supposed to regulate the expression of different protein isoforms called TRPM3α (α1 to α5) starting within exon 1 and lacking exon 2, TRPM3β (β1 to β17) starting within exon 2 and finally isoforms starting with a ATG codon located at the very end of exon 4 ([106], Figure 2-7).

The splicing events affect exons 8, 13, 15, 17, 20, 24 and 28 and hitherto at least 24 different TRPM3 variants have been described from one species (Figure 2-7). However, only by splicing at least $2^7 = 128$ isoforms may exist (Figure 2-7). The splicing pattern of these exons is highly conserved in human, rat and mouse transcripts indicating important functions of the related protein modifications. For example, mTRPM3α2 proteins differ from mTRPM3α1 proteins by the absence of 12 amino acid residues in the pore forming region of the channel and display high permeability for Ca^{2+} in contrast to mTRPM3α1 [103].
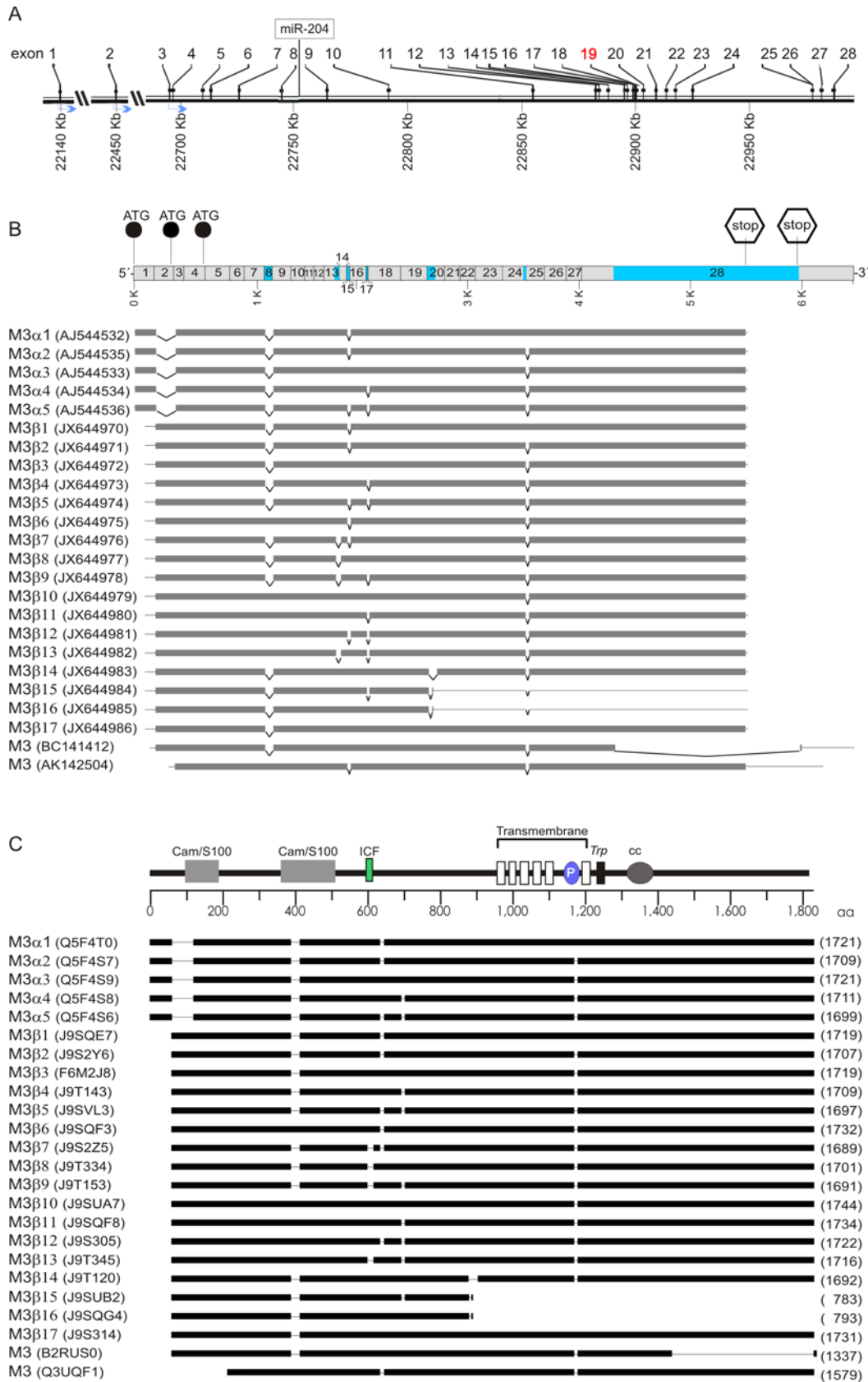
Figure 2-7: The *Trpm3* gene, its transcripts and the encoded proteins, adapted from [106].

A. Genomic organization of the mouse *Trpm3* gene on chromosome 19. Predicted transcription start sites are indicated by arrows. A microRNA sequence (miR-204) is located in intron 8. Exon 19 which was subject of the targeting strategy to obtain a TRPM3-deficient mouse line [105,107] is highlighted in red. B. Structure of *Trpm3* transcripts identified in mouse tissues. Their reading frames are flanked by stop codons establishing entire protein coding sequences with GenBank accession numbers as indicated. The coding parts of the transcripts are shown as grey bar, the noncoding parts as thin line. The upper bar indicates the relative size of the protein coding exons 1 - 28 with spliced parts highlighted in blue. Start codons (ATG) present in exons 1, 2 and 4 and stop codons (stop) in exon 28 are indicated. C. Schematic presentation of TRPM3 protein isoforms (black bars) scaled to their relative size with protein identifiers and numbers of amino acid residues (aa) indicated in brackets. Internal protein domains removed by alternative splicing are indicated as thin lines. The organization of domains of TRPM3 proteins is shown above, with calmodulin/S100 protein interacting regions (CamBS/S100), ICF region, transmembrane region including the six transmembrane domains (white rectangles), the channel pore (P), the TRP motif (TRP) and a coiled-coil region (cc) as indicated.

TRPM3 proteins are known to interact with theirselves and with other TRP channels to form homo- and hetero-multimeric channels. It has been shown by immunoprecipitation that TRPM3α1 variants interact with TRPM3α2 and with TRPM1 [108]. This interaction was also confirmed by intermolecular fluorescence resonance energy transfer (iFRET) of TRPM3 proteins fused to the fluorescent proteins CFP or YFP [109,110]. The introduction of TRPM3α1 or TRPM1 into TRPM3α2 overexpressing HEK293 cells revealed a dominant-negative effect on the TRPM3α2-dependent Ca^{2+} entry confirming a direct molecular interaction of TRPM3 and TRPM1 proteins [108]. Recently, a region that is indispensable for TRPM3 channel function (ICF) has been identified [111]. The ICF domain consists of 10 amino acid residues encoded by the last part of exon 13 and interestingly, is also subject of alternative splicing. The ICF region is conserved throughout the TRPM subfamily and was suggested to be essential for the function and the formation of operative TRPM channels. TRPM3 variants lacking the ICF domain (ΔICF) showed reduced interaction with other TRPM3 isoforms and a diminished occurrence in the plasma membrane. Furthermore, coexpression of ΔICF-proteins with functional TRPM3 subunits resulted in impaired TRPM3-mediated Ca^{2+} entry and reduced the number of channels indicating that the ICF region is necessary for the function and trafficking of TRPM3 proteins [111].

TRPM3 channel activity is suggested to be regulated by the calcium binding protein calmodulin (CaM) since the comparison of TRPM3 amino acid sequence with calmodulin-binding proteins indicated the presence of six putative calmodulin binding sites within the N-terminus of TRPM3 [112]. Recently, the presence of two of these binding sites was confirmed experimentally [113]. Interestingly, these two binding site were found to bind both calmodulin and another calcium binding protein (S100A) in calcium-dependent manner. These two proteins are able to compete for the same binding sites within the TRPM3 N-

terminus [113]. PIP$_2$ was also found to interact with the CaM/S100A binding sites, implying an important role of this region in the regulation of TRPM3 channel activity [114].

2.4.2 Expression and function of TRPM3 proteins

The expression pattern of TRPM3 in different tissues was uncovered by the use of a variety of molecular and biochemical techniques like RT-PCR, *in-situ* hybridization, immunohistochemistry as well as Northern- and Western blot analysis (Table 2-2). RT-qPCR analysis of human and mouse tissues revealed strongest expression of TRPM3 in the brain, pituitary gland, kidney and adipose tissues. For neuronal TRPM3 channels, their occurrence in dorsal root ganglia (DRG) and their function as sensor of noxious heat is well established [105]. However, in the central nervous system the *Trpm3* gene is expressed not only in neurons but also in epithelia and oligodendrocytes, where TRPM3 channels have been proposed to participate in differentiation and CNS myelination [110]. In mouse brain, transcripts could be detected in several regions (Table 2-2) with most prominent expression in epithelial cells of the choroid plexus [103]. However, as shown in Table 2-2, TRPM3 is expressed in quite a number of other tissues and cell types with hitherto unknown functions.

In isolated pancreatic β-cells, PregS induced TRPM3-mediated Ca^{2+} influx resulting in an enhanced insulin secretion of these cells (Table 2-1, [115]). This and other studies [116] suggested the importance of TRPM3 signaling in the regulation of insulin synthesis and secretion [117]. Furthermore, TRPM3 proteins contribute to pain sensation in dorsal root ganglia (DRG). TRPM3-deficient mice showed an impaired perception of noxious heat [105] and TRPM3 antagonists like Hesperetin and isosakuranetin reduced the nocifensive behavior after PregS injection [118]. TRPM3-dificient mice also showed reduced consensual pupillary responses to light suggesting that TRPM3 might play an indirect role in these responses [107]. Furthermore, TRPM3 signaling has been suggested to be coupled to aortic contraction and suppression of proinflammatory interleukin-6 secretion in vascular smooth muscle cells from human and mouse [119]. Since TRPM3 is expressed in the brain with a prominent expression in choroid plexus epithelial cells (CPECs), it was hypothesized that TRPM3 might be involved in the production of the cerebrospinal fluid and the regulation of its ionic composition [103,120]. According to TRPM3 expression in the kidney and its activation by hypotonicity, it has been suggested that TRPM3 plays a role in renal osmohomeostasis [102,121].

Table 2-2: TRPM3 expressing tissues and the methods of their detection (adopted from [106])

Tissue/cell type	RT-PCR	RT-qPCR	Micro-array	Northern	ISH	Western	IHC/ICC	cDNA library	Transgene	Function
Method of detection*										
Nervous system										
total brain	[101,102, 110,115, 122-124] [122,123]	[63,102]		[101-103,125]		[110,115]				
cerebrum		[126]					[110]			
brainstem							[110]			
locus coeruleus		[102]								
spinal cord		[102]								
hippocampus		[126]					[110]			
forebrain		[126]								
corpus callosum							[110]			
chor. plexus epithel		[102]		[103]	[103, 127-129]					
tenia tecta					[103]					
ILSN#					[103]					
hypothalamus		[102]								
cerebellum		[102,126]					[110, 130]			
purkinje cell							[130]			[130]
oligodendrocyte	[110]						[110]			
Oli-neu/OLN-93cell						[110]				[110]
basal ganglia/ substantia nigra		[102,126]								
dorsal root ganglion	[124]	[105,124, 131,132]			[105]	[105]				[105,118, 133]
trigeminal ganglion	[134]	[105,124]			[105]	[105]				[105]
nodose ganglion		[131]								
SH-SY5										
Sensory system										
eye (total)			[107]	[103]	[128]					
retina	[125]	[135,136]		[125]	[125,128, 129]			[137]	[107]	
iris								[138]		
lens		[139]			[128,129, 140]					
retinal pig. epithel.		[141,142]			[125,128, 140]			[137]		
Muller cell	[107]								[107]	
ciliary body					[125,128, 140]				[107]	
inner ear	[143,144]							[144]		
Cardiovascular system										
heart	[124]	[145]								
pulmonary artery	[122,146]	[146,147]								
coronary artery	[123]									
mesenteric artery	[123]									
femoral artery							[119]			
aorta	[119,123, 146]	[146]								[119]
saphenous	[119]	[119]					[119]			[119]

vein									
Endocrine system									
pituitary gland		[63]		[108]					
pancreas (total)	[101,115]					[115]			[115]
pancretic islet cell	[148]								[149]
INS1	[115,148]	[150]		[115]		[115,116, 151]			[115,149, 151]
Urinary system									
kidney (total)	[101,124]	[63,102]		[101,102]		[101]			
collect. tub. epithel.					[102]				
MDCKII cell	[152]								
ccRCC§		[153]							
Reproductive system									
ovary	[101]								
testis	[124]	[102,124]		[102]					
sperm cell	[154]								
prostate	[155]	[155]							
Other tissues/cells									
MG-63 cell	[156]								
SaOS cell	[156]								
U2 OS cell	[156]								
odontoblast	[157]								
adipose tissue		[63]							
buccal mucosa		[158]							
synoviocyte	[159]						[159]		[159]
glioma		[160]							

* References demonstrating expression of TRPM3 as indicated by numbers, #intermediate lateral septal nuclei, §clear cell renal cell carcinoma

2.4.3 Pharmacology of TRPM3 channels

Depending on the isoform, the activation mechanisms of TRPM3, the selectivity and the conductance of the channels turned out to be different. For example, the long variant of human TRPM3 has been suggested to be activated by store depletion [102], whereas the short variant hTRPM3$_{1325}$ mediates Ca^{2+} entry upon extracellular application of hypotonic solutions [101]. Furthermore, mouse TRPM3α1 channels are permeable for monovalent cations, whereas mouse TRPM3α2 channels allow the entry of divalent cation such as Ca^{2+} and Mg^{2+} [103]. Human TRPM3$_{1325}$ was reported to be the first cation channel activated by D-erythrosphingosine [161] but TRPM3 channels have been also described as steroid-receptors channels, since pregnenolone sulfate (PregS) is the most potent agonist of TRPM3 [115]. At body temperature of 37°C, TRPM3 is activated by ~ 100 nM PregS, which is close to serum concentrations that have been reported to be 130 and 140 nM in female and male, respectively [162,163]. However, at room temperature 100 µM PregS are needed to fully activate the channel [115]. TRPM3 channels were also shown to be activated by nifedipine which is well-known as a blocker of voltage-gated calcium channel (VGCC, [115]). It has been shown that nifedipine and PregS are able to activate TRPM3 synergistically and that they act at different binding sites [164]. Recently, an alternative permeation pathway through

TRPM3 channels has been described. This pathway is activated by the combined application of neurosteroids and clotrimazole or other structurally related drugs and is still active after desensitization or blockade of the central pore. Activation of this pathway leads to massive Na^+ influx, enhanced excitation of sensory neurons and in turn increased TRPM3 dependent pain intensity [163].

Similar to other TRP channels, TRPM3 channel activity was described to be inhibited by the extracellular application of 100 µM 2-aminoethoxydiphenyl borate (2-APB, [165]). Furthermore, 100 µM concentration of trivalent ions such as Gd^{3+} and La^{3+} also inhibit Ca^{2+} influx through TRPM3 channels [101,102]. The nonsteroidal anti-inflammatory drug mefenamic acid [151], antidiabetic PPARγ-agonists such as rosiglitazone, troglitazone, and pioglitazone [166] and cholesterol [119] have been shown to decrease TRPM3 channel activity. Finally, progesterone was shown to reduce TRPM3 activity in vascular smooth muscle cells [167]. However, none of the above mentioned substances are specific for TRPM3 as they also block a plethora of other channels. By screening a library of natural compounds, novel potent TRPM3 blockers have been discovered recently including ononetin, naringenin and Hesperetin [168]. Ononetin is a deoxybenzoin from *Ononis spinosa* while naringenin and Hesperetin belong to citrus fruit flavanones. In a following study, further TRPM3 channel blockers like liquiritigenin and isosakuranetin were identified and isosakuranetin was defined as the most potent inhibitor of TRPM3 channels with an IC_{50} of 50 nM [118].

2.5 Aim of the work

The aim of this work was the identification of TRPM3 channels in the pituitary gland and the determination of their function(s) in defined cell populations.

To accomplish this goal:

1. I constructed and screened a pituitary cDNA library and analyzed the number and identity of different TRPM3 isoforms.
2. I used mono- and polyclonal anti-TRPM3 antibodies as well as a transgenic mouse line expressing the GFP-reporter protein under the control of TRPM3 promoter to identify TRPM3 expressing cells.
3. I analyzed the functional properties of TRPM3 channels and their physiological roles in the identified cell populations using TRPM3 specific ligands and cells from wild type and TRPM3-deficient mice.

3 Materials

3.1 Chemicals

Unless otherwise indicated, chemicals used for this work were purchased from one of the following suppliers: Sigma-Aldrich, Invitrogen, Merck, Applichem, VWR, Biochrome or Roth.

3.2 Reagent systems (Kits)

Agilent RNA 6000 Nano Kit®

Alpha-MSH ELISA Kit (MyBioSource)

GeneElute™ HP Plasmid Miniprep Kit (Sigma-Aldrich)

peqGOLD RNAPure ™ (Peqlab Bio technology, Erlangen)

Phusion® High-Fidelity PCR Kit (New England Biolabs)

Milliplex MAP® Kit, Rat/Mouse Neuropeptide (Merck Millipore)

SuperScript® One-Step RT-PCR with Platinum® *Taq* DNA Polymerase (Invitrogen)

SuperScript™ First-Strand Synthesis System for RT-PCR (Invitrogen)

Thermo Scientific™ Pierce™ BCA™ Protein Assay

Western Lightning™ *Plus* ECL (Perkin Elmer)

3.3 Vectors

pUC 19

The cloning vector pUC19 (Figure 3-1) comprises a fragment carrying the sequences for the α-peptide of the lacZ gene and the multiple cloning site (MCS), in addition to portions of pBR322 and M13mp19 (Figure 3-1). The pBR322 fragment carries the ampicillin resistance gene and the origin of replication. The region of M13 mp19 vector is responsible for the single strand production. Insertion of cloned fragments into the MCS disrupts the reading frame of the α-peptide and gives rise to white-colored colonies on X-Gal / IPTG containing solid media.

pCAGGSM2-IRESGFP

The expression vector pCAGGSM2 IRESGFP [169] comprises 6153 bp and is based on the plasmid pCAGGS (Figure 3-1, [170]). The expression of the target cDNA is under the control of a chicken β-actin promoter. An internal ribosome entry site (IRES) located downstream of the multiple cloning site allows the simultaneous expression of the target cDNA and the

cDNA encoding the green fluorescent protein (GFP). This way the expression of the target cDNA can be visualized by the fluorescence of GFP.
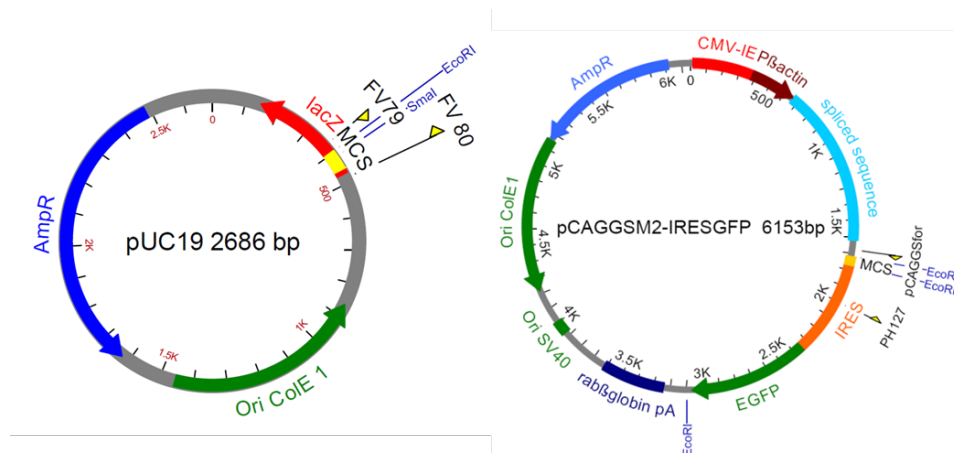
Figure 3-1: Circular map of the vectors used.
Shown are: the origin of replication derived from the ColE1 Plasmid (ColE1 ori) and the simian virus SV40 (SV40 Ori); the multiple cloning site (MCS); binding sites of the primers FV79, FV80, pCAGGSfor and PH127; the enchancer sequence from the cytomegalovirus (CMV IE); the promotor of the β-actin gene from chicken (P β-actin); the polyadenylation sequence of the rabbit β-globin gene (rabßglobin pA); the internal ribosome entry site (IRES); coding sequences for β-lactamase (AmpR); the sequence encoding the α-peptide of the β-galactosidase (lacZ) and the green fluorescent protein (EGFP), recognition sequences of the restriction endonucleases SmaI and EcoRI.

3.4 Oligonucleotides

Oligodeoxyribonucleotide primers (Table 3-1) were purchased in lyophilized form from Eurofins MWG Operon (Ebersberg) and dissolved in sterile H_2O in a concentration of 100 pmol/µl. Stock solutions were stored at -20 °C.

Table 3-1: Oligonucleotide primers used for sequencing

Primer name	Primer sequence (5'→3')	Origin of the sequence
FV 79	CACGACGTTGTAAAACGAC	pUC19
FV 80	CAGGAAACAGCTATGAC	pUC19
PH 389	CCAACTGAGCTTAGCTTTAGCC	Mouse TRPM3 cDNA
PH 401	CTACATTGTTCGCCAGAGCAG	Mouse TRPM3 cDNA
PH 422	CCCTCTAGAGCTGGAGTGAAATGTGCTTTTCC	Mouse TRPM3 cDNA
PH 427	GCCCTTAAGTTGAGGAGAGGACGGAAGACA	Mouse TRPM3 cDNA
PH 520	AGGATCATCCAAGTCGATGTCC	Mouse TRPM3 cDNA

Nucleotides which are non-homologous to the indicated sequence are underlined.

Table 3-2: Oligonucleotide primers used for RT-PCR

Primer name	Primer sequence (5'→3')	Origin of the sequence
PH 382	GAGAGCTGAGCGCAGGCTG	Mouse TRPM3 cDNA
PH 383	GAATGGGCAAGAAGTGGAGGG	Mouse TRPM3 cDNA
PH 384	AATGTGTTCACATCATACCGAGC	Mouse TRPM3 cDNA
PH 385	TCCTGCAACACACGGTAAGCC	Mouse TRPM3 cDNA
PH 386	GGTTGTGGAAGGTGCTAGAGC	Mouse TRPM3 cDNA
PH 423	GCCCTTAGGAGCAAGCTCACCGTTCTCAATAG	Mouse TRPM3 cDNA
PH 429	AAGAAGGTTCAGGGGCTCAGG	Mouse TRPM3 cDNA
PH 520	AGGATCATCCAAGTCGATGTCC	Mouse TRPM3 cDNA
PH 521	CCCAATGAGGAGCCATCTTGG	Mouse TRPM3 cDNA
PH 522	CGGGTCTCATTCTGTCCACAG	Mouse TRPM3 cDNA
PH 561	GGTACCTAACAATGTCAGGGAC	Mouse TRPM3 cDNA
PH 562	AAGTAGGGAGAAGTTGGTCACC	Mouse TRPM3 cDNA
PH 777	TGGTGGTGCTGATGAGCTTTGG	Mouse TRPM3 cDNA
PH 778	TGGATTGTCTTGCCATCCTCTCG	Mouse TRPM3 cDNA
C5-139	CGCACACCGGCCTTATTCC	IRES-GFP

Table 3-3: Oligonucleotide primers used for amplification of TRPM fragments from GLAST positive and GLAST negative cells from mouse intermediate and posterior pituitary lobe

Primer name	Primer sequence (5'→3')	Origin of the sequence
PH 773a	GCGACGAAGGAGGAGTCATAAACG	Mouse TRPM1 cDNA
PH 774a	CATCTTGCTGACCCTCGGAACC	Mouse TRPM1 cDNA
PH 775	GAAAGTGGGGAAGTATGTCCGGG	Mouse TRPM2 cDNA
PH 776	TTGAGCCACCTTGACCAAGCC	Mouse TRPM2 cDNA
PH 779	AGGTCCTCCTGGGACTGTAGAACCC	Mouse TRPM4 cDNA
PH 780	GCAACACGTGGGCAAACAGC	Mouse TRPM4 cDNA
PH 781	TCAAGGCACTTGTGAAAGCCTGC	Mouse TRPM5 cDNA
PH 782	TCACGAGGGCATCTGTCATCACC	Mouse TRPM5 cDNA
PH 783	CAGCCCTACAAATCCAAGGAGAAGC	Mouse TRPM6 cDNA
PH 784	TGCCTCTTCATGAGCACCGC	Mouse TRPM6 cDNA
PH 785	CATTCGGGATGTCAAGCAGGG	Mouse TRPM7 cDNA
PH 786	CGACCTGACCTCCGGTTATTTCC	Mouse TRPM7 cDNA
PH 787	TGCGCTGTACAAAGCCTTCAGC	Mouse TRPM8 cDNA
PH 788	TGGGTCTGTCCTTTATGAGAGCCG	Mouse TRPM8 cDNA
PH 928	TGGTGAGAAACGGTGCATGCTTA	Mouse TRPM3 cDNA
PH 930	TCTGTCCAGGACTAGGGCATCCAG	Mouse TRPM3 cDNA

3.5 Primary and secondary antibodies

Antibodies used for immunostaining and western blots are listed in the following tables.

Table 3-4: Antibodies used for immunostaining

Antibody	Host and concentrations	Dilution used	Origin
Anti-LH	Rabbit polyclonal, 0.1 mg/ml	1:5000	NHPP*
Anti-FSH	Rabbit polyclonal, 0.1 mg/ml	1:20000	NHPP*
Anti-ACTH	Rabbit polyclonal, 0.1 mg/ml	1:20000	NHPP*
Anti-TSH	Rabbit polyclonal, 0.1 mg/ml	1:5000	NHPP*

Anti-GH	Rabbit polyclonal, 1.5 mg/ml	1:20000	NHPP*
Anti-PRL	Rabbit polyclonal, 1 mg/ml	1:20000	NHPP*
Anti-LH	Guinea pig	1:5000	NIDDK**
Anti-PRL	Guinea pig	1:12000	NIDDK**
Anti-α MSH	Rabbit polyclonal, 0.1 mg/ml	1:2000	abcam
Anti-GFP	Rabbit polyclonal, 2 mg/ml	1:5000	Invitrogen
Anti-GFP	Goat monoclonal, 1 mg/ml	1:1000	Rockland
Anti-GLAST (PE)	Mouse monoclonal,100 µg/ml	1:20	Miltenyi Biotec MACS
Anti-GFAP	Rabbit polyclonal, 2.9 mg/ml	1:500	Dako
Anti-GFAP Alexa Fluor 488	Mouse monoclonal,100 µg/ml	1:50	Cell Signaling
Anti-Neurophysin I	Goat polyclonal, 200 µg/ml	1:1500	Santa Cruz
Anti-Neurophysin II	Goat polyclonal, 200 µg/ml	1:1500	Santa Cruz
Anti-Synapsin I	Goat polyclonal, 200 µg/ml	1:1500	Santa Cruz
Anti-S100B	Rabbit polyclonal, 2 mg/ml	1:500	Abcam
Anti TRPM3 (AK695)	Rabbit polyclonal, 1 mg/ml	1:1000	Lab-made
Anti TRPM3 (9F6)	Rat monoclonal, 1 mg/ml	1:200	Lab-made
Anti-rabbit Alexa Fluor 488	Donkey, 2 mg/ml	1:1000	Invitrogen
Anti-goat Alexa Fluor 488	Donkey, 2 mg/ml	1:1000	Invitrogen
Anti- guinea pig Cy 3	Donkey, 2 mg/ml	1:1000	Jackson Labs
Anti-rabbit Alexa Fluor 488	Goat, 2 mg/ml	1:1000	Invitrogen
Anti-rabbit Alexa Fluor 594	Goat, 2 mg/ml	1:1000	Invitrogen
Anti-rabbit Alexa Fluor 594	Donkey, 2 mg/ml	1:1000	Invitrogen
Anti-goat Alexa Fluor 546	Donkey, 2 mg/ml	1:1000	Invitrogen
Anti-goat Alexa Fluor 594	Donkey, 2 mg/ml	1:1000	Invitrogen
Anti-rat Alexa Fluor 594	Goat, 2 mg/ml	1:1000	Invitrogen
Anti-rat Alexa Fluor 488	Goat, 2 mg/ml	1:1000	Invitrogen

* NHPP = National Hormone & Peptide Program, Harbor-UCLA Medical Center, 1000 W. Carson St., Torrance, California 90509, U.S.A, Dr. A. F. Parlow, Scientific Director.

** NIDDK = National Institute of Diabetes and Digestive and Kidney Diseases; Maryland, USA.

Table 3-5: Antibodies used for Western blots

Antibody	Antigen	Host	Dilution used	Origin
AK695	mTRPM3-peptidsequence QEKEPEEPEKPTKEK	Rabbit polyclonal	1:200	Lab-made; 1 mg/ml
9F6	mTRPM3α, epitope ERAESNKIRSRTS	Rat monoclonal	1:200	Lab-made; 1 mg/ml
Anti-GFP	GFP	Mouse monoclonal	1:500	Roche; 0,4 mg/ml
Anti-Na$^+$/K$^+$ ATPase	Na$^+$/K$^+$ ATPase			
Anti-rabbit Horseradish peroxidase (HRP)-linked	rabbit IgG	Donkey polyclonal	1:50000	GE Healthcare
Anti-Mouse HRP -linked	mouse IgG	Goat	1:50000	Dianova; 0,8 mg/ml
Anti-Rat HRP -linked	rat IgG	Rabbit polyclonal	1:40000	Sigma; 8,3 mg/ml

3.6 Bacterial strains

In this work the *E. coli* strain XL1-Blue was used for the cloning of plasmid DNA [171]. This strain is derived from *E. coli* K12 and has the following genotype: supE44, hsdR17, recA1, endA1, gyrA46thi, relA1, lac$^-$, F'[proAB$^+$lac^{q}ZΔM15 Tn10 (tet^r)].

3.7 Mice

All animal experiments mentioned in this work were approved in accordance with the Saarland University Ethic Regulations and the animal welfare committees of Saarland's State. In this work, a mouse line lacking part of the *Trpm3* gene (TRPM3-knockout, KO) was used. Additionally, a mouse line carrying the GFP-cDNA in the *Trpm3* locus (TRPM3-GFP-knock in, short GFP-Ki) was used as reporter strain of TRPM3 expression [108]. The strategy used to generate these mouse lines is explained in Figure 3-2. For the all experiments, both male and female mice were used at an age of 2-6 months. TRPM3-GFP-Ki mice (short GFP-Ki) had a mixed 129SvJ/C57Bl6/N genetic background. For this line, mice of the F1 generation from 129SvJ and C57Bl6/N intercrosses were used as wild type controls. TRPM3-deficient mice were back-crossed for at least 10 generations to the C57Bl6/N mouse line which also served as wild type controls. All mice were bred and kept in a specific pathogen free facility (SPF). They were maintained in a 12 hour light-dark cycle, and water and standard food was available *ad libitum*. At the end of each experiment, a biopsy from the tip of the tail was taken to confirm the genotype of each mouse.
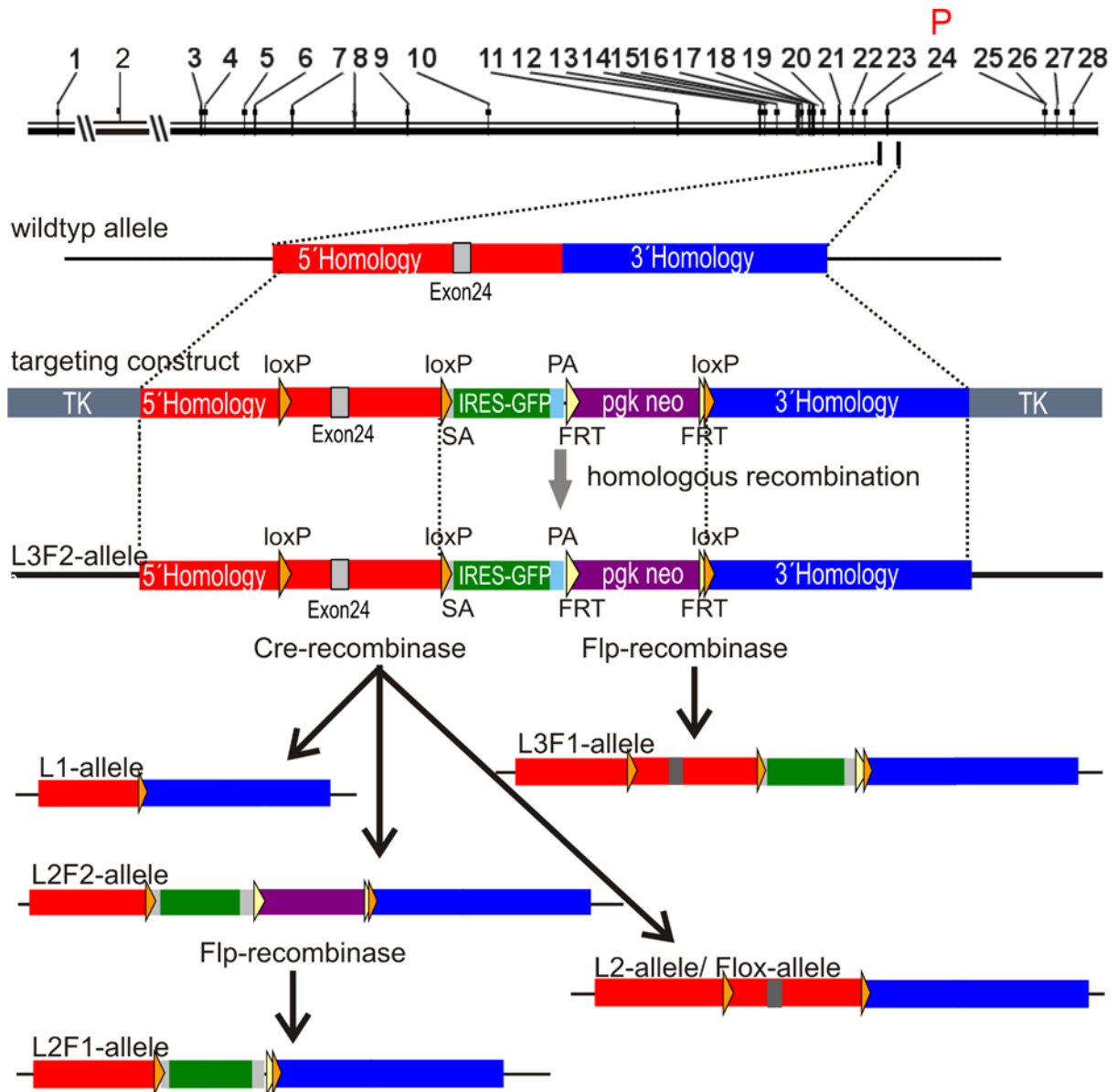
Figure 3-2: TRPM3 targeting strategy [108].

The genomic structure of the TRPM3 gene including the pore coding exon 24 (P) is shown and a higher magnification of this region is indicated below. The targeting construct included two flanking thymidine kinase cassette (TK), the 5`-homology with the floxed exon 24, the 3`-homology, the splice acceptor (SA), the IRES-GFP cassette and the polyadenylation site (PA). The location of the loxP (orange triangles) and FRT (yellow triangles) sequences is also indicated. A L3F2 allele (carrying three loxP and two FRT) was generated by the homologous recombination of the targeting construct with the wild-type allele. L1 allele (KO), L2F2 allele (conditional KO) and L2 allele (WT) were generated by the activity of Cre-recombinase. The L3F1 allele (GFP-Ki) and the L2F1 allele were generated by the activity of Flp-recombinase.

4 Methods

4.1 Molecular biological methods

4.1.1 Cultivation and transformation of eukaryotic cells

4.1.1.1 Cultivation of HEK 293 cells

Human Embryonic Kidney (HEK) 293 cells were cultured at 37°C in a humidified atmosphere containing 5 % CO_2 either in 75 cm² culture flasks with 10 - 15 ml of medium or cultured in culture dishes (∅ 3 cm) with 2 ml of medium, to passage into an appropriate culture vessel, the cells were washed once with PBS, trypsinized with 30 – 40 µl trypsin-EDTA/cm² surface area, diluted 1:2 up to 1:10 with fresh medium and transferred.

Culture medium
Minimum essential medium   (# 31095-029, Invitrogen)
10% Fetal calf serum   (# 104370-028, Invitrogen)

4.1.1.2 Preparation and cultivation of primary pituitary cells

A mouse was killed by cervical dislocation and the head was decapitated. The cover of the skull was cut using a small bone scissor and the brain was removed using spatula. The pituitary gland was directly isolated and placed in cold dispersion medium I and cut into 8-10 pieces. In some cases the posterior/intermediate lobe were dissected from the anterior lobe. The pieces were digested for 30 min at 37°C in sterile filtered, freshly prepared 3 mg collagenase (CLS type II, Biochrom)/ ml dispersion medium I. During the incubation time, the pieces were triturated several times by pipetting through 1000 and 200 µl pipette tips. Thereafter, the cells were collected by centrifugation at 800 rpm (Hettich, Rotana) for 5 min and resuspended in 125 µl dispersion medium II. 25 µl of the cell suspension were plated onto poly-L-lysine covered coverslips and incubated at 37°C, 5 % CO_2 for 1 h before 1.5 ml of the culture medium were added.

Dispersion medium I

1x   HBSS (Invitrogen, 14025)
5 mg/ml   BSA
10 mM   HEPES
10 mM   glucose
pH was adjusted to 7.3 - 7.4 with 2 mM NaOH

Dispersion medium II

1x   DMEM (Invitrogen, 41966 with Nateruimpyruvate)
5 mg/ml   BSA

<u>Culture medium</u>

1x	DMEM (Invitrogen, 41966 with Nateruimpyruvate)
10000 u/ml	Penicillin
10 mg/ml	Streptomycin
10 %	FCS

Primary "explant" cultures were prepared as described [172]. In brief, a piece of the posterior lobe (separated from the intermediate lobe) was placed onto collagen-covered coverslips, covered with culture medium and incubated at 37°C, 5 % CO_2. The medium was exchanged every two days.

4.1.1.3 Transformation of eukaryotic cells

Cells were plated one day prior to transfection at a cell density of 60 – 70 % in culture dishes (∅ 3 cm). HEK293 cells were transfected with FuGene6 reagent according to the instructions of the manufacturer (Roche, Mannheim). Highest transfection rates were achieved with 6 µl transfection reagent and 2 µg DNA or with 3 µl transfection reagent and 1 µg DNA. Transfected cells were used for experiment after 24 - 48 h.

4.1.2 Cultivation and transformation of *Escherichia coli*

4.1.2.1 Cultivation of *Escherichia coli*

The bacteria were grown in liquid LB medium or on LB Agar plates under aerobic conditions at 37°C. For the preparation of LB Agar plates LB medium was supplemented with 15 g/l of agar autoclaved and cooled to 50°C and poured into sterile petri dishes (∅ 10 cm). Selective medium was prepared by adding 50 g/ml ampicillin at 50°C.

<u>LB medium (pH 7.5)</u>

1 %	(w/v)	Tryptone / Peptone
0.5 %	(w/v)	Yeast extract
1 %	(w/v)	NaCl

4.1.2.2 Preparation of electrocompetent *E. coli* cells

To prepare electrocompetent *E. coli* cells, 2 x 500 ml LB medium in 2 l/ Erlenmeyer flasks were inoculated with 5 ml of an overnight culture of the *E. coli* strain XL-1 blue. The cells were incubated at 37°C and were shaked at 225 rpm until the optical density of the culture reached 0.6 at a wavelength of λ = 578 nm. The cell suspension was transferred into four sterile JA-10 centrifuge beakers (Beckman) and incubated on ice for 30 min. The cells were harvested by centrifugation at 4420 g at 4°C for 15 min. To remove the rest of the medium and salts, the cells were washed two times with ice-cold sterile water and one time with sterile and ice-cold 10 % (v/v) glycerol. Finally, the cells were resuspended in a total volume

of 1.5 ml 10 % glycerol. Aliquots of 60 µl were frozen immediately in dry ice/ EtOH and stored at -80°C. The competence of the cells was tested by transformation of 10 ng of the plasmid pUC 18.

4.1.2.3 Transformation of plasmid DNA into electrocompetent bacterial cells

An aliquot of electrocompetent cells (4.1.2.2) was thawed on ice and 40 µl of cells were mixed with the 2 µl of DNA. To remove salts prior to transformation, ligation reactions were precipitated with ammonium acetate / ethanol and precipitated the DNA was dissolved in 2 µl H_2O. The DNA / cells mixture was transferred into a pre-cooled electroporation cuvette with 1 mm electrode gap (peqlab). The electrical pulse was performed using a Gene-Pulser (Bio-Rad) at a capacitance of 25 µF, a voltage of 2.5 KV and a resistance of 100 Ω. The time constant of the electrical pulse was always close to 2.5. 1 ml of LB medium supplied with 50 mM magnesium sulfate, 50 mM magnesium chloride and 2 % glucose was added immediately after performing the pulse. The cell suspension was shaked at 37°C and 200 rpm for 1 h, plated onto solid LB medium supplied with ampicillin and incubated overnight at 37°C. Cells of the *E. coli* strain XL1-Blue carry the ΔM15 deletion of the lacZ gene and are therefore not capable to form a functional β-galactosidase [171]. The α-peptide of the β-galactosidase, encoded by plasmids like pUC18 and pUC19 can complement this deficiency after transformation (α-complementation). A functional ß-galactosidase can be detected by the formation of a blue indole dye after cleavage of 5-bromo-4-Chloro-3-indolyl-13ß-galactopyranoside (X-gal). The cells were therefore mixed with 200 µl X-Gal (40 mg/ml dissolved in dimethylformamide) and 50 µl of 0.1 M isopropyl-ß-thiogalactosylpyranosid (IPTG). IPTG was added to induce the gene expression of the α-peptide. The insertion of a DNA fragment into the multiple cloning site of the pUC18 or pUC19 vector led to an interruption of the reading frame of the lacZ gene. Therefore, cells carrying recombinant plasmids appeared as white colonies whereas those that were blue had been transformed with non-recombinant plasmids (blue-white screen).

4.1.3 Isolation and purification of nucleic acids

4.1.3.1 Isolation of total RNA

To inactivate RNases, amine-free solutions were treated for 12 h with 0.01 % (v/v) diethyl pyrocarbonate (DEPC) and autoclaved twice. Total RNA was extracted using peqGOLD RNAPure ^{TM} kit following the manufacturer's protocol (Peqlab Bio technology, Erlangen). Briefly, 10^7 cells or 100 mg tissue were homogenized by pipetting in 1 ml peqGOLD RNAPure ^{TM} reagent. The sample was incubated at RT for 5 min followed by the addition of

0.2 ml chloroform and vigorous mixing for 15 sec and incubation for 5 min at RT. After centrifugation at 12000 g for 15 min at 4°C, the upper aqueous phase was removed carefully. An equal volume of isopropanol was added and the sample was incubated for 5 min at 4°C followed by centrifugation at 12000 g for 15 min. The supernatant was completely removed and the RNA pellet was washed four times with 80 % ethanol. The pellet was air dried and dissolved in 500 µl of RNase-free water. To obtain highly pure RNA, an additional ethanol precipitation step was performed using potassium acetate (4.1.3.4).

4.1.3.2 Analytical quick preparation of plasmid DNA for sequencing

For isolation of recombinant DNA from *E.coli* cells, a GeneEluteTM HP Plasmid Miniprep Kit (Sigma-Aldrich) was used. Cells were collected by centrifugation of 1.5 ml overnight culture for 5 min at 3000 rpm (Biofuge pico, Heraeus) and resuspended in 200 µl resuspension buffer containing 0.1 mg/ml RNaseA. 200 µl of alkaline lysis buffer was used to lyse the cells for 5 min before 350 µl neutralization buffer was added. Samples were centrifuged at 13000 rpm for 10 min to sediment cell debris. A vacuum suction device was used for the subsequent steps of binding and washing of plasmid DNA to silica columns. The silica columns were attached to the device and equilibrated with 500 µl of preparation solution. The clear supernatant was applied to the column and fluid was sucked by vacuum whereas plasmid DNA was bound to the column. Then DNA was washed by the addition of 500 µl of wash solution 1 followed by 750 µl of wash solution 2. The column was transferred to a 2 ml micro-centrifugation tube and centrifuged for 1 min at 13000 rpm, before it was transferred into a fresh tube and plasmid DNA was eluted with 100 µl 10 mM Tris-HCl, pH 8.8 by centrifugation for 1 min at 13000 rpm. The yield and purity of the eluted DNA was analyzed spectrophotometrically (4.1.4.1) and by agarose gel electrophoresis (4.1.4.2).

4.1.3.3 Electroelution of DNA fragments from agarose gels

DNA fragments separated by gel electrophoresis (4.1.4.2) were cut from the gel and placed in sterile semipermeable dialysis tube (pore size 12 kDa; Sigma) and filled with 300 µl H_2O. The tubes were tightly closed with clamps and transferred to a chamber filled with 1x TBE buffer. 135 mA current was applied for 45 min until the DNA was totally eluted into the buffer. DNA solution was then carefully collected and the tube was washed with 100 µl H_2O to gain the remaining DNA solution.

4.1.3.4 Ethanol precipitation of nucleic acids

Ethanol precipitation [173] was used to concentrate and clean nucleic acid solutions. DNA was precipitated from the aqueous solution by addition of 250 mM NaCl and two volumes of

ethanol (-20°C) followed by centrifugation at 13000 rpm (Biofuge pico, Heraeus) for 20 min. The pellet was washed with 70 % ethanol (-20°C), dried in a vacuum evaporation centrifuge and finally dissolved in sterile water. To precipitate RNA, 0.3 M potassium acetate and 2.5 volumes of ethanol was used and the RNA sediment was washed with 80 % ethanol diluted in RNase-free water. The isolated RNA was stored at -80°C and the DNA at -20°C.

4.1.4 Analysis of nucleic acids

4.1.4.1 Photometry

A spectrogram of 1 µl nucleic acid solution was determined at a wave length of 200 to 300 nm using Nanodrop1000 spectrophotometer (peqlab biotechnology, Germany). According to Lambert–Beer's law, the concentration was calculated assuming that at an absorbance of 1, the concentration of RNA is 40 µg/ml and of DNA 50 µg/ml. The ratio of the absorbance of 260 nm and 280 nm was taken as a measure of the purity and should be between 1.7 and 2.0.

4.1.4.2 Gel electrophoresis of DNA

Negatively charged DNA molecules migrate in an electrical field towards the positive pole and can be separated in an agarose matrix according to their size. DNA molecules were visualized by Ethidium bromide (EtBr) which intercalates into the DNA double helix and fluoresces after excitation with UV light of 354 nm [174]. DNA samples and a DNA size standard, used to determine the molecular mass of the DNA samples, were both mixed with loading buffer. Agarose gels were used in different concentration according to the size of the fragment. 0.8 % (w/v) gels were used to analyze DNA fragments ranging in size from 0.5 to 8 kb, whereas 2 % (w/v) gels were used to analyze small fragments between 0.1 to 1 kb. Standard agarose (Roth) were used to prepare analytical gels whereas GTQ-agarose (Roth) was used for preparative gels. The gels were prepared by mixing the desired amount of agarose with 1x TBE buffer. The mixture was heated in a microwave oven to melt the agarose and then cooled down to 50°C by stirring. EtBr was added of a final concentration of 0.1 µg/ml before pouring the gel in a horizontal gel tray. The gel solidified at room temperature and was immersed in 1x TBE buffer in the electrophoresis chamber before use.

<u>10x TBE buffer (pH= 8.0)</u>
108	g/l	Tris-HCL
55	g/l	Boric acid
9.3	g/l	EDTA

<u>6x loading buffer</u>
15 %   (w/v)   Glycerol or ficoll
0.25 % (w/v)   Bromophenol blue
0.25 % (w/v)   Xylene cyanol

4.1.4.3 Gel electrophoretic analysis of RNA

To assess the integrity and the quantity of RNA solutions, an Agilent 2100 bioanalyzer, the Agilent RNA 6000 Nano Kit® and a RNA 6000 Nanochip were used (Agilent technologies). The chip accommodates sample wells and a well for an external standard (ladder). On the chip, micro-channels are fabricated from glass that creates an interconnected network among the wells. When filled with a sieving polymer and fluorescence dye, the channels built an integrated electrical circuit that allows the separation of RNA as well as DNA and proteins. The RNA 6000 Nano gel matrix was centrifuged through a spin filter at 1500 g for 10 min at RT and could be stored at -80°C. Before starting a single assay, 1 µl of the RNA 6000 dye concentrate was added to 65 µl of the Nano gel matrix and the mixture was vortexed and centrifuged at 13000 g for 10 min at RT. The gel-dye mixture, the marker, the ladder and RNA samples (25-500 ng/µl) were loaded into the chip according to the manufacturer's protocol. RNA samples were separated by their electrophoretic mobility and subsequently detected via laser induced fluorescence. From the electropherogram, the RNA integrity could be estimated and was indicated by the RNA integrity number (RIN, [175]).

4.1.4.4   DNA sequencing

Sequencing of plasmid DNA was performed by the StarSEQ® Sequencing Service (Mainz). 400-700 ng of plasmid DNA was mixed with 1 µl sequence specific oligonucleotide primer (10 pmol/µl) in a total volume of 7 µl per sequencing reaction. Sequence informations were analyzed using the Accelrys Gene software.

4.1.5   Amplification of nucleic acids using polymerase chain reaction (PCR)

4.1.5.1 Reverse transcription of the total RNA

Synthesis of cDNA was carried out using the SuperScript ^{TM} First-Strand Synthesis System (Invitrogen) following the manufacturer's instructions. Briefly, in a total volume of 10 µl, 5 µg of total RNA, 1 µl oligo dT$_{12-18}$ or 1 µl gene specific primer (10 µM each) and 1 mM dNTP mix were added, heated at 65°C for 5 min and then cooled on ice for 1 min. Thereafter, 2x reaction mix containing 2 µl of 10x reverse transcriptase buffer (200 mM Tris-HCl, 500 mM KCl, pH 8.4), 4 µl of 25 mM MgCl$_2$, 1 µl of RNAse inhibitor (RNAse Out, 40 units / µl) and 2 µl 0.1 M DTT was added to the mixture and incubated for 2 min at 42°C before 1 µl of

Superscript II reverse transcriptase (50 U/µl) was added and the reaction was incubated at 42°C for 50 min. The reaction was stopped by incubation at 70°C for 15 min. In order to obtain RNA-free cDNA templates, the remaining RNA was digested by addition of 1 µl RNase H (2 U/µl) and incubated at 37°C for 20 min. cDNA samples were stored at -20°C.

4.1.5.2 PCR for subcloning of DNA fragments

DNA fragment were amplified *in vitro* by the activity of a thermostable DNA polymerase directed by a pair of sequence-specific oligonucleotide primers in the presence of dNTPs. The polymerase chain reaction (PCR) was initiated by a denaturation step in which the double-stranded DNA was denatured into two single DNA strands followed by annealing of the primers to their specific recognition sequence and their elongation by the polymerase corresponding to the template sequence. This cycle of denaturation, annealing and elongation was repeated up to 45 times leading to an exponential amplification of the template DNA. For amplification of fragments that were subcloned into plasmid DNA, Phusion polymerase (NEB) was used. Oligonucleotides primers used for PCR were designed to have an average melting temperature (Tm) of 64°C to 68°C.

The following reaction was prepared:

2 µl   Template cDNA
10 µl   5x Phusion High Fidelity Buffer
1 µl   dNTPs (10 mM of dATP, dCTP, dGTP, dTTP)
2.5 µl   Oligonucleotide primer 1 (10 pmol/µl)
2.5 µl   Oligonucleotide primer 2 (10 pmol/µl)
31.5 µl DEPC-treated H_2O
0.5 µl   Phusion DNA Polymerase (2 U/µl)

The following reaction cycle was performed:

98°C   1min
98°C   5 sec ⎤
64°C   10 sec ⎬   45 cycles
72°C   3min   ⎦
72°C   5 min
4°C   ∞

4.1.5.3 One-step RT-PCR

The amplification of TRPM transcripts expressed in mouse intermediate and posterior pituitary cells was performed using the One-Step reverse transcription-PCR system (Invitrogen, Karlsruhe, Germany). It allows the reverse transcription of RNA into cDNA and followed by its amplification in one single reaction tube (one-step). Therefore, RT/ Platinum® *Taq* Mix contains a mixture of two different enzymes: the SuperScript® II Reverse

Transcriptase (RT) which exhibits reduced RNase H activity and increased thermal stability compared to Moloney Murine Leukemia Virus reverse transcriptase RT (M-MLV RT) and Platinum® Taq DNA polymerase which is inhibited at ambient temperatures by the binding of a specific antibody. As soon as the denaturation step at 94°C begins, the polymerase activity is restored by the denaturation of the antibody.

By adding the specific compounds (prepared as a supermix) directly to the tube containing the frozen sorted cells, the following reaction mixture was prepared:

50	sorted pituitary cells (4.4)
12.5 µl	2x reaction mix
0.5 µl	RT/ Platinum® Taq Mix
0.75 µl	Oligonucleotide primer 1 (10 pmol/µl)
0.75 µl	Oligonucleotide primer 2 (10 pmol/µl)
10 µl	autoclaved H_2O

The following reaction cycle was performed:

Reverse transcription:	50°C	30 min	
PCR:	94°C	2 min	
	94°C	15 sec	
	62°C	40 sec	15 cycles
	70°C	30 sec	
	94°C	15 sec	
	62°C	30 sec	30 cycles
	70°C	40 sec + 2 sec/cycle	
	72°C	5 min	
	4°C	∞	

Amplification products were analyzed by agarose gel electrophoresis (4.1.4.2)

4.1.6 Enzymatic modification of nucleic acids

4.1.6.1 Restriction mapping

Restriction endonucleases and buffers from (NEB, Biolab) were used to cleave purified plasmid DNA. Plasmid DNA in a final concentration of 50-500 ng was digested using 1-10 U of restriction enzymes in the presence of the appropriate buffer provided by the manufacture (NEB) at recommended temperatures for 1-3 h followed by electrophoretic analysis of the digestion products (4.1.4.2).

4.1.6.2 DNA phosphorylation

PCR products that were amplified with oligonucleotide primers missing the 5'-phosphate-residue were phosphorylated prior to ligation. For this purpose, the T_4 polynucleotide kinase was used in the presence of ATP. 25 µl DNA solution was mixed with 3 µl 10x T4 DNA ligase

buffer containing 10 mM ATP (NEB) and 2 µl T$_4$ polynucleotide kinase (10 U/µl, NEB). The reaction mixture was incubated at 37°C for 40 min and then the enzyme was inactivated at 75°C for 10 min.

4.1.6.3 Ligation of DNA fragments

DNA fragments were inserted into linearized plasmid DNA by T4 DNA ligase. DNA fragments and plasmid vector were mixed in a molar ratio of 3:1 in a total volume of 15 µl containing 1.5 µl 10x ligase buffer (NEB) and 1 µl T4 DNA ligase (NEB). The reaction was incubated overnight at 16°C or alternatively 3-4 h at room temperature.

4.2 Protein biochemical technologies

4.2.1 Protein extraction from mice organs

Proteins from mouse tissues like pituitary gland and choroid plexus of the brain or cultured cells were extracted in RIPA buffer containing freshly added protease inhibitors. Tissues/cells were homogenized by pipetting under permanent cooling (4°C) and then sheared through 0.9, 0.7 and 0.4 mm cannulas to solubilize the cellular proteins. Protein lysates were centrifuged at 12000 g at 4°C for 30 min and the supernatant was saved. Protein concentrations were estimated using the BCA protein assay kit (Pierce, 4.2.2). Afterwards, proteins lysates were mixed with the same volume of 2x Laemmli buffer and denatured for 5 min at 95°C or 30 min at 37°C.

RIPA-buffer (pH= 8.0)
150	mM	CaCl$_2$
50	mM	Tris-HCl
1 %	(v/v)	Nonidet P40
0.5 %		Sodium deoxycholate
0.1 %	(w/v)	SDS

Protease inhibitors
1	µg/ml	Leupeptin
1	µg/ml	Antipain
0.1	mM	PMSF
1	µM	Benzamidin
1	µM	Pepstatin A
0.3	mM	Jodoacetamid
0.3	µM	Aprotinin
1	mM	Phenanthrolin C

2 x Laemmli buffer
120   mM   Tris-HCl, pH 6.8
8 %   (w/v)   SDS
20 %   (v/v)   Glycerin
0.01 %   (w/v)   Bromphenol blue
10 %   (v/v)   ß-mercaptoethanol (14.3 M freshly added before use)

4.2.2 Determination of protein concentration

Protein concentrations were determined using the BCA method [176] and the BCA protein assay kit from Pierce® (Rockford, USA). The method is based on the fact that Cu^{2+} is reduced to Cu^+ in an alkaline solution by the oxidation of peptide groups. The resulting Cu^+ ions chelate with BCA forming purple-colored products which absorb light at 562 nm. The amount of this product is proportional to the amount of the proteins present in the solution. 1:50, 1:100 and 1:250 dilutions of the protein lysate were prepared and three times 25 µl of each were pipetted into 3 wells of a 96-well plate. In parallel, 0.02, 0.04, 0.06, 0.08, 0.1, 0.15 and 0.2 µg/µl BSA solutions were used to generate a calibration curve. 200 µl of a mixture of BCA reagent A and BCA reagent B (50:1) was added to each sample. The reaction was incubated at 37°C for 1 h and the absorbance was measured at a wave length of λ= 540 nm in a plate spectrophotometer (Tecan Sunrise, Switzerland). The concentration of the tested protein was calculated using the standard calibration curve.

4.2.3 Discontinuous sodium dodecyl sulfate-polyacrylamide gel electrophoresis (SDS-PAGE)

In an electric field, proteins were separated according to their molecular mass in the presence of sodium dodecyl sulfate (SDS) and polyacrylamide gel (PAGE, [177]). Proteins were denatured and molecules became negatively charged by their interactions with SDS. For the reduction of disulfide bonds, ß- mercaptoethanol was added to Laemmli buffer directly before use. Proteins samples, as well as a molecular mass standard (Precision Plus Protein™ Dual Color Standards, 10-250 kD; BioRad, München), were loaded into the pockets of the polyacrylamide gel. Electrophoresis was carried out in 1x SDS buffer at 75 volts until the migration front reached the resolving gel. Then 120 volts were applied. The content of polyacrylamide used to prepare the stacking and the resolving gels was adapted according to the size of proteins to be separated. To separate proteins with a molecular mass > 100 kD, 4 % and 6.5 % polyacrylamide were used in the stacking gel and the resolving gel, respectively. For the separation of proteins with a molecular mass of 20 – 100 kD, 5 % and 10 % polyacrylamide were used.

Stacking gel 4 % or 5 %

125	mM	Tris-HCl, pH 6.8
0.1 %	(w/v)	SDS
4 % or 5 %	(v/v)	Acrylamid: Bisacrylamid (29:1)
0.075 %	(w/v)	APS
0.15 %	(v/v)	TEMED

Resolving gel 6.5 % or 10 %

375	mM	Tris-HCl, pH 6.8
0.1 %	(w/v)	SDS
6.5 % or 10 %	(v/v)	Acrylamid: Bisacrylamid (29:1)
0.075 %	(w/v)	APS
0.15 %	(v/v)	TEMED

10x SDS electrophoresis buffer

250	mM	Tris-HCl, pH 8.3
1.92	M	Glycin
1 %	(w/v)	SDS

4.2.4 Western blot analysis

The aim of this technique is to transfer proteins separated by SDS-PAGE onto a membrane where they can be detected with antibodies. To assemble the so called blotting sandwich, a PAGE gel with separated proteins was covered with a nitrocellulose membrane (Hybond C extra; Amersham Biosciences; Piscataway/New Jersey). The gel and the membrane were placed between two pairs of Whatman 3 M filter paper and a pair of pads which were rinsed with blotting buffer. The blotting sandwich was then placed in a blotting chamber (Peqlab Biotechnologie, Erlangen) filled with blotting buffer. A current of 350 mA was applied for 90 min at 4°C to transfer the negatively charged proteins from the gel to the positively charged membrane where the proteins became tightly attached by the hydrophobic interaction with the membrane.

Blotting buffer (pH= 8.3)

20 %	Methanol
10 %	10x SDS electrophoresis buffer

To check the transfer efficiency, the membrane was transiently submersed in a solution of 2 % of the dye Ponceau-S in 3 % trichloroacetic acid. The membrane used for blotting had high affinity for proteins and therefore, the unoccupied areas were blocked by shaking the blot in 5 % non-fat dry milk dissolved in TBST for at least 1 h at RT. The membrane was submersed overnight at 4°C with gentle shaking in a solution containing primary antibodies dissolved in 1 % BSA / TBS / 0.05 % NaN3 (Table 3-5).

10x TBS

500 mM	Tris-HCl pH 7.5
1.5 M	NaCl

TBST

1x	TBS
1 %	Tween 20

4.2.5 Enhanced chemiluminescence development (ECL-Reaction)

The primary antibody (4.2.4) was discarded and the nitrocellulose membrane was washed three times for 10 min at RT with TBST and then incubated with secondary antibodies coupled to horseradish peroxidase in 5 % solution of non-fat dry milk for 1 h at RT. Next, the membrane was washed two times 10 min with TBST and finally for 10 min with TBS. The ECL reagents A and B containing the substrate of horseradish peroxidase (Perkin Elmer, Waltham/Massachusetts) were mixed in 1:1 ratio and added to the blot. The chemiluminescent reaction product was visualized and subsequently quantified for 15 sec, 1 min, 5 min and 60 min using a charge-coupled device (CCD) camera (LAS-3000; Fujifilm, Düsseldorf)

To remove antibodies bound to the blot (stripping), the membrane was washed four times for 5 min with TBST, incubated with 20 ml of stripping buffer at 55°C with shaking, washed six times for 5 min with 20-30 ml TBST and finally blocked in 20 ml 5 % non-fat dry milk in TBST before it was incubated with the another antibody.

Stripping buffer

62.5 mM	Tris-HCl pH 6.8
2%	SDS
100 mM	ß-mercaptoethanol

4.3 Immunostaining

4.3.1 Fixation of proteins by whole body perfusion of mice

The goal of the perfusion fixation of the whole body with a fixative is to preserve the tissue morphology and retain the antigenicity of the target molecules for following immunostaining experiments. The vascular system of an anesthetized mouse was used to deliver the fixative *in vivo* to the organs to fix proteins before autolysis of cells begins. The method described below is used to fix the organs which are supplied by the left ventricle. The perfusion was performed inside a fume hood. Before starting the procedure, the whole tubing of the perfusion system were filled with PBS (37°C) and all air bubbles were removed. Mice were

anesthetized with a mixture of ketamine (Serumwerk, Bernburg) and xylazine (Rompun, Bayer, Leverkusen) in concentration of 140 µg/g body weight and 10 µg/g body weight, respectively. As a measure of persisting nociception and the deepness of anesthesia, the withdrawal reflex upon strong pinching of the hind paw was tested repetitively. Thereafter, the mouse was taped on a tray with the chest upward and the abdominal site was cleaned with 70 % ethanol. A midline skin incision from the thoracic inlet to the pelvis was made with a scissor and then the abdomen was opened carefully to expose the liver and intestines. To expose the heart, the thoracic cavity was opened by an incision down the midline of the sternum, removing the diaphragm and by cutting the ribs along the lateral surface on the right and left side. Then the pulsative heart was gently grasped using a forceps and a blunt butterfly injection needle connected to a tube filled with PBS was inserted directly into the apex of the left ventricle. The right atrium was incised to allow the perfused solutions to exit the circulation. 20-40 ml PBS was perfused slowly and constantly into the heart to flush the blood from the circulatory system. Blanching of the liver and the mesenteric arteries from blood were good indicators to start the perfusion with the fixative. 60-80 ml of 4 % paraformaldehyde (PFA)/PBS was perfused for a mouse with body weight of 20-30 g. Skeletal muscle contractions indicated successful and complete perfusion of the body. Finally, the pituitary gland was dissected and post-fixed for additional 15-30 min in ice cold 4 % PFA/PBS.

Phosphate buffered saline (PBS) (pH= 7.4)

137	mM	NaCl
2.7	mM	KCl
10	mM	Na_2HPO_4
1.47	mM	KH_2PO_4

4.3.2 Preparation of pituitary microsections for immunostaining

Following the fixation process, the fixed pituitaries were washed with PBS three times for 2 min and transferred into 30 % sucrose overnight to remove PFA and to cryo-protect the tissues. Pituitaries were placed in disposable plastic molds (Peel-A-Way ®, Thermo Fisher) filled with Jung tissue freezing medium (Leica Microsystems GmbH). A snap freezing chamber was made of a coplin jar filled with isopentane up to a height of 1 cm which was placed in an ice box filled with dry ice and 100 % ethanol up to a height of 3-4 cm. The molds were placed in the isopentane until the tissue freezing medium was totally frozen. Frozen organs were wrapped with parafilm and stored at -80°C at least overnight before they were cut into micro-sections. Using a CM3050 S microtome (Leica), 14 µm-slices were placed

onto SuperFrost® plus glass slides (R. Langenbrinck) and stored in slide saver boxes at -80°C.

4.3.3 Immunohistochemistry

The immunostaining procedure was started by washing the slices (4.3.2) with PBS three times for 10 min at RT to remove Jung tissue freezing medium. Next, the slices were next permeabilized and blocked by incubation of the slides in coplin jars containing 20-50 ml of blocking solution. Depending on the amount of antibodies available, the staining procedure was performed either by incubation of the slides in coplin jars containing 20-50 ml of primary antibody solution (Table 3-4) dissolved in PBS or alternatively by the application of at least 50 µl of antibody solution on the top of each slice followed by incubation of the slides in a humidified chamber overnight at 4°C. Control slices excluding the primary antibodies were always included (only shown in Figure 5-18) and never showed signals different from the background. Excess antibody was washed three times for 20 min with PBST in a coplin jar. The secondary antibody (Table 3-4) was diluted in PBS and applied for 2 h at RT in the dark. Excess secondary antibody was washed three times for 10 min with PBST. For staining of the cell nucleus, Hoechst 33258 (Sigma) was prepared in a concentration of 5 µg/µl in PBS, applied for 10 min at RT and then washed two times for 2 min with PBST. To reduce the decrease of fluorescence, stained slices were covered with a drop of anti-fading agent Roti®-Mount FluorCare (Roth) and then with glass coverslips. Glass slides were sealed with nail polish to avoid desiccation.

<u>Blocking solutions</u>
5 % normal goat serum in 0.2 % Triton-X 100/ 0.02 % NaN3/ PBS
5 % normal donkey serum in 0.2 % Triton-X 100/ 0.02 % NaN3/ PBS

<u>PBST</u>
1x   PBS
1%   Tween 20

Stained slices were analyzed using an Observer. Z1 fluorescence microscope (Carl Zeiss AG, Göttingen) coupled to a CCD camera and photos were acquired and archived by Axiovision Rel.4.6 image processing software (Carl Zeiss AG, Göttingen). To compare fluorescence emission intensities observed in different samples, slices were illuminated with identical light intensities and for identical time intervals.

4.4 Fluorescence-activated cell sorting (FACS)

For fluorescence-activated cell sorting (FACS), pituitary cells were prepared as described under (4.1.1.2). Following centrifugation, the cells were kept on ice until being sorted. In some cases the cells were stained with anti-GLAST antibodies (1:11) in 0.5 % BSA/PBS for 10 min at 4°C and the excess antibody was washed with 0.5 % BSA/PBS. Cell sorting was performed by Dr. Stephan Philipp on a MoFlo-XDP cell sorter (Beckman Coulter, Germany) using a 488 nm laser excitation.

4.5 Fluorescence-based Ca^{2+} imaging

For Ca^{2+} imaging experiments, pituitary cells were prepared as described under (4.1.1.2). For functional analysis of TRPM3 channel, changes of the intracellular Ca^{2+} concentration [Ca^{2+}]$_i$ were recorded using Fura-2. Fura-2 is a ratiometric fluorescent dye excited by light of 340 nm and 380 nm wavelengths [178]. Upon binding of Ca^{2+}, Fura-2 changes its excitation maximum which shifts from 380 nm towards 340 nm whereas the emission maximum at 510 nm is an affected. As a consequence, the ratio of the fluorescence intensities successively measured after excitation with 340 nm and 380 nm (F$_{340}$/F$_{380}$) is a good measure of [Ca^{2+}]$_i$. This ratio is independent of dye concentration, cell thickness, excitation intensity, dye leakage, photo-bleaching as well as the camera sensitivity because these factors all affect the measurements at both excitation wavelengths to the same extent. Fura-2 is used as an acetoxymethyl ester (Fura-2 AM), a nonpolar substance which can pass the plasma membrane of the cell. Fura-2 AM is cleaved in the cytoplasm of the cell by endogenous esterases to the polar molecule Fura-2 which is no longer able to pass the cell membrane again.

Measurements were performed on an inverted microscope (Carl Zeiss AG; Göttingen) equipped with a 20x Flour objective and a polychrom II illumination system that can switch its output wavelength within 3 ms (TILLVision-Systems, TILL Photonics; Gräfelfing). 1 mM Fura-2 AM stock solution were prepared in dimethyl sulfoxide (DMSO). Primary pituitary cells plated onto poly-L-lysine covered coverslips were loaded at 37°C for 30 min in the dark with 5 µM Fura-2 AM (Biotium, Austria) in the medium. Cells were washed twice with Ringer's solution before the coverslip was inserted into a perfusion chamber. The cells were perfused with a perfusion rate of 1 ml/min. 100 µM pregnenolone sulfate (PregS) dissolved in Ringer's solution was used to activate TRPM3, whereas 10 µM Hesperetin was used to block the channel activity. Both PregS and Hesperetin were prepared as a stock solution of 100 mM in DMSO. F$_{340}$/F$_{380}$ ratios were obtained every 3 sec and the fluorescence emissions at λ > 440

nm were captured, digitized, and analyzed for individual cells after background subtraction using TILLVision software. Results were given as mean ± S.E.M.

<u>Ringer's solution</u>

135	mM	NaCl
5.4	mM	KCl
2	mM	$MgCl_2$
1	mM	$CaCl_2$
20	mM	glucose
10	mM	HEPES

pH = 7.25 adjusted with NaOH, 315 mosmol/kg

4.6 Electrophysiological recordings (Dr. Andreas Beck)

For patch-clamp experiments, cells from the posterior and intermediate lobe were prepared as described under (4.1.1.2). High resolution current recordings were performed at room temperature in the tight-seal whole-cell configuration using an EPC-9 patch-clamp amplifier (HEKA Electronics, Lambrecht, Germany). Patch pipettes were pulled from glass capillaries GB150T-8P (Science Products, Hofheim, Germany) at a vertical Puller (PC-10; Narishige, Tokyo, Japan) and had resistances between 2 and 4 MΩ. All bath and pipette solutions had an osmolarity of 285 to 305 mosM. For the recording of voltage-activated sodium current (Na_V) and TRPM3 currents, voltage ramps spanning from -100 mV to +100 mV within 50 ms from a holding potential (Vh) of -80 mV (Na_V) or within 400 ms from a Vh of 0 mV (TRPM3) were applied every 2 s using the patchMaster software (HEKA). All voltages were corrected for a 10 mV liquid junction potential. Currents were filtered at 2.9 kHz and digitized at 100 µs intervals. Capacitive currents and series resistances were determined and corrected before each voltage ramp using the automatic capacitance compensation of the EPC-9. Inward and outward currents were extracted from each individual ramp current recording by measuring the current amplitudes at -80 and +80 mV, respectively, and plotted versus time. Representative current-voltage relationships (IVs) were extracted at the indicated time points. To display the IVs of the net PregS-induced current, basic currents before application of PregS were subtracted. All currents were normalized to the cell size (picoamperes/picofarads).

<u>Bath solution</u>

140	mM	NaCl
2.8	mM	KCl
2	mM	$MgCl_2$
1	mM	$CaCl_2$
10	mM	HEPES

10   mM   glucose

<u>Pipette solution 1</u>

140   mM   Cs- Glutamate
8   mM   NaCl
1   mM $MgCl_2$
10   mM   HEPES
10   mM   Cs-BAPTA + 3.1 mM $CaCl_2$ => 100 nM free Ca^{2+} (calculated with webMaxC, http://web.stanford.edu/~cpatton/webmaxcS.htm)
This solution was used for (Figure 5-40, Figure 5-42).

<u>Pipette solution 2</u>

140   mM   Cs- Methanosulfonate
8   mM   NaCl
1   mM $MgCl_2$
10   mM   HEPES
10   mM   Cs-BAPTA + 3.1 mM $CaCl_2$ => 100 nM free Ca^{2+} (calculated with webMaxC, see above)
This solution was used for all other electrophysiological experiments.

<u>Application solution</u>

100 µM PregS in bath solution
10 µM Hesperetin in bath solution

<u>Monovalent-free (MVF) solution</u>

140   mM   NMDG-Cl
2   mM $MgCl_2$
1   mM $CaCl_2$
10   mM   HEPES
10   mM   glucose

5   Results

5.1   Identification of TRPM3 transcripts in mouse pituitary gland

5.1.1   Detection of TRPM3 transcripts in whole pituitary

Northern blot analysis revealed TRPM3 expression in the pituitary gland and other tissues of the mouse with transcripts of different sizes [108]. The *Trpm3* gene encodes a large number of variants due to alternative splicing of their primary transcript (Figure 2-7). Furthermore, the variability of TRPM3 transcripts is increased by the presence of at least three promoters that give rise to three alternative transcription start sites and lead to alternative amino-termini of the encoded proteins.TRPM3α variants start with exon 1 and lack exon 2 but TRPM3β variants start with exon 2. Thus, the presence of exon1 and exon2 in the transcripts is mutually exclusive. Furthermore, isoforms have been described starting with an ATG-codon located at the very end of exon 4, which is the start codon for transcripts lacking both exon 1 and 2 ([106], Figure 2-7).

To analyze the identity of TRPM3 transcripts present in the mouse pituitary, I isolated total RNA which was reversed transcribed using oligo (dT) primers and amplified by PCR. Using forward primers PH383 located in exon1 in combination with different reverse primers PH385, PH386, PH561 and PH562 located in exon 28 (Figure 5-1), I found PCR products matching in size to a complete reading frame of TRPM3 α-variants. No amplification products of corresponding size were obtained using forward primer PH429 in combination with the same set of reverse primers indicating no or low expression of TRPM3 β-variants. Strong bands were obtained using primer PH384 which hybridize to the common exon 3 indicating prominent expression of TRPM3 proteins whose translation start codon is located at the very end of exon 4. Such TRPM3 proteins have already been described in human [102] and the result is in good agreement with recent findings of Alexander Becker who demonstrated that nearly 70 % of the TRPM3 transcripts present in the pituitary encode proteins with truncated amino termini [179].
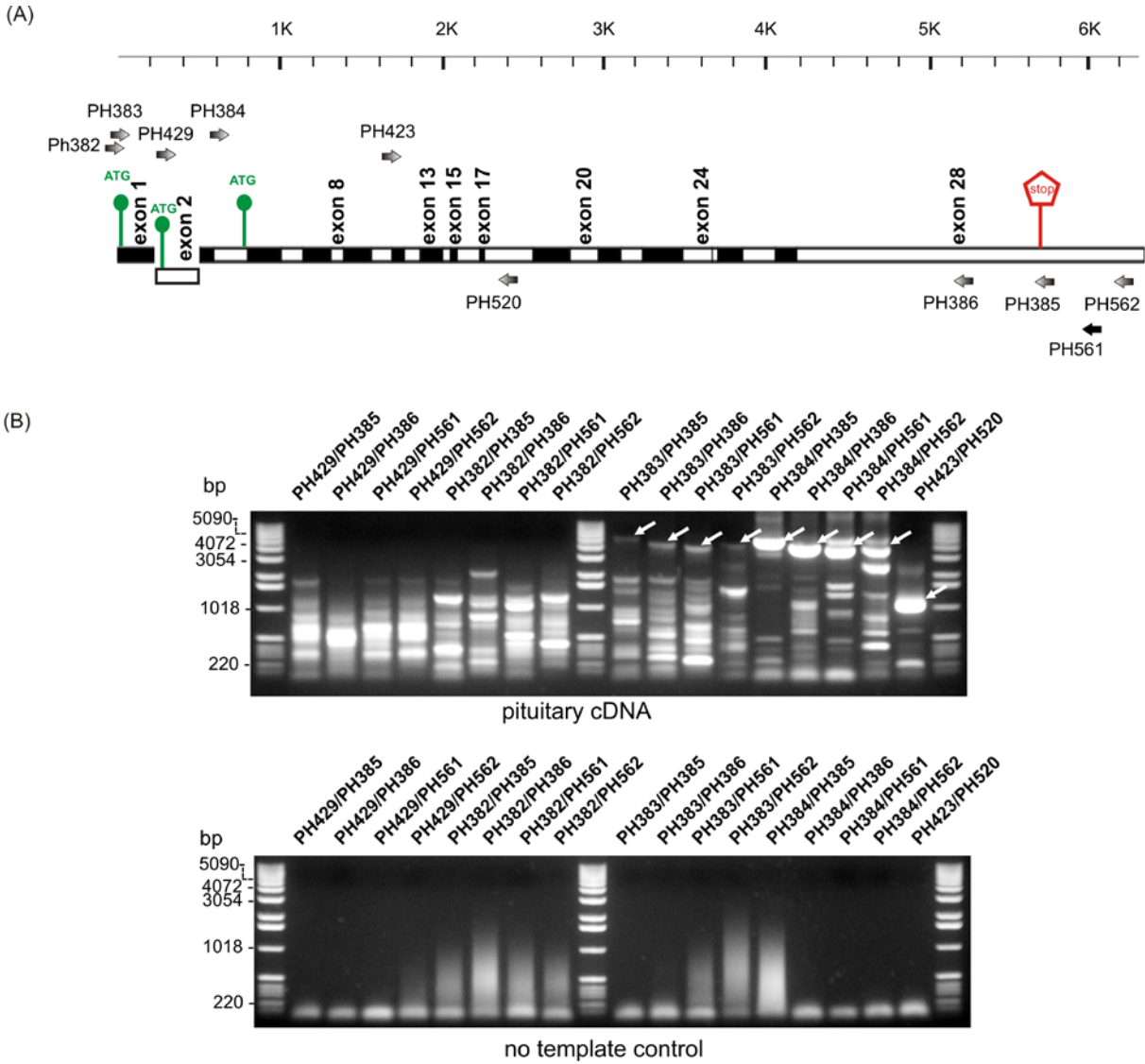
Figure 5-1: Amplification of TRPM3 cDNA from mouse pituitary gland.
(A) Schematic representation of the coding exons of TRPM3. Start codons (ATG) present in exon 1, 2 and 4 and a stop codon (stop) in exon 28 are indicated in green and red, respectively. Forward and reverse primers used to amplify TRPM3 cDNA are presented by arrows. (B) Gel electrophoretic separation of RT-PCR products obtained from mouse pituitary gland or a no template control using different primer combinations as indicated. Products matching to the appropriate size of the expected products are labeled with arrows. Additional bands of low size might be related to mispriming during PCR.

5.1.2 Analysis of splice events in TRPM3 transcripts of the pituitary

RT-PCR experiments using primers located upstream of the translations start codons in exon 1, 2 or 3 combined with a downstream primer PH385 located downstream of the stop codon confirmed my previous findings (Figure 5-1): primers PH429 and PH385 again failed to

amplify TRPM3 transcripts, indicating the absence of ß-variants in the mouse pituitary which is in contrast to what has been described for the mouse choroid plexus [111]. However, when I combined the downstream primers PH385 with primers PH383 located upstream of a start codon in the predicted exon 1, I obtained amplification products of ~ 5.2 kb similar to what I found before (compare to Figure 5-1).
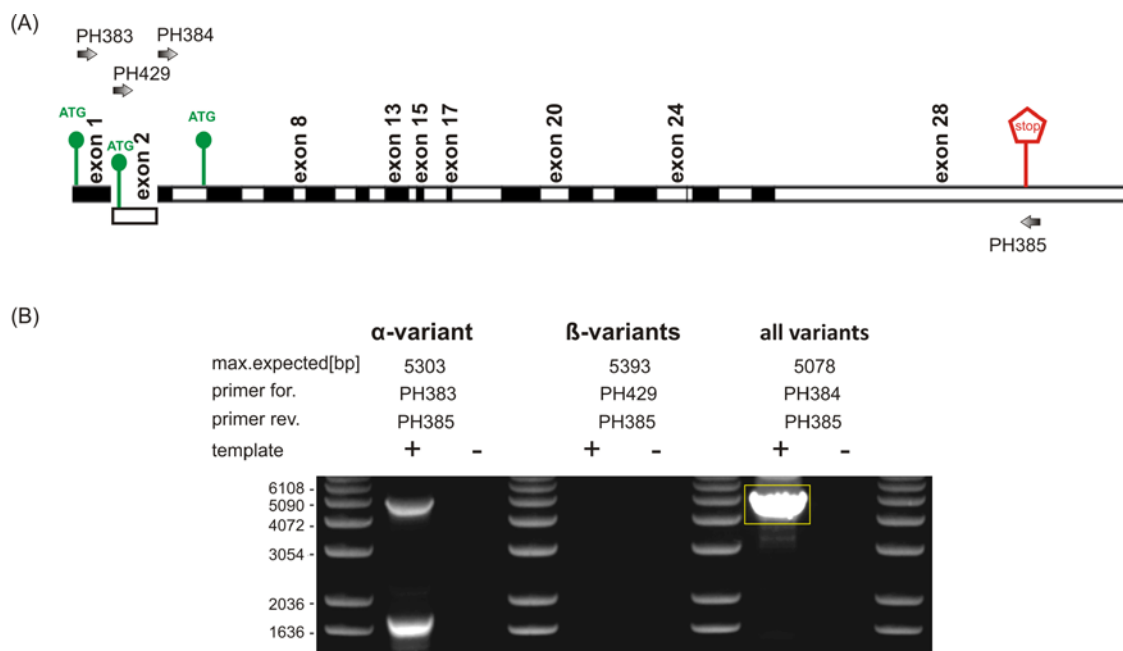
Figure 5-2: Amplification of TRPM3 cDNA from mouse pituitary gland.
(A) Strategy for the amplification of TRPM3 cDNA from mouse pituitary gland. Arrows indicate the position of the primers. (B) PCR products obtained after separation by gel electrophoresis. Fragments used to analyze the TRPM3 transcriptome of the pituitary are highlighted which were common to all TRPM3 isoforms.

I analyzed the splicing frequency between exon 3 and exon 28. For that purpose, I subcloned the amplification products obtained with primers PH384 and PH385. Sequencing of 98 independent clones identified 12 different combinations of alternative splice events that happened in five different exons 8, 13, 15, 17 and 20 (Figure 5-3). Four of them displayed splicing within the reading frame, whereas splicing in exon 20 led to a truncation of the protein upstream of the transmembrane region due to splicing outside of the reading frame. Exons 8, 15 and 17 were removed by exon skipping whereas in exons 13 and 20, a part of the exons were removed using an alternative 5´splice site.

Confirming the results obtained by one-step RT-PCR (Figure 5-4), I did not find any clone containing the long pore encoding sequence of exon 24 (Table 5-1). Thus, all TRPM3 channels expressed in the pituitary are expected to be permeable for Ca^{2+}. The second most

frequent splice event happened in exon 8 (76.5 %, Table 5-1) and correspondingly, variant 1 was most abundant with a rate of close to 40 % of all variants found. Splicing within exon 13 was rare. Only ~ 3 % of the clones lacked the ICF-encoding region. Thus, most of the TRPM3 proteins may encode functionally active subunits of TRPM3 cation channels.

Table 5-1: Frequency of splice events in TRPM3 mRNA of the pituitary gland.

Spliced exon No.	8	13	15	17	20	24
[%]	76.5	3.06	42.8	8.16	3.06	100
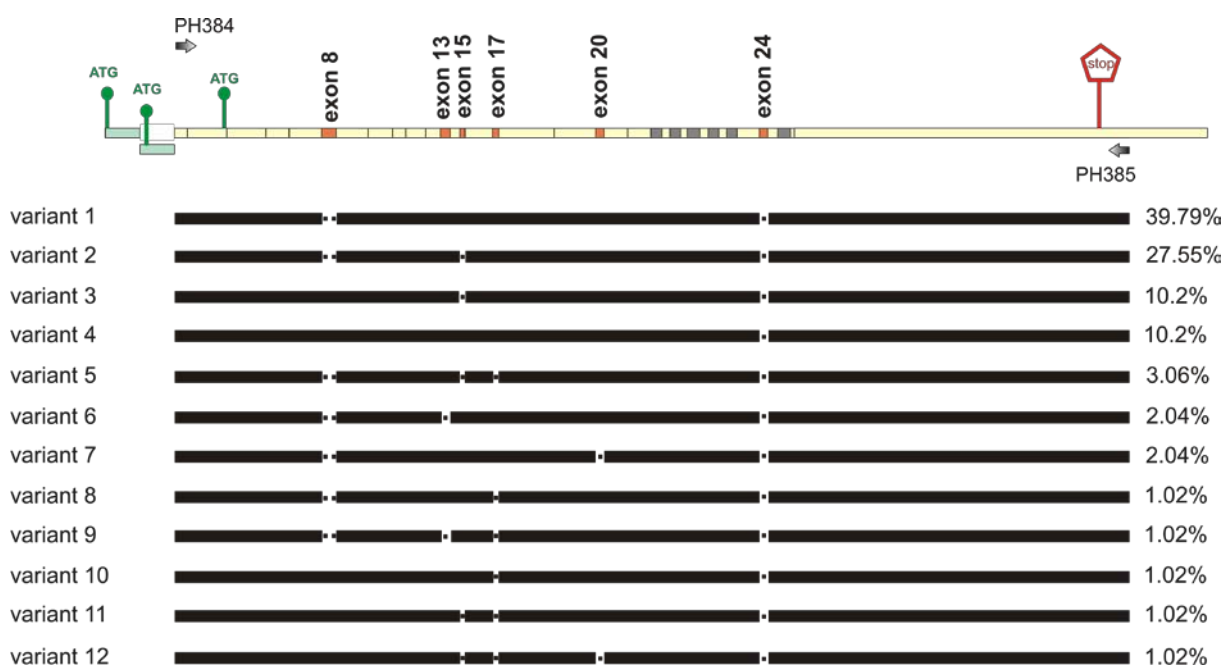
Figure 5-3: Cloning of TRPM3 splice variants in mouse pituitary gland.
The organization of TRPM3 cDNA is shown in yellow with each box representing an individual exon. Exons which are alternatively spliced are highlighted in orange and defined by their numbers. Sequences encoding transmembrane regions are highlighted in gray and the alternative aminotermini are shown in green. The locations of primers used to amplify the cDNA are indicated. Identified TRPM3 variants are shown as black boxes and their frequency is indicated. Areas missing by alternative splicing are presented as dotted line.

5.1.3 Identification of TRPM3 transcripts in different regions of the pituitary

I analyzed the presence of TRPM3 transcripts in different pituitary lobes by RT-PCR. The anterior lobe was dissected from the intermediate/posterior lobe from three different mice and total mRNA was prepared. One-step PCR (4.1.5.3) was performed using two primer combinations PH928/PH930 and PH777/PH778 which hybridize to exons 12/13 and to exons

24/25, respectively. The latter primer combination allowed the identification of alternative splicing within the pore coding exon 24, which was indicated by a shortened amplification product of 187 bp. As shown in Figure 5-4, amplification products of the expected size (109, 187 bp) indicated expression of TRPM3 transcripts in both pituitary regions of all three samples. Interestingly, only products of 187 bp were obtained using primers PH777/PH778 indicating the absence of transcripts encoding Ca^{2+}-impermeable long pore variants.
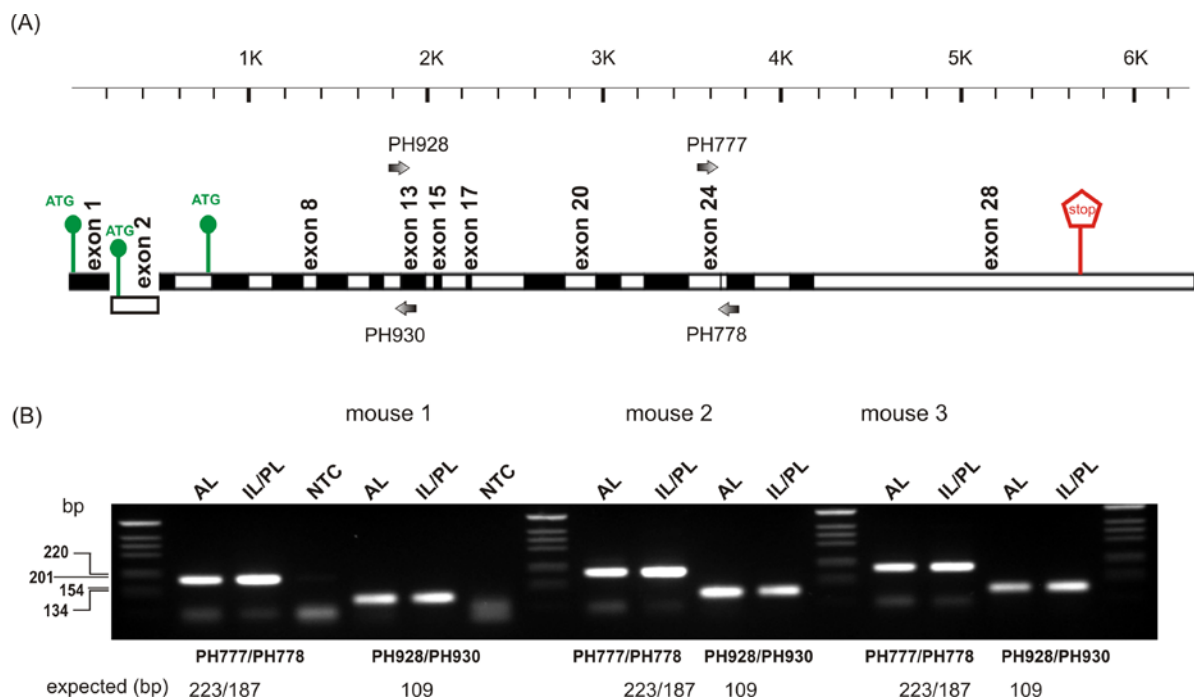
Figure 5-4: Expression of TRPM3 transcripts in the anterior and in the intermediate/posterior lobe of the pituitary gland.
(A) Schematic representation of the coding exons of TRPM3. Oligonucleotide primers (arrows) flanking the region between exon 12 and exon 13 and the pore coding exon 24 and 25 were used to amplify TRPM3 cDNA. (B) Gel electrophoretic separation of PCR products obtained from anterior lobe (AL) and intermediate/posterior lobe (IL/PL) of the pituitary using primers shown in (A) in three individual RNA preparations. NTC = no template control.

5.1.4 Distribution of TRPM transcripts in FACS-sorted cells of the posterior lobe/intermediate lobe

In contrast to the adenohypophysis which contains at least five types of neuroendocrine cells and in addition folliculostellate cells, the posterior lobe (PL) mainly consist of axon terminals of hypothalamic neurons and one single glial cell type called pituicytes. These cells are reported to express glutamate aspartate transporter proteins (GLAST) which can be taken as a cellular marker of these cells. Similarly, the intermediate lobe (IL) also contains mainly one

single cell type: α-MSH releasing melanotrophs which may not express the glial cell surface marker GLAST. To dissect the origin of TRPM3 transcripts obtained from RNA of the intermediate lobe/posterior lobe (5.1.3), cells from PL/IL of wild type pituitaries were prepared and the living cells were stained with anti-GLAST antibodies in a dilution of 1:11 in 0.5 % BSA/PBS for 10 min on ice. After sorting of 50 GLAST-positive and GLAST-negative cells each in single tubes by fluorescence-activated cell sorting (FACS, see also 5.4.2.4), one-step RT-PCR was performed to analyze the expression of TRPM3 transcripts (Figure 5-5).

Again different primer combinations to identify splice events within exon 13 (PH885/ PH907) and exon 24 (PH521/PH522) were included, as well as primer pairs (PH400/PH395, PH374/PH405) common to all splice variants. Using primers PH521/PH522 specific to exon 24 and exon 25 in both GLAST-positive and GLAST-negative cells, 119 bp fragments were amplified. These fragments derived from transcripts which were spliced within exon 24 and suggested the presence of Ca^{2+}-permeable channel in these cells.

Figure 5-5: Analysis of TRPM3 transcripts expressed in GLAST-positive and GLAST-negative cells from intermediate/posterior lobe of the pituitary gland.
(A) Schematic representation of the coding exons of TRPM3. Oligonucleotide primers (arrows) flanking the region between exons 4 and 5, exon 12 and 13, the pore coding exon 24 and 25 and exon 27 and 28 were used to amplify TRPM3 cDNA. (B) Gel electrophoretic separation of PCR products obtained from brain RNA (as positive control) and from cells that were stained with anti-GLAST antibodies (GLAST pos.) or not (GLAST neg.) using primers shown in (A). NTC = no template control. The expected sizes of the amplification products are indicated.

The aim of using primers PH885 and PH907 was to explore the splice events within exon 13, which may lead to the removal of a protein domain indispensable for channel function (ICF, [111]). The expected lengths of the amplified fragments were 204 or 150 bp, respectively. Only fragments originating from an unspliced exon 13 were amplified from both cell populations (Figure 5-5) indicating the absence of the non-functional variants in pituicytes as well as in melanotrophs.

In addition to TRPM3 isoforms, I also analyzed the expression of other members of TRPM subfamily (Figure 5-6) using gene-specific primer pairs. TRPM3, TRPM4 and TRPM7 transcripts were amplified in GLAST-positive cells (pituicytes) whereas in GLAST-negative cells (melanotrophs), TRPM2, TRPM3, TRPM4, TRPM6 and TRPM7 transcripts were amplified.
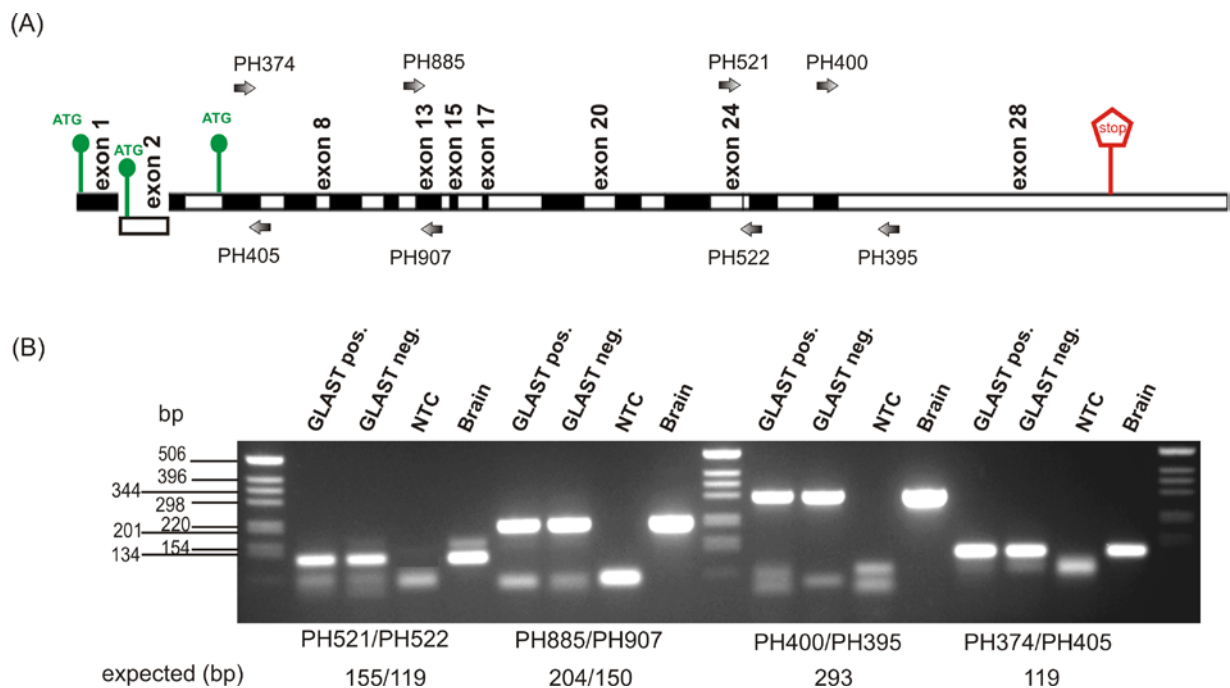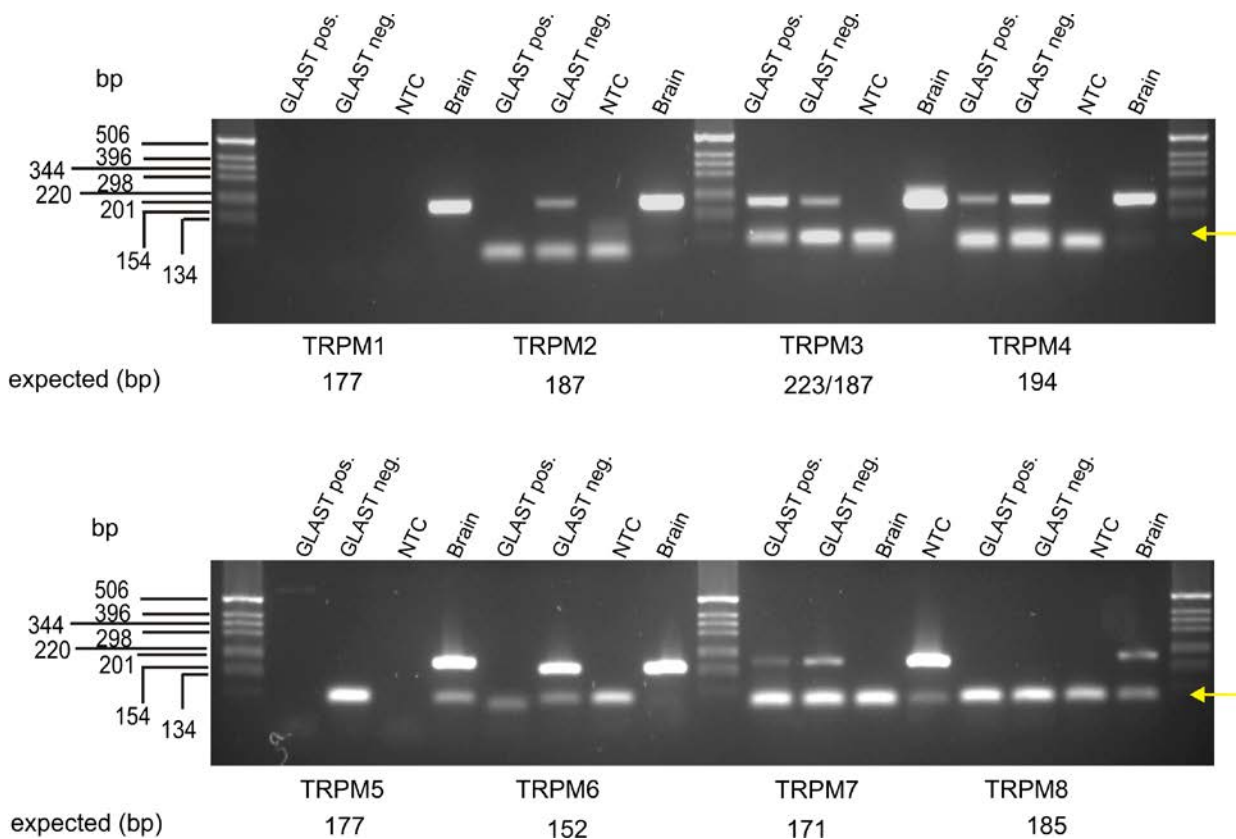

Figure 5-6: Expression of TRPM transcripts in GLAST-positive and GLAST-negative cells from the intermediate/posterior lobe of the pituitary gland.
Gel electrophoretic separation of PCR products obtained from brain RNA (as positive control) and from cells that were stained with anti-GLAST antibodies (GLAST pos.) or not (GLAST neg.) using primers specific for TRPM1-TRPM8 transcripts. NTC = no template control. The expected sizes of the amplification products are indicated. Yellow arrows label unspecific PCR products (primer dimers).

5.2 Identification of TRPM3 proteins in mouse pituitary gland using anti-TRPM3 antibodies

5.2.1 Detection of TRPM3 proteins by western blot

I analyzed the expression of TRPM3 proteins in the pituitary gland by western blot using affinity purified monoclonal anti-TRPM3 antibodies (9F6) which recognize an epitope within the C-terminus of the protein (Figure 5-7, A). In pituitary glands and choroid plexus of the brain from wild type (WT) mice, I found proteins that matched to recombinant TRPM3α2 proteins expressed in HEK293 cells (HEK-TRPM3α2, Figure 5-7 B) and to the expected molecular mass of 194.794 kDa calculated from the primary TRPM3α2 sequence. Similar bands were missing in protein extracts from the pituitary gland and choroid plexus obtained from TRPM3-deficient mice (KO, Figure 5-7 B), demonstrating that the antibody detected the right protein. However, other proteins of lower mass that might be unrelated to TRPM3 were also detected by the antibody. The data provides strong evidence that TRPM3 proteins are expressed in the pituitary. Interestingly, TRPM3 proteins found in the choroid plexus were slightly smaller and may represent different TRPM3 isoforms.

A polyclonal anti-TRPM3 antibody AK695 raised against the sequence QEKEPEEPEKPTKEK within the N-terminus of mouse and rat TRPM3 proteins (Figure 5-7, A), also detected protein of similar molecular mass as the recombinant protein in protein extract from WT pituitaries that were not detected in TRPM3-deficient mice (KO, arrow in Figure 5-7 C). Again TRPM3 proteins of lower molecular mass were identified in the choroid plexus of the brain. However, these antibodies also detected unrelated proteins of similar size that were still present in tissues from the KO. Taken together, the data confirmed my finding obtained with RT-PCR and demonstrate TRPM3 expression in the pituitary and the choroid plexus.
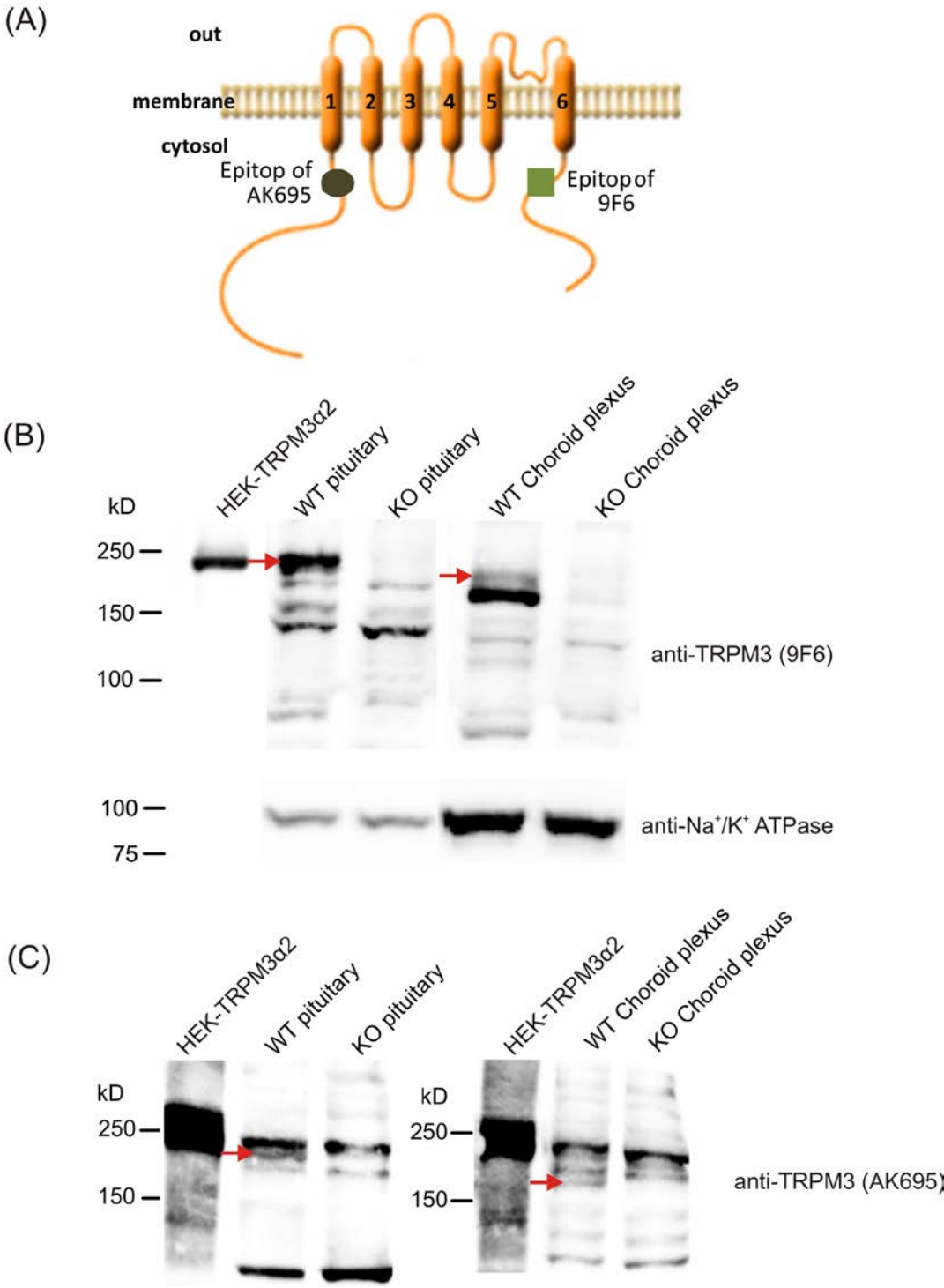
Figure 5-7: Expression of TRPM3 proteins in mouse tissues.
(A) Schematic presentation of the TRPM3 protein with six transmembrane domains. The epitopes of anti-TRPM3 antibody 9F6 at the C-terminus and AK695 at the N-terminus are indicated. (B) Western blot using 9F6 antibodies to detect TRPM3 proteins in pituitary gland and choroid plexus from WT and KO mice. HEK293 cells stably expressing TRPM3α2 (HEK-TRPM3α2) served as positive control. Anti-Na$^+$/K$^+$ ATPase antibodies were used as loading controls. (C) Western blot using antibody AK695 to detect TRPM3 proteins in pituitary gland and choroid plexus from WT and KO mice.

5.2.2 Immunohistochemical detection of TRPM3 proteins

I used the antibodies tested in western blot (5.2.1) to analyze TRPM3 expression in the pituitary by immunohistochemical staining. For this purpose, age and sex-matched WT and KO mice were perfused transcardially with 4 % PFA (4.3.1) and 14 µm pituitary slices were prepared from both genotypes (4.3.2). Using monoclonal 9F6 antibodies in different dilutions, TRPM3 proteins were not detectable probably due to low affinity of the antibodies or masking of the epitope in fixed tissues (not shown). Using polyclonal AK 695 antibodies in a 1:1000 dilution, I found strong signals in the intermediate lobe of the pituitary (Figure 5-8). These signals were largely reduced in the anterior lobe which was co-stained with anti-LH antibodies as a marker of gonadotropic cells. However, these signals were also present in the pituitary from TRPM3-deficient animals (Figure 5-8) even with increased intensity, indicating false positive signals of the antibodies as it was the case in western blot (5.2.1). On the other hand, AK695 antibodies may recognize truncated TRPM3-proteins present in KO-animals, since the recognized epitope is located N-terminally of the targeted pore region.
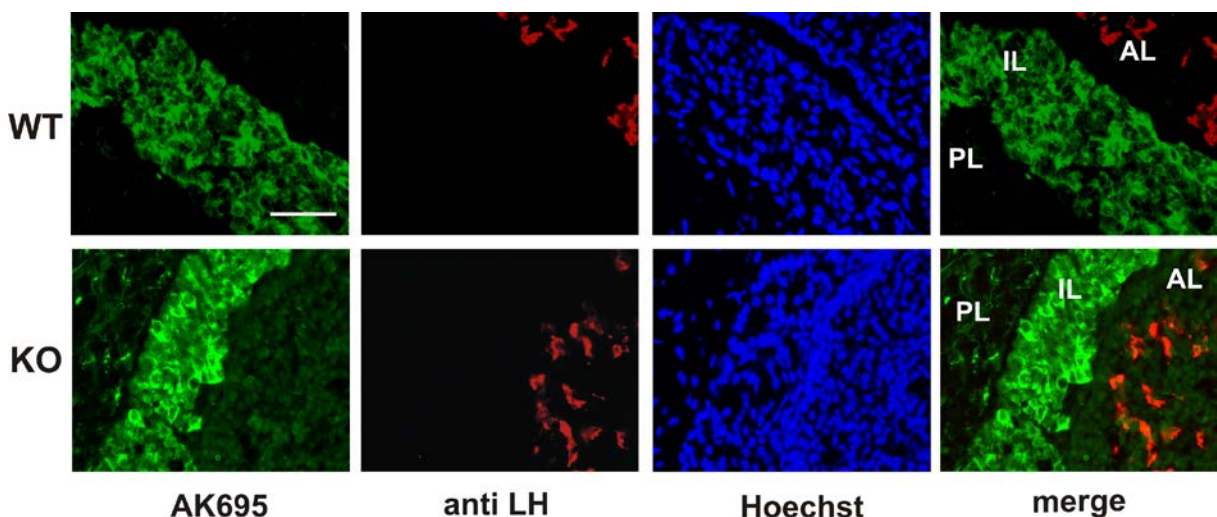
Figure 5-8: Distribution of immunoreactivity to anti-TRPM3 antibodies (AK695) in the anterior (AL), intermediate (IL) and posterior lobe (PL) of the pituitary gland.
Fluorescence images of 14 µm pituitary sections prepared from WT and KO mice and stained with AK 695 (green), anti-LH (red) and Hoechst 33258 for nucleus staining (blue). Overlays of AK695 and LH staining are shown on the right. Scale bar = 50 µm.

Therefore, tissues from TRPM3-KO mice might be an inappropriate control for immunohistochemical experiments using these antibodies and, the experiment was repeated with pituitary sections from WT animals (Figure 5-9). As controls, the antibodies were incubated with a 10000-fold molar excess of peptide P873. This peptide has the amino-acid

sequence of QEKEPEEPEKPTKEK and was used for immunization to obtain the antibody. As a negative control, I used an unrelated control peptide P281. Similar to the last experiment, I found strong signals in the intermediate lobe which was largely reduced in the neighboring areas. In the presence of P873 but not P281, the signals disappeared indicating that at least the antibodies recognized (a) protein(s) containing an epitope similar to the sequence of P873. Taken together these data provide first and preliminary evidence that TRPM3 channels are expressed in the intermediate lobe of the pituitary. On the other hand, it is pretty clear from these data that neither 9F6 nor AK695 antibodies are reliable and specific tools to identify TRPM3 expressing cells in the pituitary.
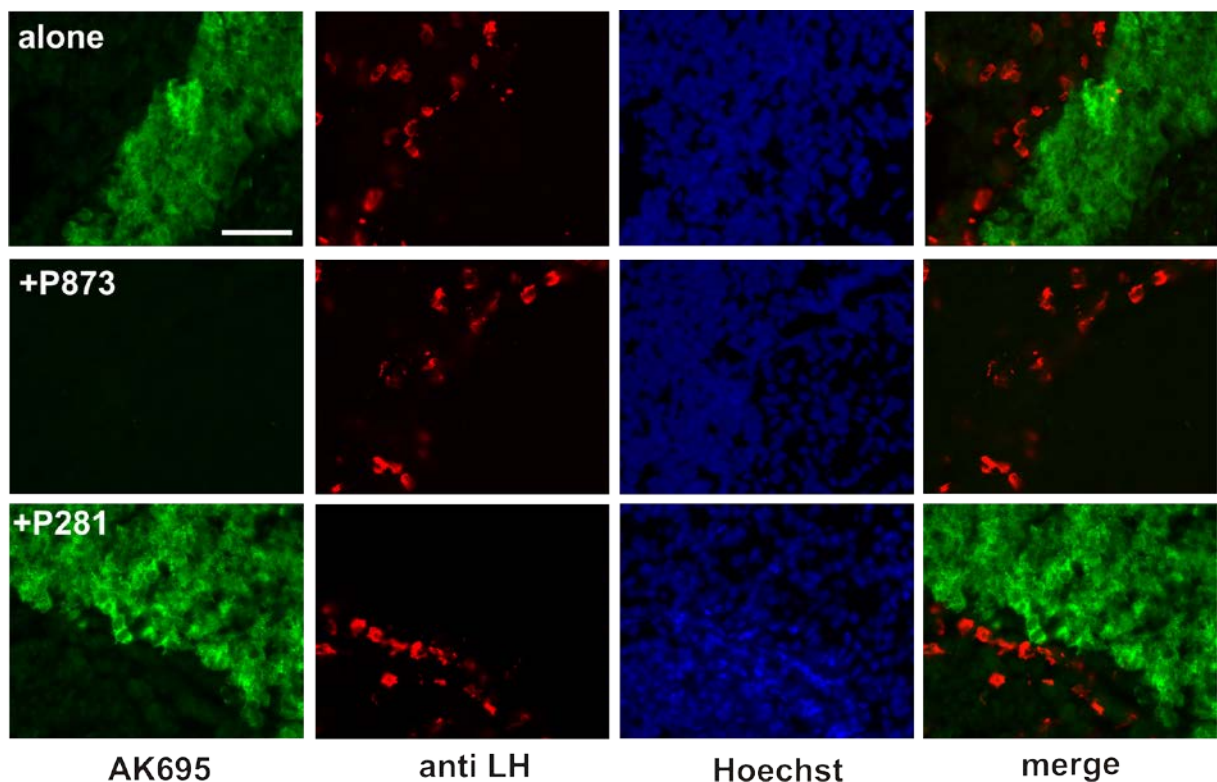
Figure 5-9: Distribution of immunoreactivity to anti-TRPM3 antibody (AK 695) in the pituitary gland.
Fluorescence images of 14 µm pituitary sections prepared from WT mice and stained with AK695 (green) alone or after preincubation with a 10000-fold molar excess of peptide P873 or P281, anti-LH (red) or Hoechst 33258 for nucleus staining (blue). Overlays of AK 695 and LH staining are shown on the right. Scale bar = 50 µm.

5.3 Analysis of TRPM3 expression using GFP-Ki mice

As shown in the previous chapter (5.2), anti-TRPM3 antibodies provided strong evidence that TRPM3 is expressed in the pituitary. However, my data also demonstrated that these

antibodies were rather unsuitable to identify TRPM3 expressing cells within this tissue. Therefore, I chose an alternative approach and made use of TRPM3-GFP-Knock in (GFP-Ki) mice which carry an IRES-GFP-cassette within the TRPM3 gene locus (Figure 3-2). These mice should express the enhanced green fluorescent protein (EGFP) under the control of the TRPM3 promoter(s).

5.3.1 GFP-Ki mice as a model to analyze TRPM3 expression

Since this mouse line has not been characterized before, I checked whether it is an appropriate model to analyze TRPM3 expression in the pituitary gland.

5.3.1.1 Detection of the green fluorescence of GFP in GFP-Ki mice by FACS

First, I analyzed the green fluorescence of GFP in vital cells from tissues, where TRPM3 expression has already been described, and compared it to pituitary cells. For that purpose, single cells were prepared from both pituitary gland and choroid plexus of the brain and were tested by FACS (Figure 5-10). Cells isolated from WT mice served as negative controls.

Figure 5-10: FACS analysis of tissues from GFP-Ki mice.
GFP-fluorescence histograms (log scale) comparing cells from choroid plexus and pituitary gland of wild type (WT) and TRPM3-GFP-Ki (GFP-Ki) mice.

As shown in Figure 5-10, FACS analysis of choroid plexus cells from GFP-Ki mice showed a strong rightward shift of the fluorescence peak compared to control cel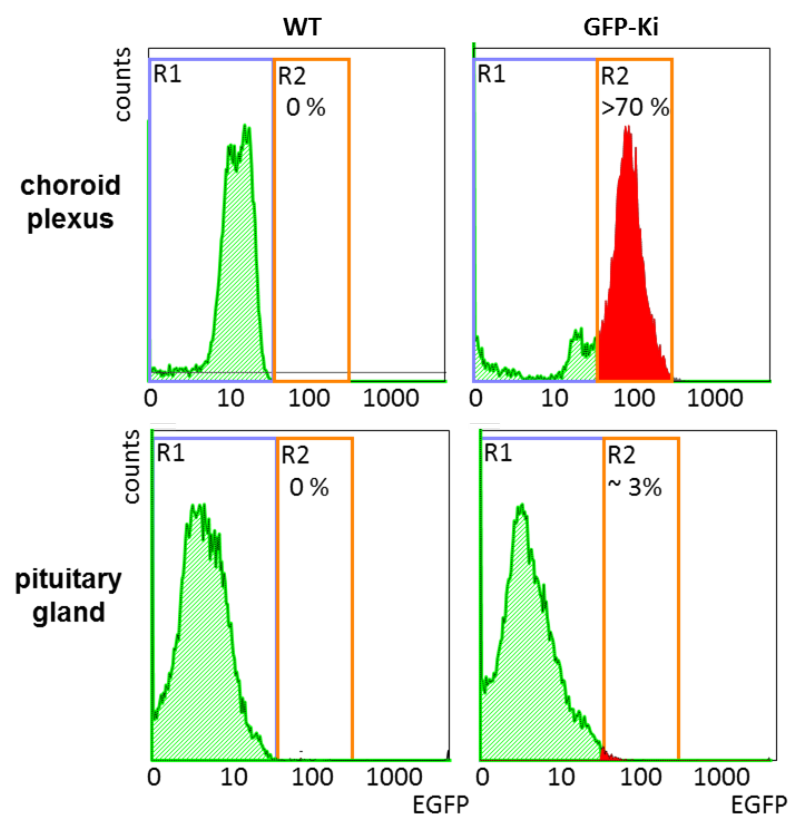ls indicating that more than 70 % of the cells were green fluorescent. This is in good agreement with the finding that TRPM3 is expressed in the epithelial cells of the choroid plexus [103] which provide the main fraction of cells within this tissue. It demonstrates that green fluorescent proteins are expressed in TRPM3 expressing tissues of GFP-Ki mice. In cell preparations of the pituitary gland, I also noticed green fluorescent cells. However, their proportion was only 3 % indicating that only few cells express TRPM3 within this multifunctional tissue.

5.3.1.2 Detection of TRPM3 proteins in tissues of GFP-Ki mice

The targeting strategy of the TRPM3 gene locus included the insertion of a splice acceptor site (SA) into the L3F1 allele (GFP-Ki), with the intention that the IRES-GFP sequence should be fused to exon 24 and the TRPM3 reading frame should be interrupted by stop codons present in the sequence of the IRES-GFP cassette (Figure 3-2). Therefore, only truncated non-functional TRPM3 proteins should be formed in TRPM3 $^{GFP-Ki/GFP-Ki}$ mice which are homozygous for the GFP-Ki allele.

In western blots, I tested, whether full length TRPM3 proteins are generated in the pituitary gland and choroid plexus in different mouse lines containing targeted TRPM3-alleles. For that purpose, I used monoclonal 9F6 antibodies which recognize an epitope C-terminally located from the targeted pore region (Figure 5-7, A). To my surprise, I found that entire TRPM3 proteins were present each in the pituitary glands pooled from five mice that were homo- or heterozygous for the GFP-Ki (L3F1) allele (Figure 5-11). In contrast, I found a gene-dose-dependent reduction of TRPM3 proteins in the choroid plexus from the very same mice leading to complete absence of TRPM3 in homozygous GFP-Ki mice. The data suggest that TRPM3 channels are unaffected in the pituitary gland but functionally inactive in the choroid plexus of TRPM3 $^{GFP-Ki/GFP-Ki}$.

Using anti-GFP antibodies I also tested the presence of GFP proteins in GFP-Ki mice. In the choroid plexus I found a gene-dose-dependent presence of GFP proteins. However, in the pituitary gland no GFP proteins were detectable probably due to the lower number of cells expressing TRPM3 in this tissue (compare Figure 5-10)
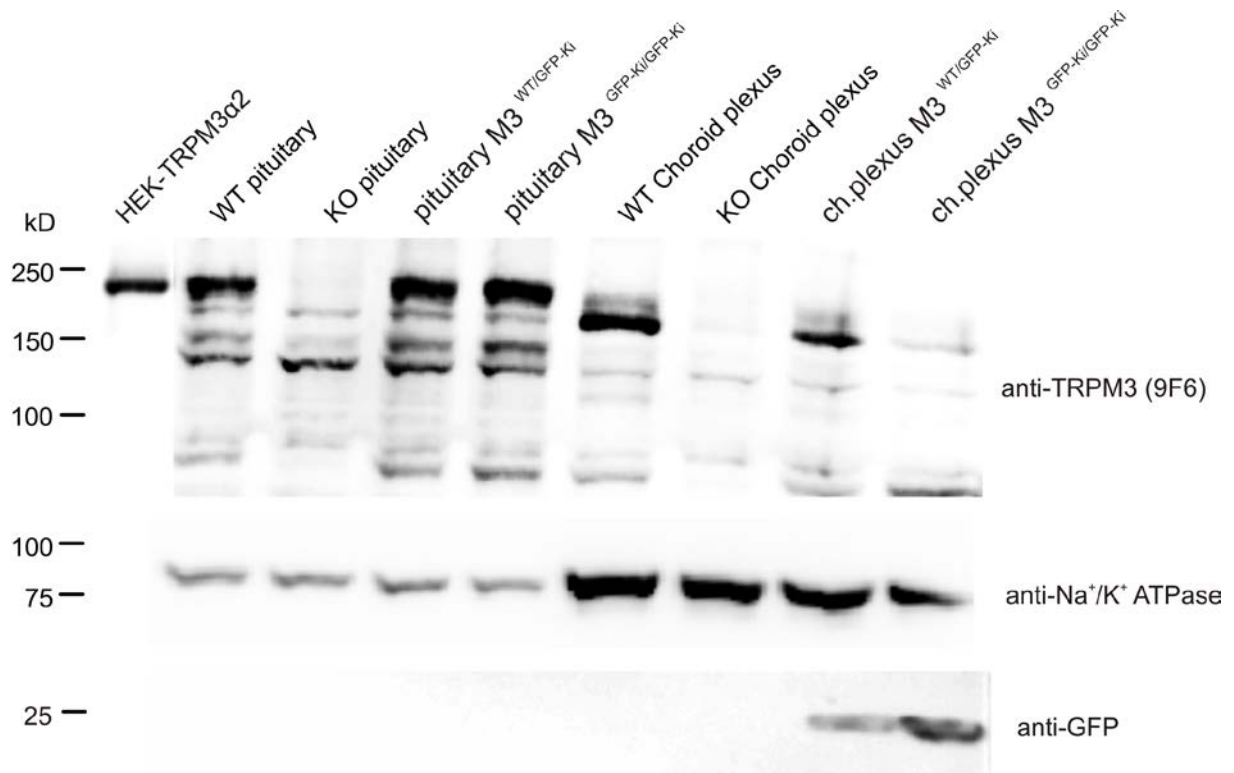
Figure 5-11: Expression of TRPM3 proteins in different mouse lines.
Western blot using 9F6 antibodies to analyze TRPM3 proteins in pituitary gland and choroid plexus of mice heterozygous (M3$^{WT/GFP-Ki}$) or homozygous (M3$^{GFP-Ki/GFP-Ki}$) for the L3F1 allele shown in comparison to tissues from wild type (WT) and TRPM3-deficient mice (KO, L1 allele). The blot was cut into three pieces, which were tested with anti-TRPM3 antibodies (9F6), anti-GFP antibodies and anti-Na$^+$/K$^+$-ATPase antibodies as a control of comparable amounts of proteins loaded to each lane.

5.3.1.3 Analysis of TRPM3 transcripts in GFP-Ki mice

Western blot analysis suggested the presence of entire and functional TRPM3 proteins in pituitaries of GFP-Ki mice but their absence in the choroid plexus. Most likely, this could be explained by alternative splicing of TRPM3 transcripts in these tissues. Therefore, I analyzed TRPM3 transcripts in total RNA from these tissues of five homozygous GFP-Ki mice by RT-PCR (Figure 5-12). I used primer combinations that allowed the detection of three different splicing scenarios as shown in Figure 5-12, A.

PCR confirmed different processing of TRPM3 transcripts in pituitary and choroid plexus from the very same mice (Figure 5-12, B). From pituitary RNA but not from choroid plexus RNA, I obtained fragments matching in size to transcripts with fused exon 24 to exon 25 using primer combination PH521/PH522 and PH777/PH778. This indicates the preservation of the TRPM3 reading frame leading to functional TRPM3 proteins. This finding is in line with the detection of TRPM3 proteins of similar size in GFP-Ki pituitaries (Figure 5-11) and I could

confirm the presence of TRPM3-mediated Ca^{2+} entry pathways in Ca^{2+} imaging experiments using the fluorescent Ca^{2+} indicator dye Fura-2 (see 5.4.3). In this scenario the IRES-GFP cassette would be spliced out and would serve as an independent molecule for translation of GFP.

The opposite was true for primer combination PH521/C5-139 and PH777/ C5-139. No amplification products were obtained with RNA from pituitary gland but from choroid plexus, indicating the fusion of exon 24 to the splice acceptor site upstream to the IRES-GFP sequence. This conclusion was confirmed by sequencing of the PCR fragments after they were cut out of the agarose gel. As shown in Figure 5-12, C, the fusion of exon 24 to the IRES-GFP sequence led to an introduction of a stop codon shortly after exon 24 and thereby to a truncation of the TRPM3 protein.

Using primer combinations SM61/C5-139, PH521/SM24 and PH777/ SM24, I also obtained PCR products of 307, 403 and 450, respectively. Although, I can't rule out that these amplification products derived from contaminating genomic DNA present in the RNA preparations, these data indicate that also unspliced TRPM3 transcripts exist in GFP-Ki mice. These transcripts would also lead to non-functional TRPM3 channel proteins, since again stop codons present in intron 24 would shorten the reading frame.

(A)
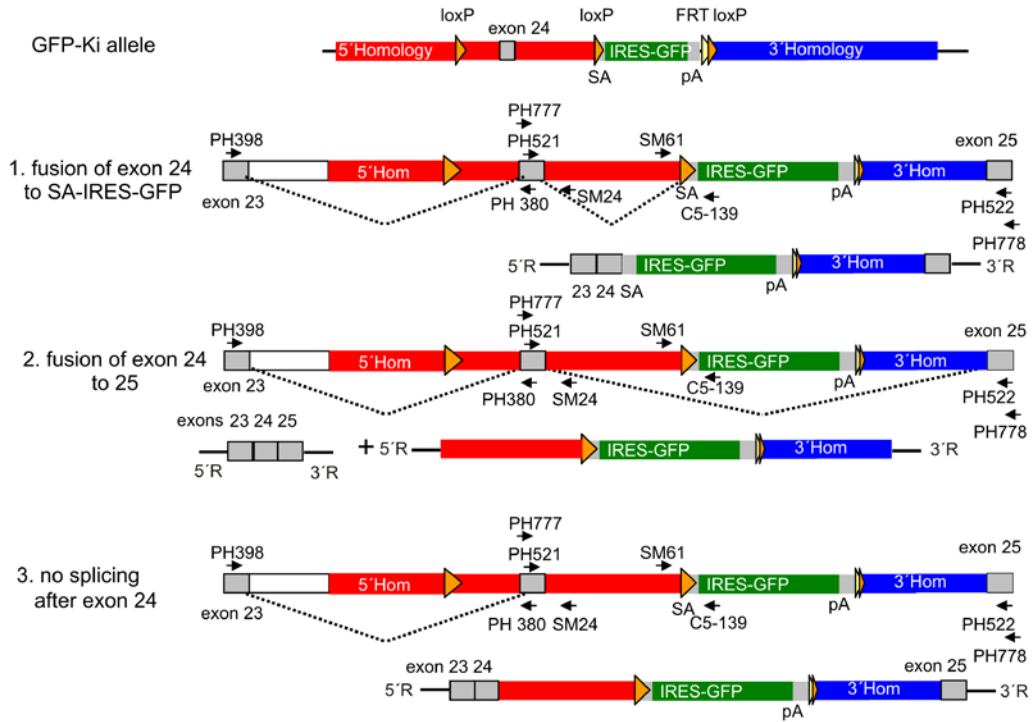
Forward primer	Reverse primer	Expected length (bp) after fusion of exon 24 to SA-IRES-GFP	Expected length (bp) after fusion of exon 24 to exon 25	Expected length (bp) in case of no splicing after exon 24
PH521	PH522	1741 / 1705	155 / 119	>2000
PH777	PH778	1809 / 1773	223 / 187	>2000
PH521	C5-139	210 / 174	No product	1616
PH777	C5-139	257 / 221	No product	1663
SM61	C5-139	No product	307	307
PH521	SM24	No product	No product	403
PH777	SM24	No product	No product	450
PH398	PH380	354	354	7736

(B)

GFP-Ki pituitary gland   GFP-Ki choroid plexus
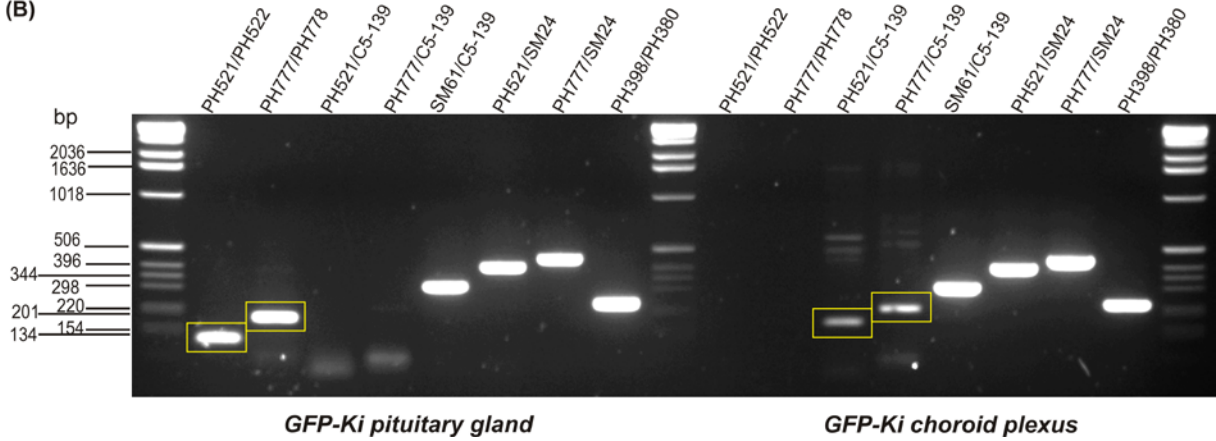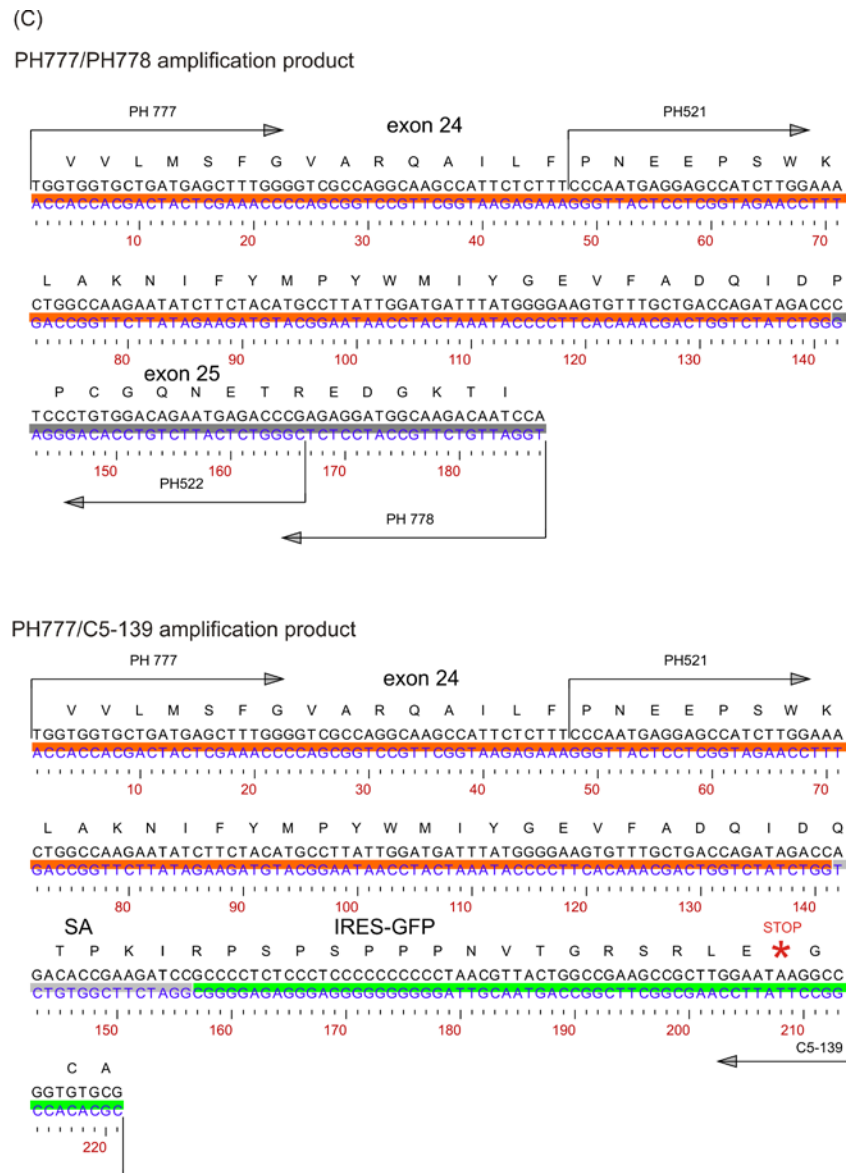
Figure 5-12: TRPM3 transcripts are differentially spliced in pituitary gland and choroid plexus of GFP-Ki mice.
(A) Structure of the TRPM3-GFP-Ki allele including the 5`-homology, the floxed exon 24, the 3`-homology, the splice acceptor (SA), the IRES-GFP cassette and the polyadenylation signal (pA). The location of the loxP sequences (orange triangles) and FRT sequences (yellow triangles) are also indicated. The scenarios of three splicing events are explained and the primers used to identify each splice event are indicated by arrows and names. The table shows the expected length of the fragments obtained with the indicated primer combinations. (B) Gel electrophoretic separation of the PCR products obtained from mouse pituitary gland and choroid plexus of GFP-Ki mice using primers indicated in A. Amplification products labelled with rectangles were purified and sequenced. (C) Sequence of the amplification products obtained with primer combination PH777/PH778 from pituitary and PH777/C5-139 from choroid plexus with primer sequences and TRPM3 reading frame indicated. Sequence sections belonging to exon 24, exon 25, the splice acceptor sequence left after fusion to exon 24 and the IRES-GFP cassette are highlighted in colors. Note the stop codon in the TRPM3 reading frame when the IRES-GFP cassette is fused to exon 24.

5.3.1.4 Microscopic detection of GFP fluorescence in native tissues of GFP-Ki mice

I analyzed the presence of fluorescent GFP proteins in native tissues of GFP-Ki mice. Pituitary glands and choroid plexus of the brain were dissected and placed immediately in ice-cold PBS. The pituitary gland was opened up between anterior lobe (AL) and intermediate lobe/posterior lobe (IL/PL). Tissues prepared from WT mice served as negative controls. Microscopic analysis of the epifluorescence revealed expression of GFP in the choroid plexus and IL/PL of the pituitary gland of GFP-Ki mice which was absent in tissues of WT mice (Figure 5-13). This result confirmed that GFP is expressed in choroid plexus and pituitary gland of GFP-Ki mice and indicate the presence of native GFP proteins in vital cells of whole mount tissue preparations.
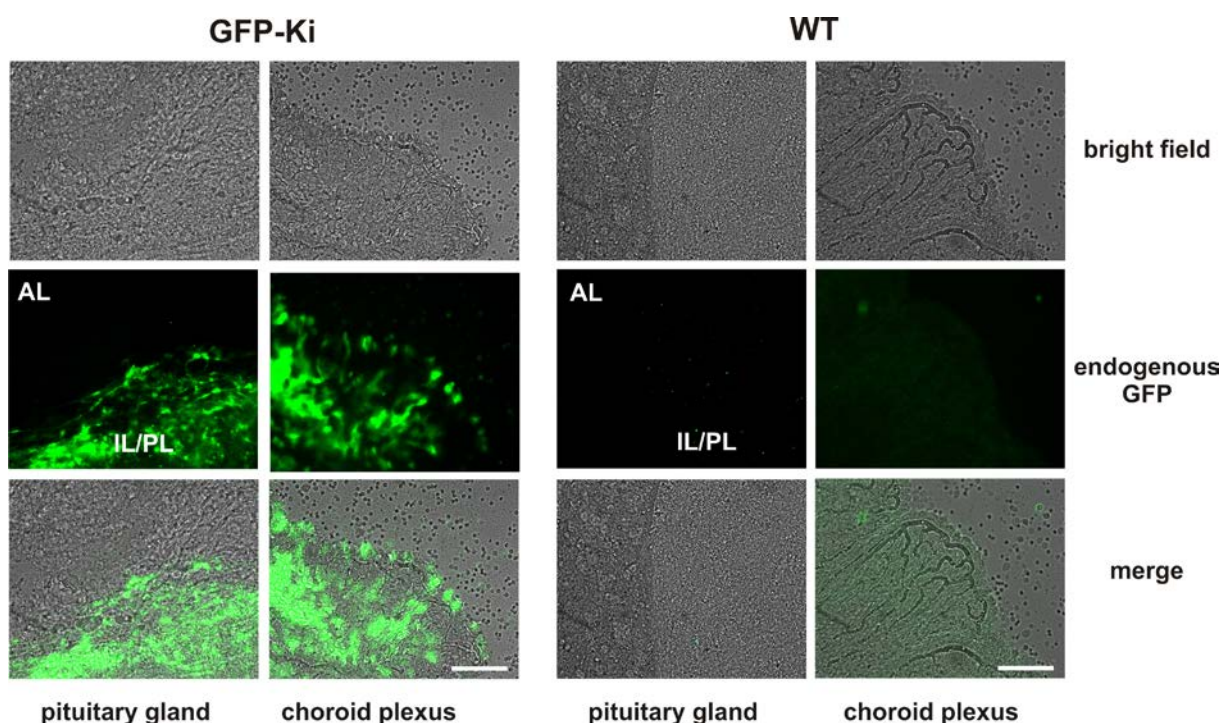
Figure 5-13: Expression of GFP in the pituitary gland and choroid plexus of GFP-Ki mice.
Bright field (upper panel), fluorescence (middle panel) and merged (lower panel) photographs of whole mount pituitary gland (left) and choroid plexus (right) isolated from GFP-Ki and WT mice (scale bar = 100 μm).

5.3.1.5 Loss of GFP fluorescence after fixation of tissues

To define the identity of GFP expressing cells in tissues, I had to use cell type-specific antibodies for immunostaining. To prevent the degradation of their target epitopes and to allow their access into the cells, fixation and permeabilization of the tissues were necessary.

However, this procedure has been described to affect the fluorescence intensity emitted by GFP [180]. Therefore, I analyzed the GFP fluorescence after removal of fresh tissues prepared from GFP-Ki mice and overnight post-fixation in 4 % PFA/PBS. As shown in Figure 5-14, GFP fluorescence was still detectable in the choroid plexus of the brain but was largely reduced in slices prepared from the pituitary, indicating that the fluorescence intensity of GFP expressed in GFP-Ki mice is not sufficient to determine the identity of TRPM3 cells in the pituitary gland.
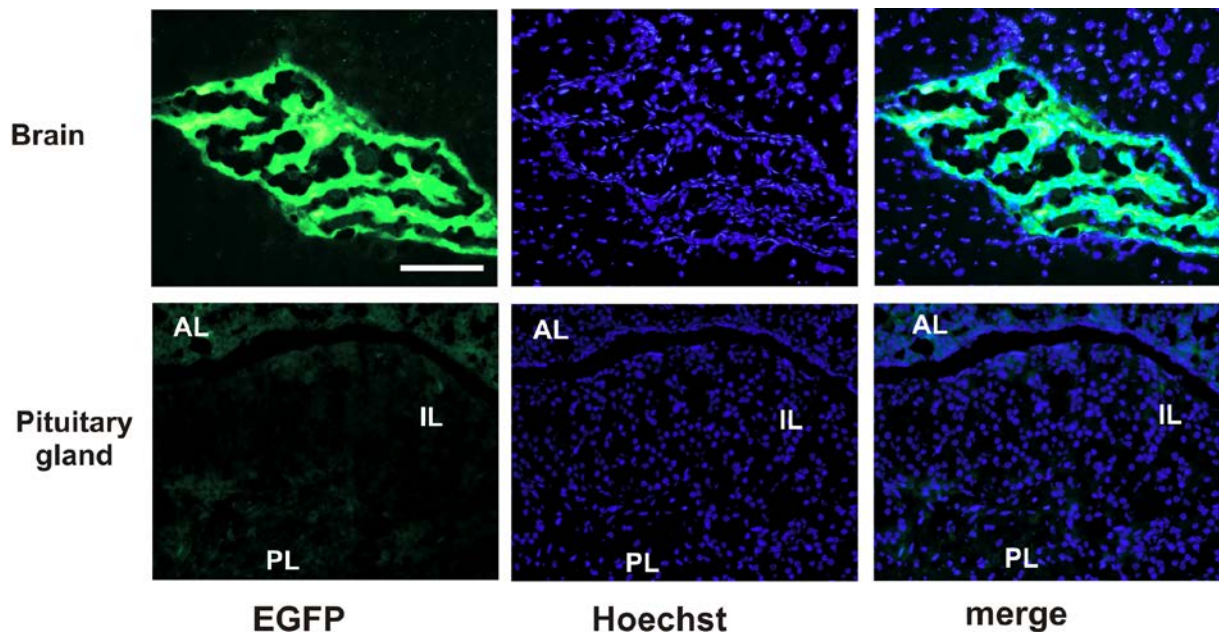
Figure 5-14: Reduction of GFP fluorescence in post-fixed slices of the brain and pituitary gland. GFP fluorescence, nucleus staining with Hoechst3342 (Hoechst) and merge image of slices obtained from brain and pituitary. Anterior lobe (AL), intermediate lobe (IL) and posterior lobe (PL) regions are indicated (scale bar =100 µm).

I analyzed this effect in more detail using HEK293 cells transiently expressing recombinant GFP. 48 h after transfection of the GFP encoding plasmid pCAGGSM2-IRESGFP, cells were fixed with different concentrations of PFA and the GFP fluorescence was compared to unfixed cells (Figure 5-15). Using imageJ software, the fluorescence intensities of 7-10 cells from five different figures were quantified. In line with my observation, that pituitaries showed only week GFP fluorescence after fixation with PFA (Figure 5-13), I noticed a concentration-dependent decrease of fluorescence intensity. Fixation with 4 % PFA reduced the GFP fluorescence by 62.7 %.
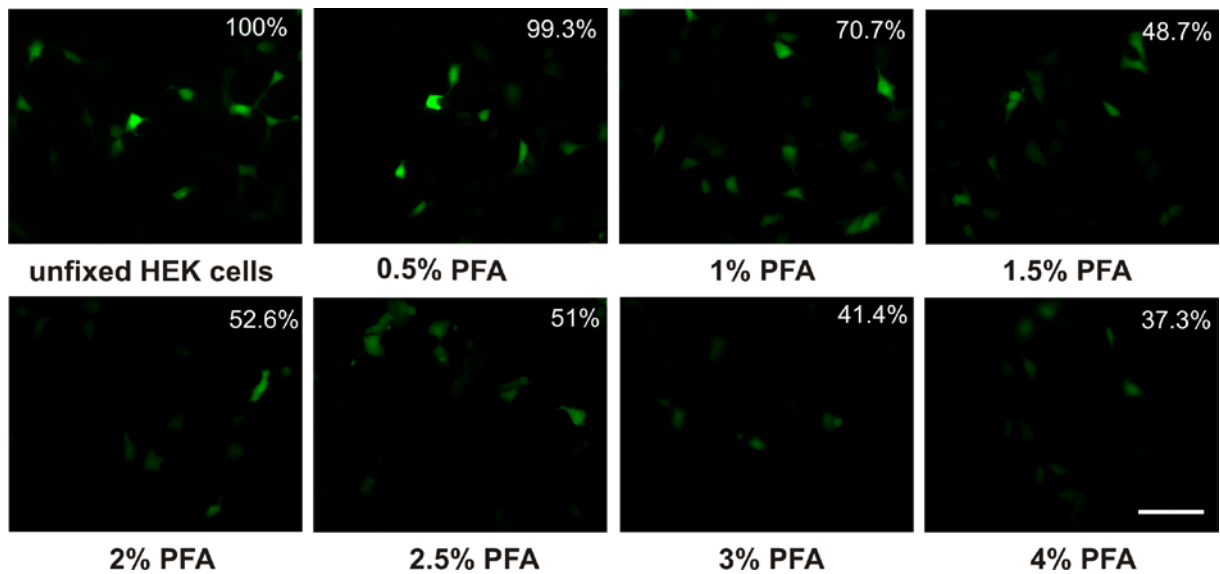
Figure 5-15: Reduction of GFP fluorescence in transfected HEK293 cells after fixation with different PFA concentrations.
Signal intensities of GFP in unfixed HEK cells and after fixation with different concentrations of PFA are indicated in each image. Scale bar =100 µm

In order to visualize green fluorescent proteins as a molecular marker of TRPM3 expression and to increase fluorescence associated with GFP, I introduced in the following experiments Alexa Flour 488- or Alexa Flour 594 labelled anti-GFP antibodies. Control slices excluding anti-GFP antibodies were always included and are shown exemplarily in Figure 5-18. In these controls, I never observed signals different from the background.

5.3.2 Identification of TRPM3 expressing cells of GFP-Ki mice using anti-GFP antibodies

In the previous chapter 5.3.1, I could demonstrate that GFP-Ki mice provide a suitable model with GFP as a reporter protein to analyze the expression pattern of TRPM3.

5.3.2.1 Overview of GFP expression in the whole pituitary

In an initial series of experiments, pituitary glands were dissected from PFA-perfused GFP-Ki and WT mice and 14 µm sections were prepared from. Rabbit polyclonal anti-GFP antibodies (anti-GFP) were used in a dilution of 1:5000 to detect GFP proteins in pituitary glands of GFP-Ki mice. Anti-LH antibodies (anti-LH) were used to stain gonadotropic cells of the anterior pituitary. Staining with anti-GFP antibodies revealed prominent GFP expression in the posterior lobe (PL), weaker expression in the intermediate lobe (IL) as well as expression in single cells of the anterior lobe (AL, Figure 5-16). The signal obtained with anti-GFP

antibodies did not match to the signal of anti-LH antibodies indicating that TRPM3 is not expressed in gonadotrophs.

This experiment revealed the expression of GFP in all three lobes of the pituitary gland of GFP-Ki mice and therefore, this expression was analyzed in more details in the following experiments.

anti-GFP + anti-LH   Hoechst
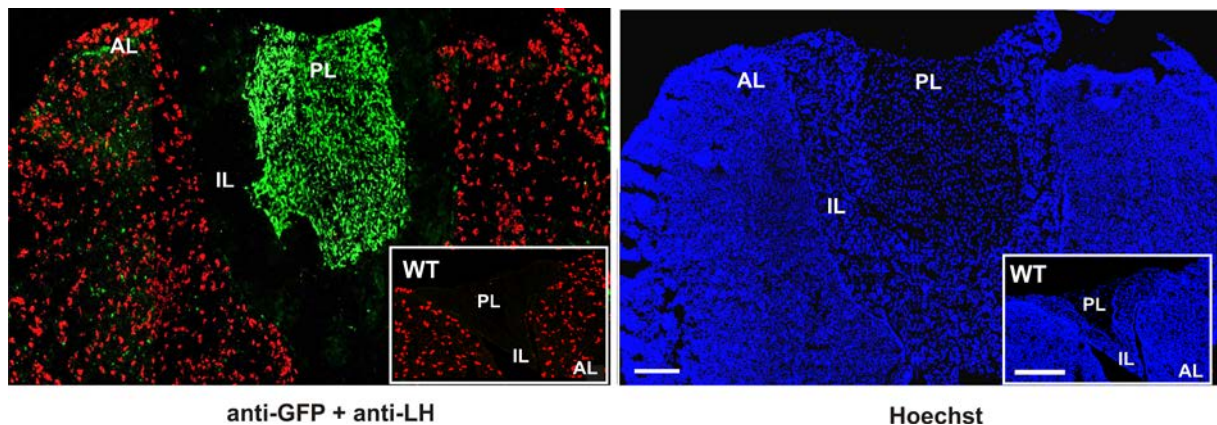
Figure 5-16: Distribution of immunoreactivity to GFP as an indicatior of TRPM3 expression in the anterior (AL), intermediate (IL) and posterior lobe (PL) of pituitary glands from GFP-Ki mice. Fluorescence image of 14 µm pituitary sections prepared from GFP-Ki mice stained with anti-GFP antibodies (green), anti-LH antibodies (red) (left figure) and Hoechst 33258 for nucleus staining (blue, right figure). The insets show fluorescence images of pituitary sections prepared from WT mice which served as controls. Scale bar = 200 µm.

5.3.2.2 Analysis of TRPM3 expression in the posterior lobe

5.3.2.2.1 TRPM3 proteins are absent in vasopressin or oxytocin-releasing nerve terminals.

The posterior lobe of the pituitary consists in principle of four different elements including VP-releasing nerve terminals, OXT-releasing nerve terminals, non-secretory nerve terminals and specialized glial cells called pituicytes. As the staining using anti-GFP antibodies displayed prominent GFP expression in this region, different co-staining experiments were performed to identify TRPM3 expressing cells. Oxytocin and vasopressin and their carrier molecules neurophysin I and neurophysin II, respectively are all synthesized in the cell bodies of the magnocellular neurons (MCNs) of the hypothalamus and released in the posterior pituitary from nerve terminals. To investigate the expression of TRPM3 in these nerve terminals, 14 µm pituitary slices were stained with both anti-GFP antibodies and mixture of anti-neurophysin I and anti-neurophysin II antibodies (anti-neurophysins). The staining showed no co-localization of the fluorescence of anti-GFP antibodies and anti-neurophysins

antibodies indicating the absence of TRPM3 protein in the VP- or OXT-releasing nerve terminals (Figure 5-17).
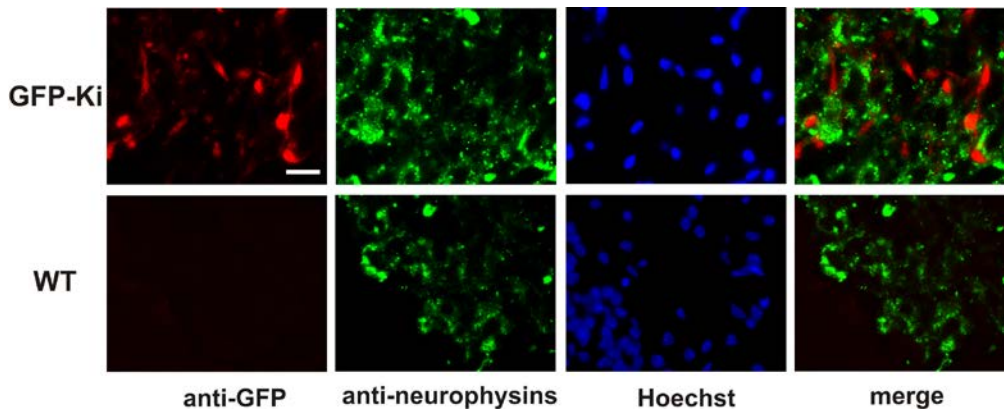
Figure 5-17: Distribution of immunoreactivity to GFP and neurophysins I and II in the posterior lobe of GFP-Ki and WT pituitaries.
Fluorescence images of 14 µm pituitary sections prepared from GFP-Ki and WT mice and stained with anti-GFP (red), anti-neurophysins (green) and Hoechst 33258 (blue) for nucleus staining. Overlay of GFP and neurophysins staining is shown in the right merged image. Scale bar = 20 µm.

Next, I analyzed whether TRPM3 proteins are expressed in hypothalamic-non-neurosecretory axons that are also known to terminate in the posterior lobe (Figure 5-18).
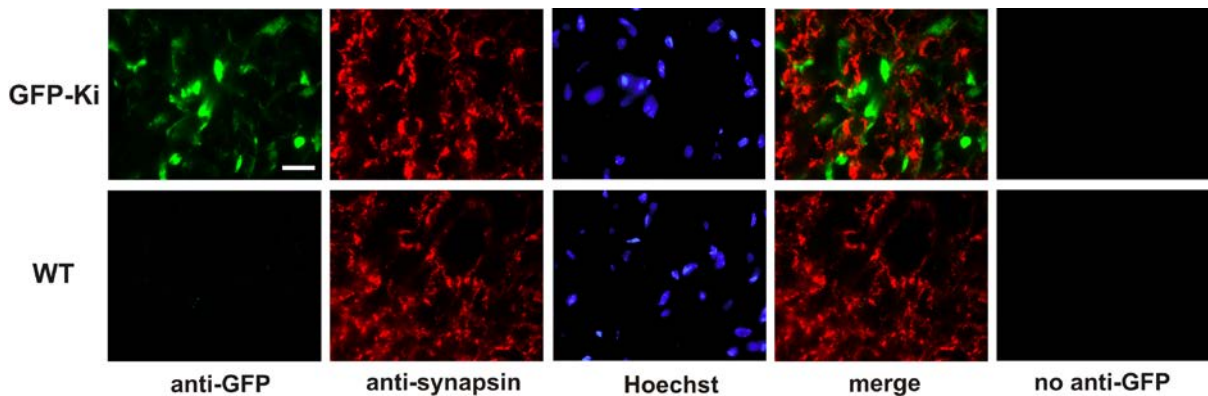
Figure 5-18: Distribution of immunoreactivity to GFP and synapsin in the posterior lobe of GFP-Ki and WT pituitaries.
Fluorescence images of 14 µm pituitary sections prepared from GFP-Ki and WT mice and stained with anti-GFP (green), anti- synapsin (red) and Hoechst 33258 (blue) for nucleus staining. Overlay of GFP and synapsin staining is shown in the right merged image. Photographs of control slices excluding the primary anti-GFP antibodies (no anti-GFP) were taken using the same exposure time and the same filter set as used for the detection of Alexa 488-coupled anti-GFP antibodies. Scale bar = 20 µm.

The staining was performed using both anti-GFP antibodies and antibodies directed against the synaptic vesicle associated protein synapsin I (anti-synapsin) which is expressed in the synaptoid contact with pituicytes [181]. Again, the staining showed no co-localization of signals obtained with anti-GFP antibodies and anti-synapsin I antibodies indicating the absence of TRPM3 proteins expression in non-neurosecretory nerve terminals of the posterior lobe (Figure 5-18).

5.3.2.2.2 TRPM3 proteins are expressed in pituicytes of the posterior lobe

Pituitary glial cells or pituicytes are known to express different astroglial markers like GLAST, GFAP and S100B. To investigate TRPM3 expression in the pituicytes, GFP-Ki and WT pituitary slices were stained using both anti-GFP antibodies in a dilution of 1:5000 and phycoerythrin-conjugated anti-GLAST antibodies in a dilution of 1:20 (Figure 5-19). The staining showed clear co-localization of signals derived from anti-GLAST antibodies and anti-GFP antibodies indicating that TRPM3 proteins are expressed in pituicytes. However, in the merged image obtained with anti-GFP and anti-GLAST antibodies, I found no complete overlap of signals and a spectrum of coloration, probably due to differences of the intensities of each immune reaction.
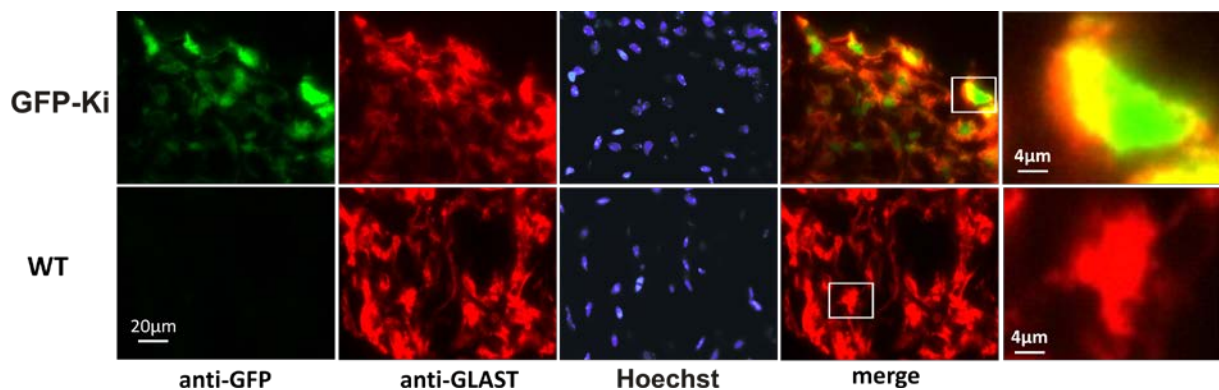
Figure 5-19: Expression of GFP and GLAST-positive cells of the posterior lobe.
Fluorescence images of 14 μm pituitary sections prepared from GFP-Ki and WT mice and stained with anti-GFP (green), anti-GLAST (red) and Hoechst 33258 (blue). Overlay of GFP and GLAST staining is shown in the merged image. Scale bar = 20 μm. The very right panels show single pituicytes in higher magnification (scale bar = 4 μm) highlighted by rectangles in the merged image.

Therefore, additional experiments were performed using anti-GFP and anti-GFAP antibodies (anti-GFAP). As shown in Figure 5-20, the staining revealed co-localization of signals derived from both antibodies confirming TRPM3 expression in pituicytes (Figure 5-20). However, not all GFP positive cells were stained with anti-GFAP antibodies, which may rely on the presence of different subtypes of pituicytes expressing GFAP [182]. S100B is an acidic, glial-

specific, calcium binding protein known to be expressed in all pituicytes of the neurohypophysis. Anti-S100B antibodies (anti-S100B) were used to label pituicytes in GFP-Ki and WT pituitary slices. All cells which showed GFP-positive signals were also positive to S100B (Figure 5-21) confirming the expression of TRPM3 proteins in pituicytes. In summary, using three different pituicytes marker proteins all showed co-localization with GFP, demonstrating that TRPM3 is expressed in pituicytes.
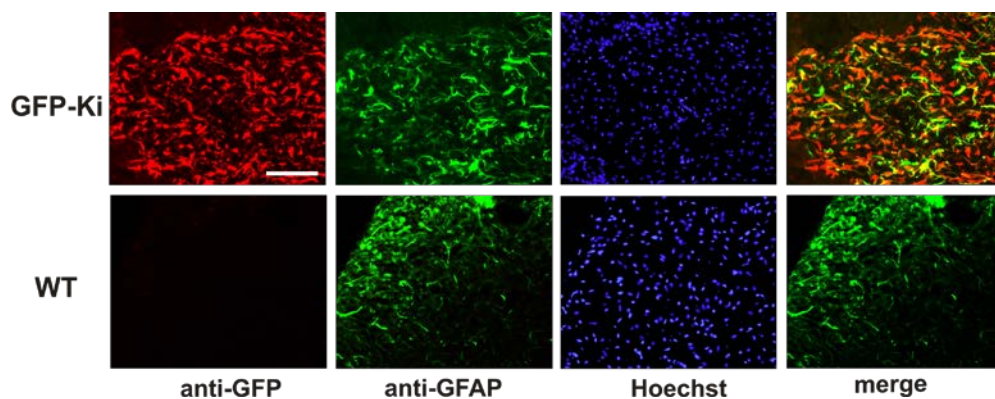
Figure 5-20: Co-staining of GFP and GFAP in pituicytes of the posterior lobe.
Fluorescence images of 14 µm pituitary sections prepared from GFP-Ki mice and WT and stained with anti-GFP (red), anti- GFAP (green) and Hoechst 33258 (blue). Overlay of GFP and GFAP staining is shown in the right merged image. Scale bar = 100 µm.
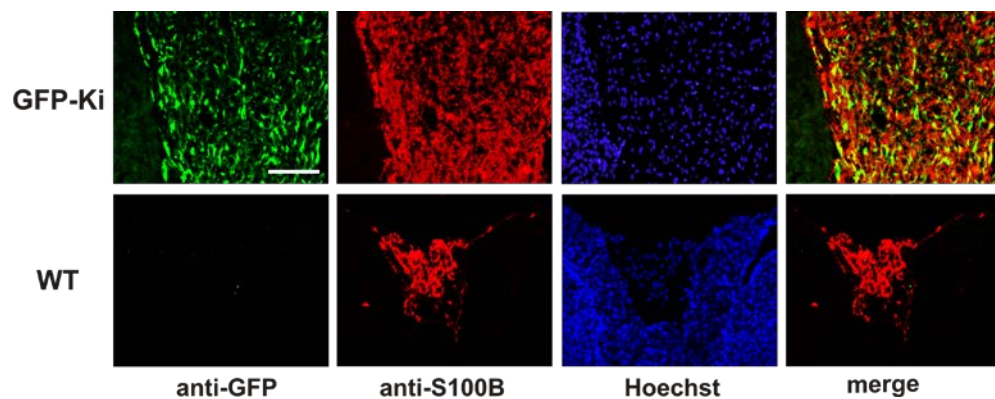
Figure 5-21: Co-staining of GFP and S100B in pituicytes of the posterior lobe.
Fluorescence images of 14 µm pituitary sections prepared from GFP-Ki and WT mice stained with anti-GFP (green), anti-S100B (red) and Hoechst 33258 (blue). Overlay of GFP and S100b staining is shown in the right merged image. Scale bar = 100 µm.

The presence of TRPM3 proteins in the pituicytes was further supported by co-staining of slices from WT pituitary with anti-TRPM3 antibodies AK695 and phycoerythrin-conjugated anti-GLAST conjugated antibodies. The signals of both antibodies again co-localized in all

pituicytes but not in the presence of the antigenic peptide P873, confirming the expression of TRPM3 proteins in these cells (Figure 5-22).
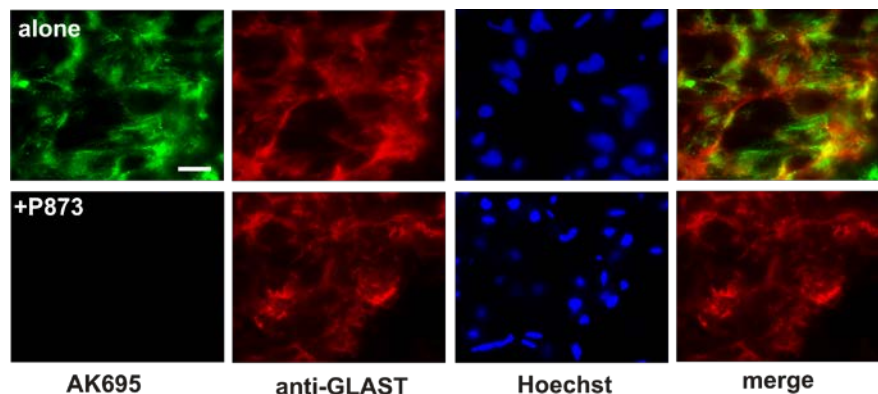
Figure 5-22: Immunoreactivity to anti-TRPM3 AK 695 and anti-GLAST antibodies in the posterior pituitary gland.
Fluorescence images of 14 µm pituitary sections prepared from WT mice and stained with AK695 (alone or after preincubation with a 10000-fold molar excess of peptide P873, green), anti-GLAST (red) and Hoechst 33258 (blue). Overlay of AK 695 and GLAST staining is shown in the right merged image. Scale bar = 50 µm.

5.3.2.3 Analysis of TRPM3 expression in the anterior lobe

The anterior lobe of the pituitary gland consists of five different endocrine cells including gonadotrophs, somatotrophs, thyrotrophs, corticotrophs and lactotrophs [1]. In addition to the endocrine cells, agranular star-shaped cells called folliculostellate (FS) cells were shown to be present in the anterior lobe [1]. As shown above (5.3.2.1), GFP expression in the pituitary of TRPM3 GFP-Ki mice revealed the presence of TRPM3 proteins in single cells of the anterior lobe. The following chapter describes a series of experiments to identify TRPM3 expressing cells in the adenohypophysis.

5.3.2.3.1 TRPM3 proteins are absent in endocrine cells of the adenohypophysis

To analyze the expression of TRPM3 proteins in gonadotrophs, 14 µm pituitary sections from WT and GFP-Ki mice were co-stained with antibodies directed against GFP and both gonadotropins LH and FSH and GFP proteins. Microscopic analysis of the slices confirmed the expression of GFP in the pituitaries of GFP-Ki mice but not of WT mice. Anti-LH and anti-FSH antibodies (anti-LH/anti-FSH) stained gonadotropic cells in pituitaries of both genotypes. In line with the result shown in Figure 5-16, I found no co-staining of GFP and gonadotropins indicating the absence of TRPM3 proteins in gonadotrophs (Figure 5-23).

Figure 5-23: Distribution of immunoreactivity to GFP and FSH/LH in the anterior lobe of GFP-Ki and WT pituitaries.
Fluorescence images of 14 µm pituitary sections prepared from GFP-Ki and WT mice and stained with anti-GFP (green), anti-FSH/LH (red) and Hoechst 33258 (blue). Overlay of GFP and FSH/LH staining is shown in the right merged image. Scale bar = 20 µm.

To investigate the expression of TRPM3 proteins in GH-releasing somatotrophs, pituitary slices were co-stained with anti-GFP and anti-GH antibodies (anti-GH). As shown in Figure 5-24, the staining showed no co-localization of signals derived from anti-GFP and anti-GH antibodies indicating the absence of TRPM3 proteins in the somatotrophs.

Figure 5-24: Distribution of immunoreactivity to GFP and GH in the anterior lobe of GFP-Ki and WT pituitaries.
Fluorescence images of 14 µm pituitary sections prepared from GFP-Ki and WT mice and stained with anti-GFP (green), anti-GH (red) and Hoechst 33258 (blue). Overlay of GFP and GH staining is shown in the right merged image. Scale bar = 20 µm.

Similarly, staining of GFP-Ki pituitary slices with anti-GFP antibodies and antibodies directed against TSH (anti-TSH, Figure 5-25), ACTH (anti-ACTH, Figure 5-26) or PRL (anti-PRL, Figure 5-27) revealed the absence of TRPM3 proteins in the thyrotrophs , corticotrophs or lactotrophs, respectively.
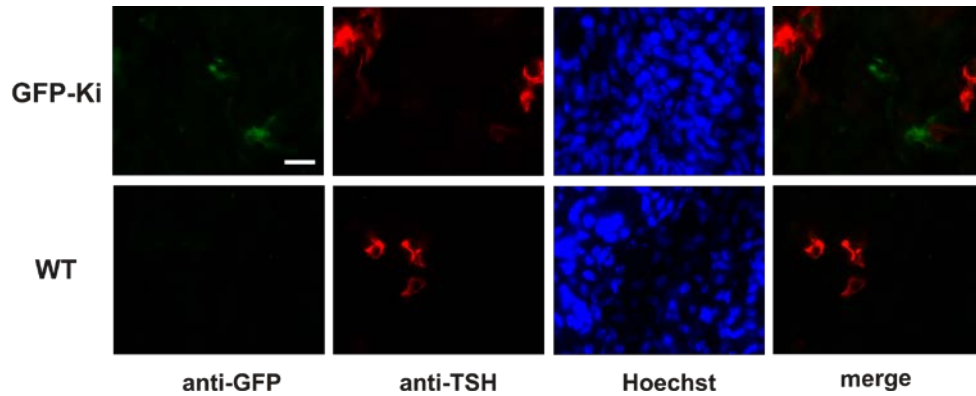
Figure 5-25: Distribution of immunoreactivity to GFP and TSH in the anterior lobe of GFP-Ki and WT pituitaries.
Fluorescence images of 14 μm pituitary sections prepared from GFP-Ki and WT mice and stained with anti-GFP (green), anti-TSH (red) and Hoechst 33258 (blue) for nucleus staining. Overlay of GFP and TSH staining is shown in the right merged image. Scale bar = 20 μm.
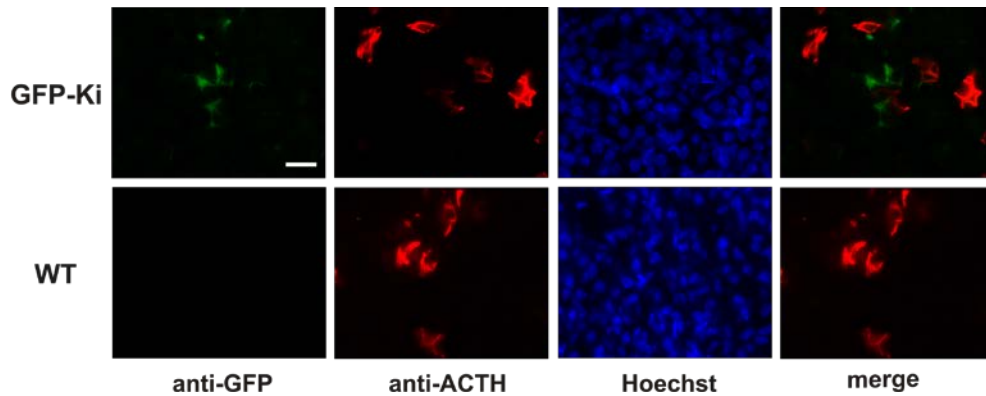
Figure 5-26: Distribution of immunoreactivity to GFP and ACTH in the anterior lobe of GFP-Ki and WT pituitaries.
Fluorescence images of 14 μm pituitary sections prepared from GFP-Ki and WT mice and stained with anti-GFP (green), anti-ACTH (red) and Hoechst 33258 (blue) for nucleus staining. Overlay of GFP and ACTH staining is shown in the right image. Scale bar = 20 μm.
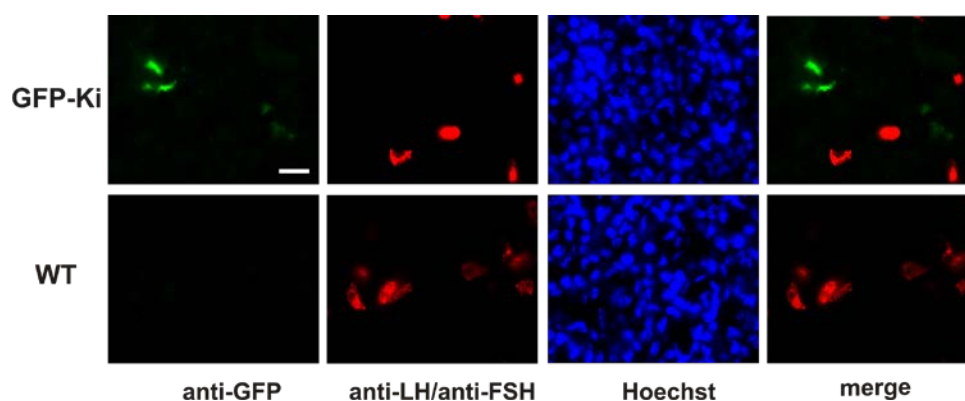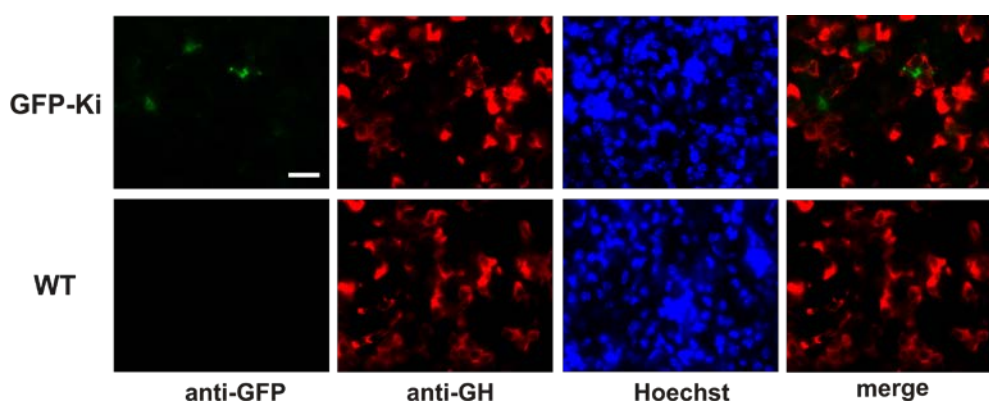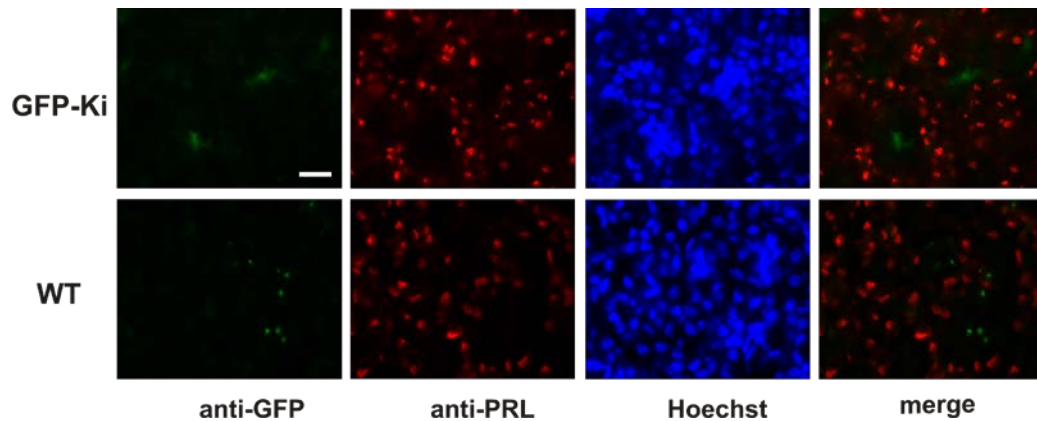
Figure 5-27: Distribution of immunoreactivity to GFP and PRL in the anterior lobe of GFP-Ki and WT pituitaries.
Fluorescence images of 14 µm pituitary sections prepared from GFP-Ki and WT mice and stained with anti-GFP (green), anti-PRL (red) and Hoechst 33258 (blue). Overlay of GFP and PRL staining is shown in the right merged image. Scale bar = 20 µm.

5.3.2.3.2 TRPM3 proteins are expressed in folliculostellate cells of the adenohypophysis

The result that TRPM3 proteins were not detected in any type of endocrine cells (5.3.2.3.1) and the fact that folliculostellate cells are the only remaining cell type present in the anterior lobe raised the idea that TRPM3 proteins might be expressed in these cells. To prove this idea, 14 µm pituitary sections from WT and GFP-Ki mice were stained with antibodies directed against glutamate aspartate transporter (GLAST) and anti-GFP antibodies (Figure 5-28). Staining with anti-GLAST antibodies labelled the soma and the processes of star-shaped cells. Staining with anti-GFP antibodies showed the labelling of the very same cells indicating that TRPM3 proteins are expressed in folliculostellate cells.
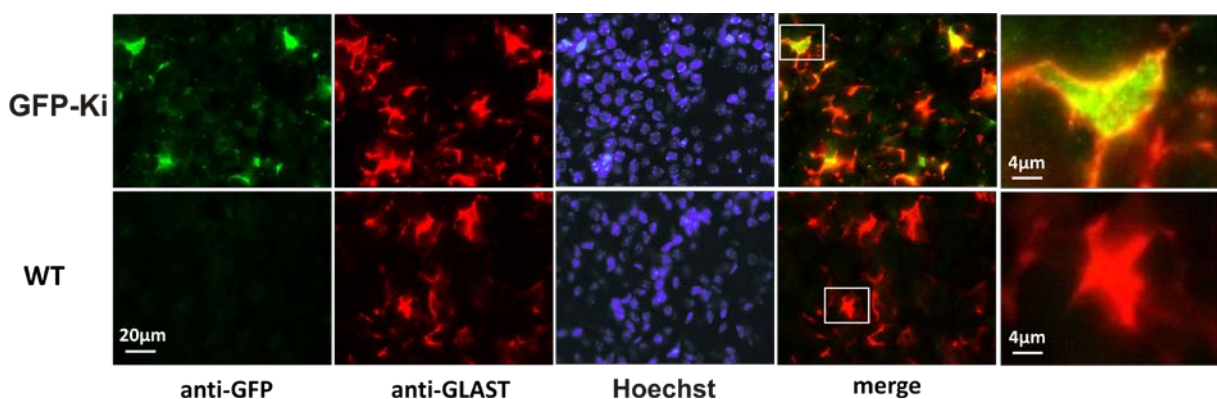
Figure 5-28: Expression of GFP in GLAST positive cells of the anterior pituitary.
Fluorescence images of 14 µm pituitary sections prepared from GFP-Ki and WT mice and stained with anti-GFP (green), anti-GLAST (red) and Hoechst 33258 (blue). Overlay of GFP and GLAST staining is

shown in the merged image. Scale bar = 20 µm. The very right panel show magnifications (scale bar = 4 µm) of single cells highlighted by rectangles in the merged image.

5.3.2.4 Analysis of TRPM3 expression in α-MSH-producing cells of the intermediate lobe

In addition to very rare non-endocrine marginal cells and astrocytes-like cells, the intermediate lobe of the pituitary gland consists mainly of one single endocrine cell type: the melanotrophs. Staining of pituitary slices from wild type mice using anti-TRPM3 antibodies (5.2.2) as well as analysis of GFP expression in pituitary slices from GFP-Ki mice already revealed the presence TRPM3 in the main fraction of intermediate lobe cells, suggesting the presence of TRPM3 in melanotrophs. Melanotrophs release mainly α-melanocyte stimulating hormones (α-MSH) which stimulate the melanocytes to produce melanin. To analyse the expression of TRPM3 proteins in melanotrophs of the intermediate lobe, 14 µm pituitary sections from WT and GFP-Ki mice were stained with antibodies directed against α-MSH (anti- α-MSH) and GFP. Anti-α-MSH antibodies stained most cells of the intermediate lobe of both WT and GFP-Ki pituitaries. The slices also showed faint signals of GFP staining in melanotrophs from GFP-Ki mice that were absent in slices obtained from WT mice indicating the expression of TRPM3 proteins in melanotrophs. However, the GFP signals were weak in comparison to signals obtained from PL (pituicytes, 5.3.2.2.2), which may be related to lower stability of GFP proteins or lower activity of the TRPM3 promoter(s) in these cells.
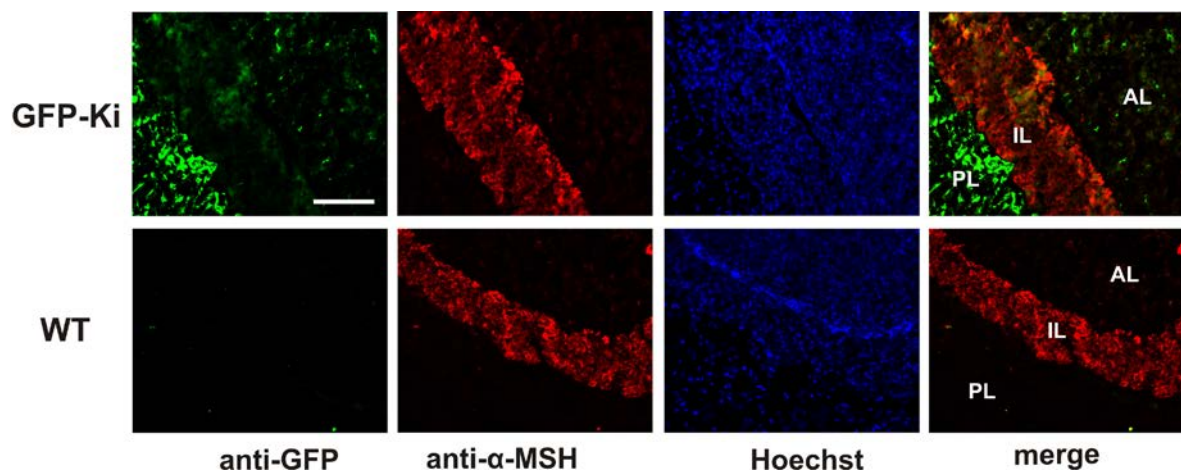
Figure 5-29: Expression of GFP in α-MSH expressing cells of the intermediate lobe.
Fluorescence images of 14 µm pituitary sections prepared from GFP-Ki and WT mice and stained with anti-GFP (green), anti-α-MSH (red) and Hoechst 33258 (blue). Overlay of GFP and α-MSH staining is shown in the right merged image. Scale bar = 100 µm

Co-staining of slices from wild type mice using anti-TRPM3 and anti- α-MSH antibodies was prevented by the fact that both antibodies were raised in rabbits. However, parallel staining of slices obtained from the very same mouse (Figure 5-9) showed strong staining of the intermediate lobe again supporting the finding that TRPM3 is expressed in melanotrophs.
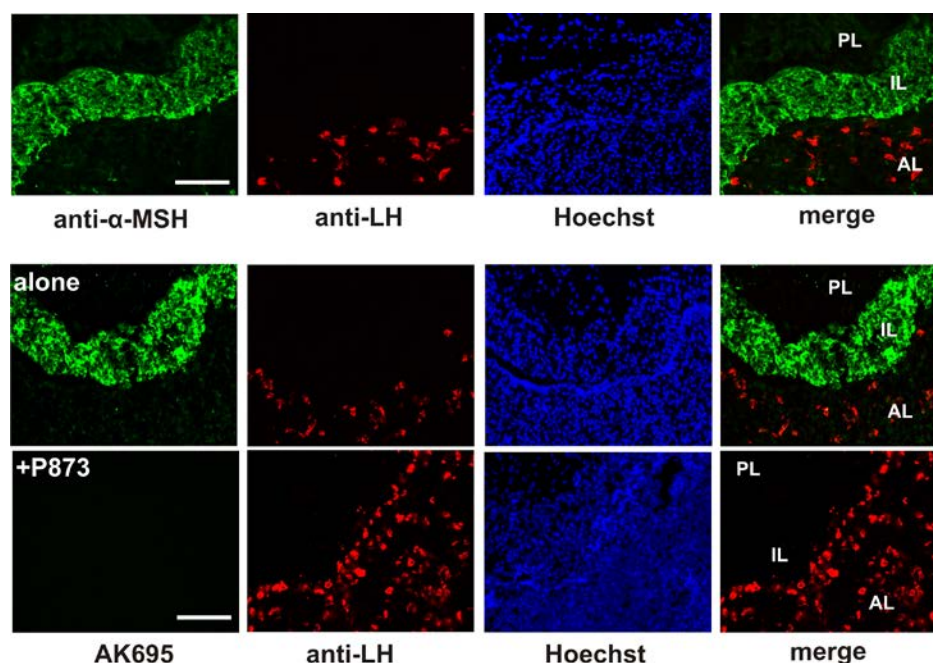
Figure 5-30: Distribution of immunoreactivity to α-MSH, LH and TRPM3 in the pituitary gland of a wild type mouse.
The upper panel show fluorescence images of 14 μm pituitary sections from WT stained with anti-α-MSH (green), anti-LH (red) and Hoechst 33258 (blue). An overlay of α-MSH and α-LH stainings is shown in the right merged image. The middle and the lower panels show fluorescence images of 14 μm sections of the same pituitary stained in parallel with AK695 in the absence or presence of peptide P873 (green), anti- LH (red) and Hoechst 33258 (blue). Overlays of AK695 and α-LH staining are shown on the right. Scale bars = 100 μm.

5.4 Analysis of Pregnenolone Sulfate (PregS)-induced Ca^{2+} signals in pituitary cells

In the latter section (5.3), immunohistochemical experiments indicated the expression of TRPM3 proteins in folliculostellate cells of the anterior lobe, pituicytes from the posterior lobe and finally melanotrophs of the intermediate lobe. In the following section, I investigated the functional role of TRPM3 channels in pituitary cells. TRPM3 proteins form Ca^{2+}-permeable cation channels in the plasma membrane that are activated by the neurosteroid pregnenolone sulfate (PregS, [115]) and efficiently blocked by flavonones like Hesperetin [168]. I analyzed the function of TRPM3 channels in pituitary cells in Ca^{2+} imaging

experiments using the fluorescent Ca^{2+} dye Fura-2. I recorded the changes of the intracellular Ca^{2+} concentration $[Ca^{2+}]_i$ upon application of specific ligands of TRPM3: the agonist PregS and the antagonist Hesperetin. Reactivity of cells to a combination of both ligands was defined as the pharmacological fingerprint of TRPM3 and served as an indicator for the presence of functional TRPM3 ion channels in primary cells.

5.4.1 PregS-induced Ca^{2+} signals in cells of the anterior lobe

The anterior lobe consist of at least six different cell populations and the folliculostellate cells account for ~ 10 % of the anterior lobe cells [1]. I analyzed TRPM3 channel activity in anterior lobe cells of wild type mice (WT) which were compared to control cells from TRPM3-deficient mice (KO). The anterior lobe was dissected from the intermediate/posterior lobe and the cells were prepared as described (4.1.1.2). The cells were loaded with 5 µM Fura-2 AM at 5 % CO_2, 37°C in the dark for 30 min. The measurements were started by perfusion of Ringer solution for 75 s followed by perfusion of a saturating concentration of 100 µM PregS [115] for 300 s. Finally, a concentration high enough to completely block TRPM3 channels of 10 µM Hesperetin was added (Figure 5-31). The application of PregS evoked an increase of $[Ca^{2+}]_i$ in 292 cells from WT mice (Figure 5-31, A and B) whereas the rest of the cells (1101) did not respond. However, in the responding cell population, I observed three different types of responders. 221 cells (15.9 %) also responded to Hesperetin with a clear decrease of the $[Ca^{2+}]_i$. These cells displayed the pharmacological fingerprint of recombinant TRPM3 channels and are therefore defined as TRPM3 expressing cells. In addition to the PregS/Hesperetin-sensitive population, 33 cells were insensitive to the application of Hesperetin and are therefore not considered to express TRPM3 channels. Finally, another minor population of 38 cells showed only a transient response to PregS (Figure 5-31) which declined to steady-state levels before Hesperetin has been applied. These cells may still express TRPM3 channels but may also respond to PregS because of other PregS-sensitive channels like TRPA1 [183]. In contrast to WT cells isolated from the anterior lobe of TRPM3-KO mice were lacking the population sensitive to both PregS and Hesperetin, whereas transient responders and Hesperetin insensitive cells were still detectable (Figure 5-31). These findings confirm the presence of functionally active TRPM3 ion channels in ~ 15 % of the anterior lobe cells.
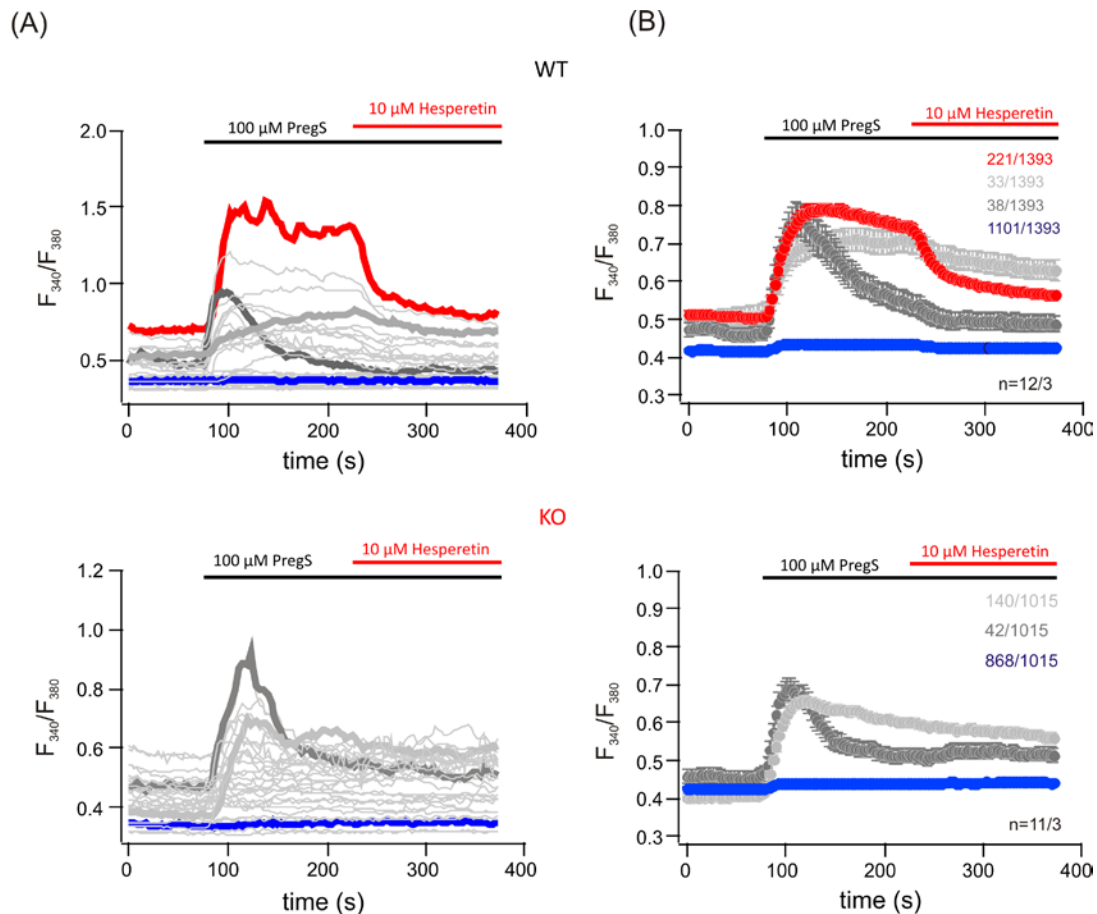
Figure 5-31: Ca^{2+} imaging of anterior lobe cells.
(A) Exemplary measurements of anterior lobe cells prepared from wild type (WT, upper panel) or TRPM3-deficient mice (KO, lower panel) in the presence of Ringer solution, during application of 100 µM pregnenolone sulfate (PregS) and 10 µM Hesperetin. Single traces each belonging to one type of responding cell is highlighted in red, dark gray, light gray and blue. (B) Mean values (± S.E.M) of experiments as shown in (A). The numbers of cells of each cell population/the total number of cells, as well as the number (n) of measurements/experiments are indicated. Note that cells responding to both PregS and Hesperetin are missing in cells prepared from TRPM3-deficient mice.

The presences of PregS-sensitive Ca^{2+} entry pathways in anterior lobe cells unrelated to TRPM3 channels were further analyzed. Cells were pre-incubated with TRPM3 blocker Hesperetin before PregS was applied (Figure 5-32). This treatment was expected to block PregS-induced TRPM3-mediated Ca^{2+} influx while TRPM3-unrelated Ca^{2+} entry pathways remain unaffected. Figure 5-32 shows that PregS induced a comparable increase of [Ca^{2+}]$_i$ in a similar number of both WT and KO anterior lobe cells confirming the presence of additional PregS-sensitive Ca^{2+} entry mechanisms in anterior lobe cells.
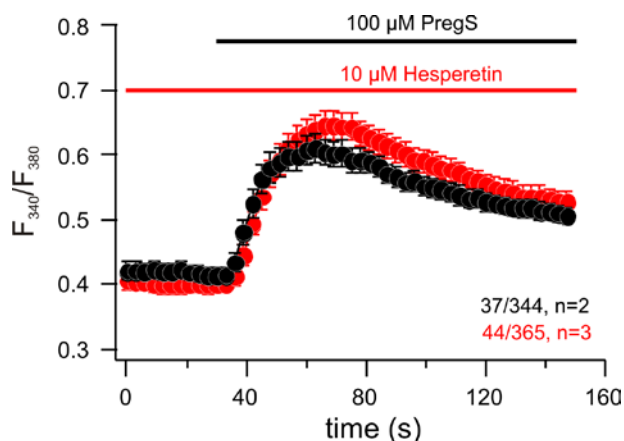
Figure 5-32: Presence of PregS-induced Ca^{2+} entry unrelated to TRPM3 in anterior lobe cells.
Response to Pregnenolone sulfate (PregS) in anterior pituitary cells from wild type (black) and TRPM3-deficient (red) mice after pre-incubation with the TRPM3 blocker Hesperetin. Mean values of 37 and 44 responding cells ± SEM detected in a total number of 344 and 365 WT and KO cells are indicated. The number of measurements (n) is indicated.

5.4.2 PregS-induced Ca^{2+} signals in cells of the intermediate/posterior lobe

Due to the fact that a microscopic separation of the posterior lobe and the intermediate lobe was impossible, the cells from these two lobes were prepared and analyzed together in the following Ca^{2+} imaging experiments and patch-clamp recordings.

5.4.2.1 Immunohistochemical characterization of primary pituitary cells obtained from the intermediate and posterior lobe

First, cells that were prepared as described in (4.1.1.2), were characterized immunohistochemically. Cells were co-stained with anti-α-MSH antibodies, anti-GFAP antibodies and Hoechst 33258 for staining of the nucleus. As shown in Figure 5-33, I found two main populations of cells: 1. α-MSH-positive and GFAP-negative round-shaped cells which were thought to represent melanotrophs derived from the intermediate lobe and 2. α-MSH-negative and GFAP-positive cells with irregular shape thought to represent pituicytes derived from the posterior lobe.
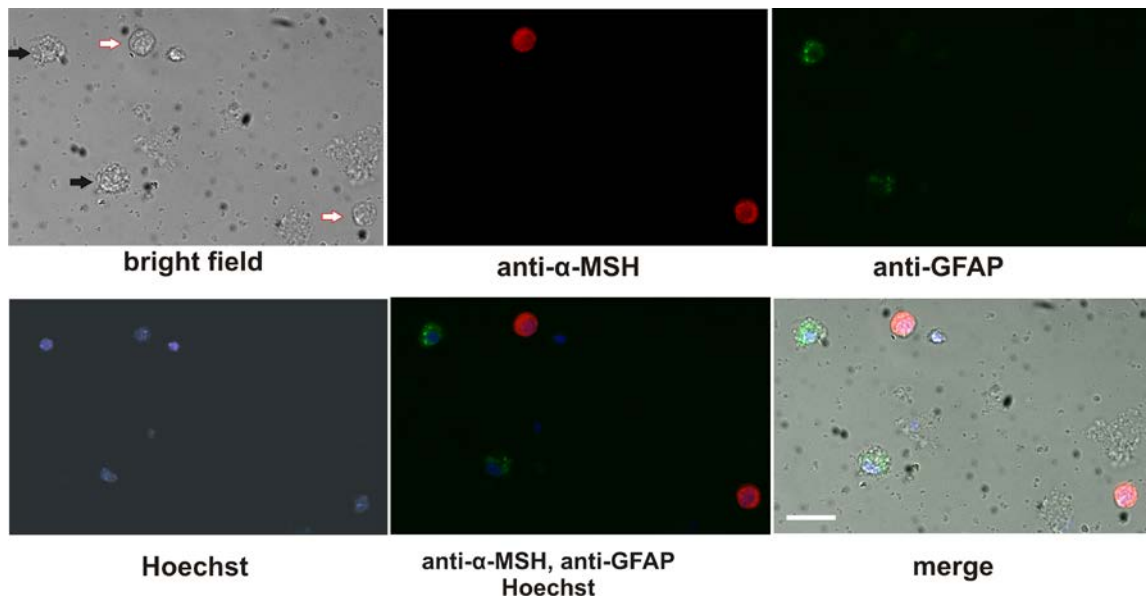
Figure 5-33: Characterization of primary cells obtained from the intermediate/posterior lobe.
Single primary cells from the IL/PL in a bright field microscopic image (upper left) and fluorescence images of the same cells after staining with anti-α-MSH (red), anti-GFAP staining (green) antibodies and Hoechst 33258 (blue) are shown. Merged images of fluorescence stainings (lower middle) and of all images (lower right) are also presented. Round cells are highlighted by white arrows, flat cells by black arrows. Additional nuclei which may belong to dead cells (see merged image) were also detectable. Scale bar = 100 µm.

5.4.2.2 Identification of PregS-sensitive Ca^{2+} entry pathways in cells of the intermediate/posterior lobe

Next, I analyzed in Ca^{2+} imaging experiments whether Ca^{2+} entry pathways which can be activated by PregS exist in cells of the intermediate/posterior lobe (IL/PL). Using the same protocol as described in the previous section (5.4.1), I found within a total number of 179 cells, 61 cells that responded to the application of PregS (Figure 5-34). Within this population of responders, I identified again three subpopulations. The PregS induced increase of [Ca^{2+}]$_i$ in 44 cells was sensitive and effectively blocked by Hesperetin. These cells are therefore defined as TRPM3 expressing cells, which represent 24.5 % of the total number of cells. Cells sensitive to both PregS and Hesperetin were missing in cell population from TRPM3-deficient (KO) mice (Figure 5-34) confirming this definition. Similar to anterior lobe cell preparations, I also found in WT cell preparations, few cells (6/179) which were insensitive to the application of Hesperetin or which responded only transiently to PregS (11/179). These cells were not expected to express TRPM3 but may contain other PregS-sensitive Ca^{2+} entry pathways. Consistent with this idea, these cells were also detectable in cell preparations of TRPM3-deficient mice (Figure 5-34, lower panel and Figure 5-35).

In summary, these experiments demonstrated that in addition to other Ca^{2+} entry pathways, TRPM3 ion channels allow the influx of Ca^{2+} into pituitary cells derived from the intermediate/posterior lobe.
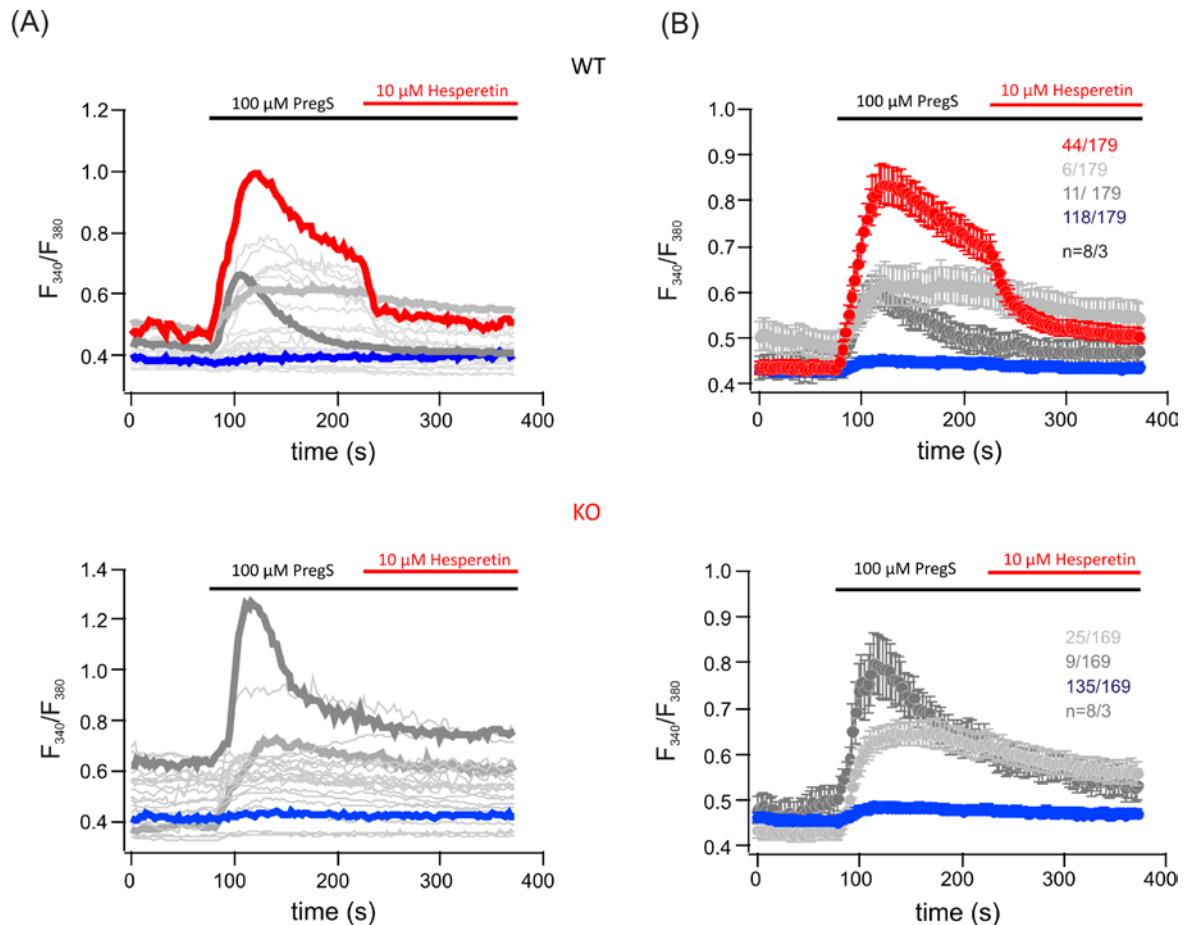
Figure 5-34: Ca^{2+} imaging of intermediate/ posterior (IL/PL) lobe cells.
(A) Exemplary measurements of intermediate/ posterior lobe cells prepared from wild type (WT, upper panel) or TRPM3-deficient mice (KO, lower panel) in the presence of Ringer solution, during application of 100 µM pregnenolone sulfate (PregS) and 10 µM Hesperetin. Single traces each belonging to one type of responding cell is highlighted in red, dark gray, light gray and blue. (B) Mean values (± S.E.M) of experiments as shown in (A). The number of cells of each cell population/the total number of cells, as well as the number (n) of measurements/experiments is indicated. Note that cells responding to both PregS and Hesperetin are missing in cells prepared from TRPM3-deficient mice.
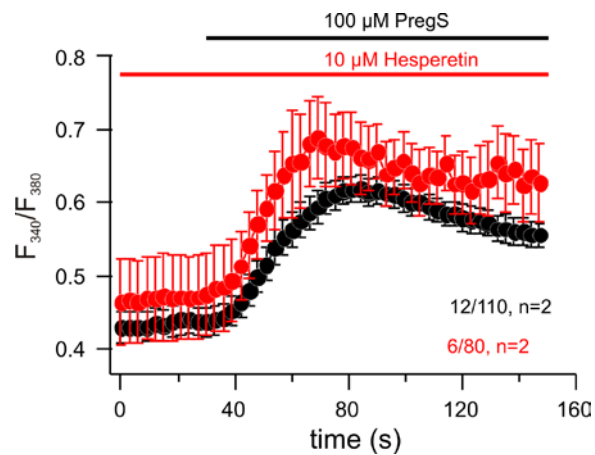
Figure 5-35: Presence of PregS-induced Ca^{2+} entry unrelated to TRPM3 in intermediate /posterior lobe cells.

Response to Pregnenolone sulfate (PregS) in PL/IL cells from wild type (black) and TRPM3-deficient (KO) mice after pre-incubation with the TRPM3 blocker Hesperetin. Mean values of 12 and 6 responding cells ± SEM detected in a total number of 110 and 80 WT and KO cells are shown, respectively. The number of measurements (n) is indicated.

5.4.2.3 Identification of TRPM3-mediated Ca^{2+} entry pathways in melanotrophs of the intermediate lobe

In order to determine the identity of PregS/Hesperetin-sensitive cells in the mixed cell preparation (5.4.2.2), cells derived from IL/PL were plated onto grid coverslips (BELLCO Biotechnology, USA) and analyzed in Ca^{2+}-imaging experiments (Figure 5-36). Subsequent to the measurement, cells were fixed, permeabilized, and stained with anti α-MSH antibodies. The grid on the coverslips allowed the identification of those cells which responded to PregS and Hesperetin. I found that 95.8 % of the responders (46/48) were stained with anti-α-MSH antibodies, whereas no other cells were stained. This experiment provided strong evidence that melanotrophs of the intermediate lobe express active TRPM3 ion channels.
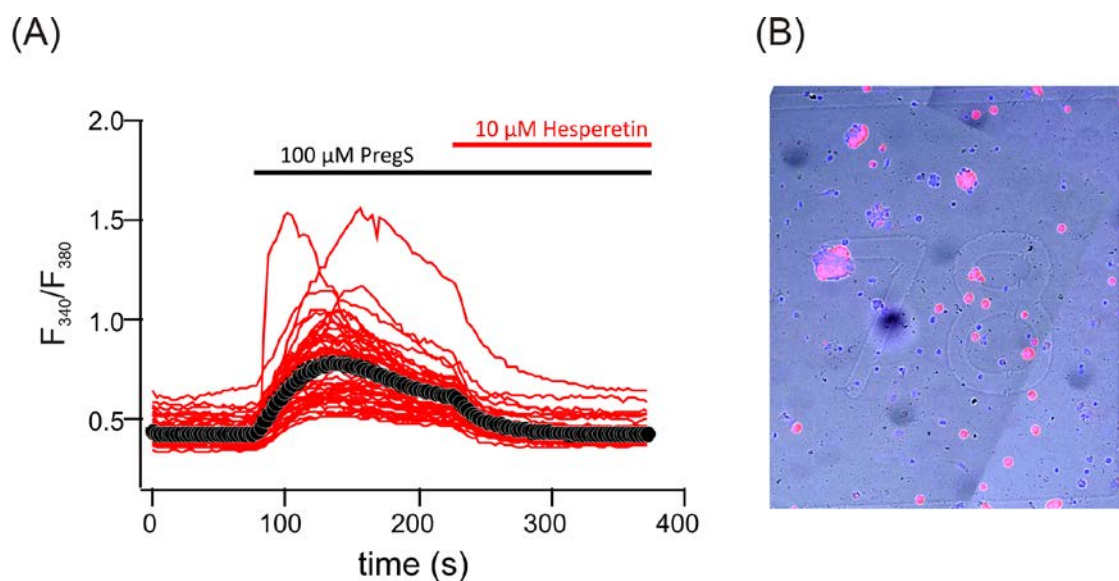
Figure 5-36: α-MSH expressing cells display TRPM3-mediated Ca^{2+} signals.
(A) Cells prepared from the IL/PL were analyzed in Ringer solution, during application of 100 μM pregnenolone sulfate (PregS) and 10 μM Hesperetin. Ca^{2+} signals of 48 cells responding to PregS/Hesperetin (red traces) and their mean ± SEM (black trace) are shown. Non responding cells (69) are not displayed. (B) Merge of a bright field image to visualize the grid on the coverslip, a fluorescence image demonstrating immunoreactivity to α-MSH antibodies (red) and Hoechst 33258 (blue) staining of the cell nuclei.

5.4.2.4 Isolated melanotrophs but not pituicytes display PregS-inducible Ca^{2+} signals

In the preceding section, I could show that α-MSH expressing cells display Ca^{2+} signals that are sensitive to PregS and Hesperetin and are therefore likely to contain active TRPM3 channels. However, only α-MSH-positive cells but not other cells were stained. This raised the question, whether pituicytes which also express TRPM3 transcripts (Figure 5-5, Figure 5-6) and TRPM3 proteins (5.3.2.2.2) contain active TRPM3 channels. To address this question, I chose an alternative approach. Cells prepared from the IL/PL were stained with anti-GLAST antibodies and were separated by fluorescence-activated cell sorting (FACS). Staining with anti-GLAST antibodies (GLAST-positive cells) was attributed to pituicytes, whereas the absence of immunoreactivity to these antibodies (GLAST-negative cells) was attributed to melanotrophs. The cells were sorted onto poly-L-lysine covered coverslips for functional and morphological analysis. In addition, 50 GLAST-positive or GLAST-negative cells were sorted into tubes for analysis of TRPM3 expression by PCR (see 5.1.4).

To allow recovery of cells after sorting, Ca^{2+} imaging experiments were performed as described (5.4.1) 24 h after the sorting procedure. After loading of the cells with Fura-2,

morphological differences were analyzed microscopically (Figure 5-37, A). GLAST-positive cells (pituicytes) looked bigger in size and more flat with processes and extensions whereas GLAST-negative cells were smaller with a round shape (Figure 5-37, A). While all GLAST-negative cells (5) showed clear response to the application of both PregS and Hesperetin, GLAST-positive cells did not respond to the application of 100 µM PregS (Figure 5-37, C and B, respectively). This result again demonstrated the presence of functional TRPM3 channels in melanotrophs (GLAST-negative cells) and also confirmed their absence in pituicytes although these cells express TRPM3 transcripts and proteins. The absence of functional TRPM3 proteins function in pituicytes was proved by additional experiment using the patch-clamp technique (5.5).
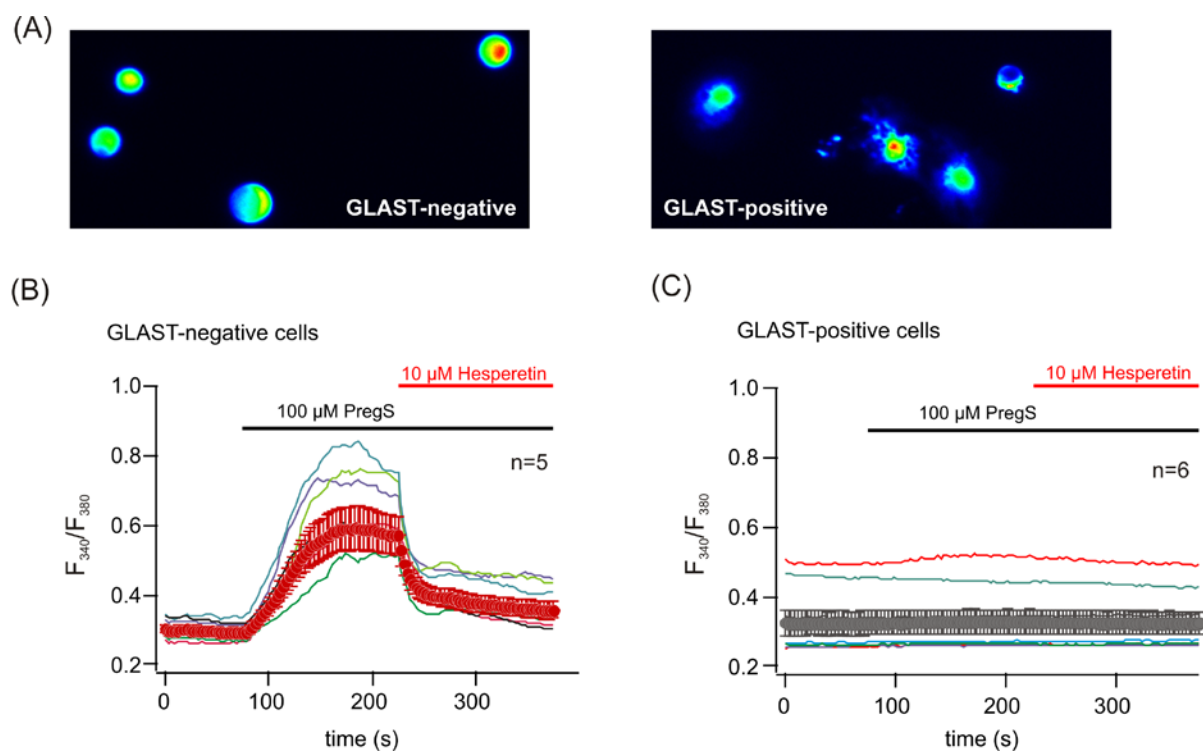
Figure 5-37: Morphological and functional analysis of sorted posterior/intermediate lobe cells. (A) A microscopic view of Fura-2 AM loaded GLAST-negative cells (left) and GLAST-positive cells (right). (B) GLAST-negative cells were analyzed in Ringer solution, during application of 100 µM pregnenolone sulfate (PregS) and 10 µM Hesperetin. Ca^{2+} signals of 5 cells responding to PregS/Hesperetin (colored traces) and their mean ± SEM (red trace) are shown. (C) GLAST-positive cells were analyzed similarly and displayed no response to PregS. Single cells are shown in colored traces and their mean ± SEM as gray trace.

5.4.2.5 Long-term culture of pituicytes did not recover TRPM3 activity

The absence of Ca^{2+} entry into pituicytes after PregS stimulation might be related to the preparation of cells and their culture conditions. Therefore, I tested whether primary "explant"

cultures of pituicytes displayed PregS-inducible Ca^{2+} entry. For that purpose, explant cultures were prepared as described ([172], 4.1.1.2). The cells proliferated and grew for period of at least 12 days. After this time, cells were fixed and stained either with anti-GFAP or anti-S100B antibodies providing evidence of their identity (Figure 5-38, A). Furthermore, I performed Ca^{2+} imaging experiments. Cells were loaded with Fura-2, but again after addition of 100 µM PregS, the cells did not display any change in the intracellular Ca^{2+} concentration (Figure 5-38, B). This experiment demonstrated that living and proliferating pituicytes do not respond to PregS albeit they may express TRPM3 proteins.
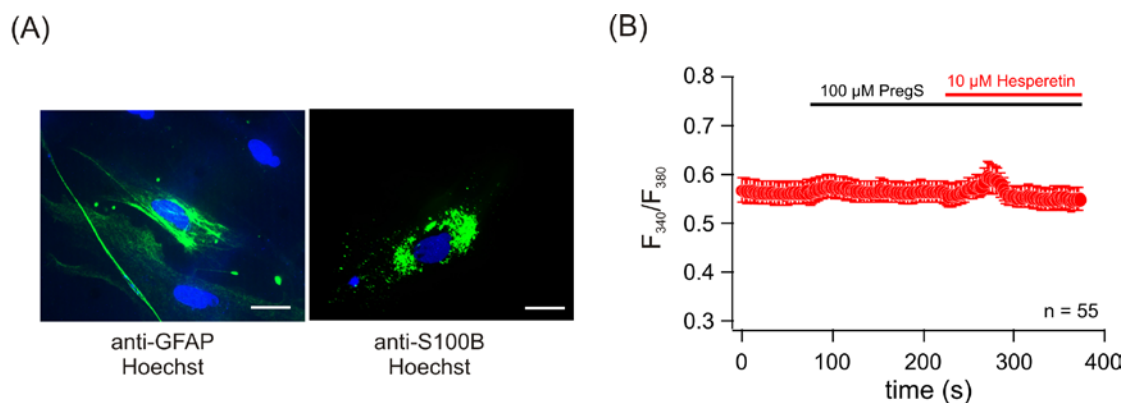
Figure 5-38: Properties of long-term cultures of pituicytes.
(A) Fluorescence images of explant pituicytes cultures stained with anti-GFAP antibodies (left image) or with anti-S100B antibodies (right image) and Hoechst 33258 (scale bar = 100 µm) (B) Cells were analyzed in Ca^{2+} imaging experiments in Ringer solution, during application of 100 µM pregnenolone sulfate (PregS) and 10 µM Hesperetin. The mean ± SEM of 55 cells is shown.

5.4.3 TRPM3-mediated Ca^{2+} entry is preserved in TRPM3-GFP-Ki mice

The targeting strategy to generate GFP-Ki mice included the fusion of exon 24 to the splice acceptor site of the IRES-GFP cassette which would lead to a frame shift of the TRPM3 reading frame and a premature stop of translation. However, I observed in the pituitaries of mice homozygous for the L3F1 (GFP-Ki) allele that long TRPM3 proteins similar in size to the recombinant TRPM3α2 proteins are still expressed (5.3.1.2). Consisting with that finding, PCR analysis revealed splicing of exon 24 to exon 25, preserving the TRPM3 reading frame (5.3.1.3). Therefore, I tested in Ca^{2+} imaging experiments whether active TRPM3 channels are still present in pituitary cells (Figure 5-39). Cells from the anterior lobe and from the intermediate/posterior lobe of TRPM3[GFP-Ki/GFP-Ki] mice both showed a reliable number of cells which displayed PregS-induced Ca^{2+} entry which was blocked by the addition of Hesperetin. This finding demonstrates that active TRPM3 channels are present in the pituitary of GFP-Ki

mice. Although the IRES-GFP cassette is spliced out from the primary TRPM3 transcript (Figure 5-12), the cells express in addition to TRPM3 the GFP protein.
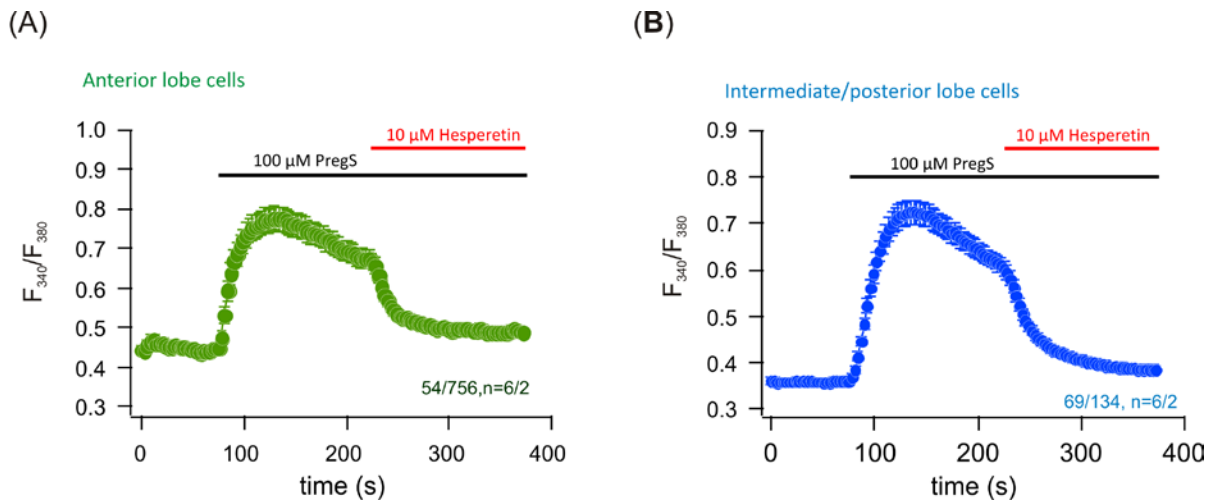
Figure 5-39: Ca^{2+} imaging of pituitary cells from mice homozygous for the L3F1 allele (TRPM3$^{GFP-Ki/GFP-Ki}$).
Ca^{2+} signals in anterior lobe cells (A) and intermediate/posterior lobe cells (B) from GFP-Ki mice in the presence of Ringer solution, during application of 100 µM pregnenolone sulfate (PregS) and 10 µM Hesperetin. Mean values ± SEM are displayed of 54 and 69 cells detected in 756 and 134 anterior and intermediate/posterior lobe cells, respectively. The number of measurements (n) is indicated.

5.5 Analysis of ionic currents in pituitary cells of the intermediate and the posterior lobe (Dr. Beck)

The results of the preceding chapters provided strong evidence that TRPM3 proteins are expressed in melanotrophs of the intermediate lobe (5.3.2.4), and pituicytes of the posterior lobe (5.3.2.2.2). However, Fura-2 measurements of the IL/PL cell preparations indicated that only round and smooth cells that were stained with anti-α-MSH antibodies responded to PregS and Hesperetin (5.4.2), whereas sorted flat and irregular pituicytes which were stained with anti-GLAST antibodies did not (Figure 5-37). In the following chapter, we characterized the biophysical properties of ionic currents of these two cell populations by whole-cell patch-clamp recordings. The electrophysiological experiments were kindly performed by Dr. Andreas Beck.

5.5.1 Characterization of voltage-gated ionic currents in IL/PL cell preparations

In the culture of primary intermediate and posterior lobe cells, the only endocrine cells were the melanotrophs (Figure 5-33), which has been shown to express different types of voltage-activated sodium channels [3].

To characterize the primary cells electrophysiologically and to distinguish melanotrophs and pituicytes not only by their morphology, but also by their biophysical properties, voltage ramps from -100 to +100 mV over 50 ms duration were applied in the whole-cell configuration at 0.5 Hz starting from a holding potential (Vh) of -80 mV (Figure 5-40).

Round cells (Figure 5-40, A) displayed voltage-dependent inward currents when the cells were depolarized to ~ -40 mV which inactivated at a membrane potential of ~ -10 mV (Figure 5-40, B). When the holding potential between the ramps was increased to 0 mV these inward currents disappeared (Figure 5-40, C). The current/voltage relationship at Vh = -80 mV (Figure 5-40, B) and the absence of the current at Vh = 0 mV (Figure 5-40, C) strongly resembled typical features of voltage-gated Na^+ channels and confirm the identity of these cells as melanotrophs. In contrast, application of the same protocol to the irregular-shaped cells (Figure 5-40, D) did not reveal any current, indicating the absence of voltage-gated Na^+ channels in these cells (Figure 5-40, E and F).

To ensure the identity of Na_V channels in the round-shaped melanotrops, whole-cell patch-clamp experiments were performed in the absence of extracellular Na^+ (replaced by 140 mM N-Methyl-D-glucamin, NMDG). Removal of extracellular Na^+ led to a complete disappearance of the inward current (Figure 5-41, A) whereas removal of Ca^{2+} did not change the appearance of the voltage-activated inward current (Figure 5-41, B). These experiments proof that the voltage-activated inward current seen in the melanotrophs are mediated by Na_V channels.
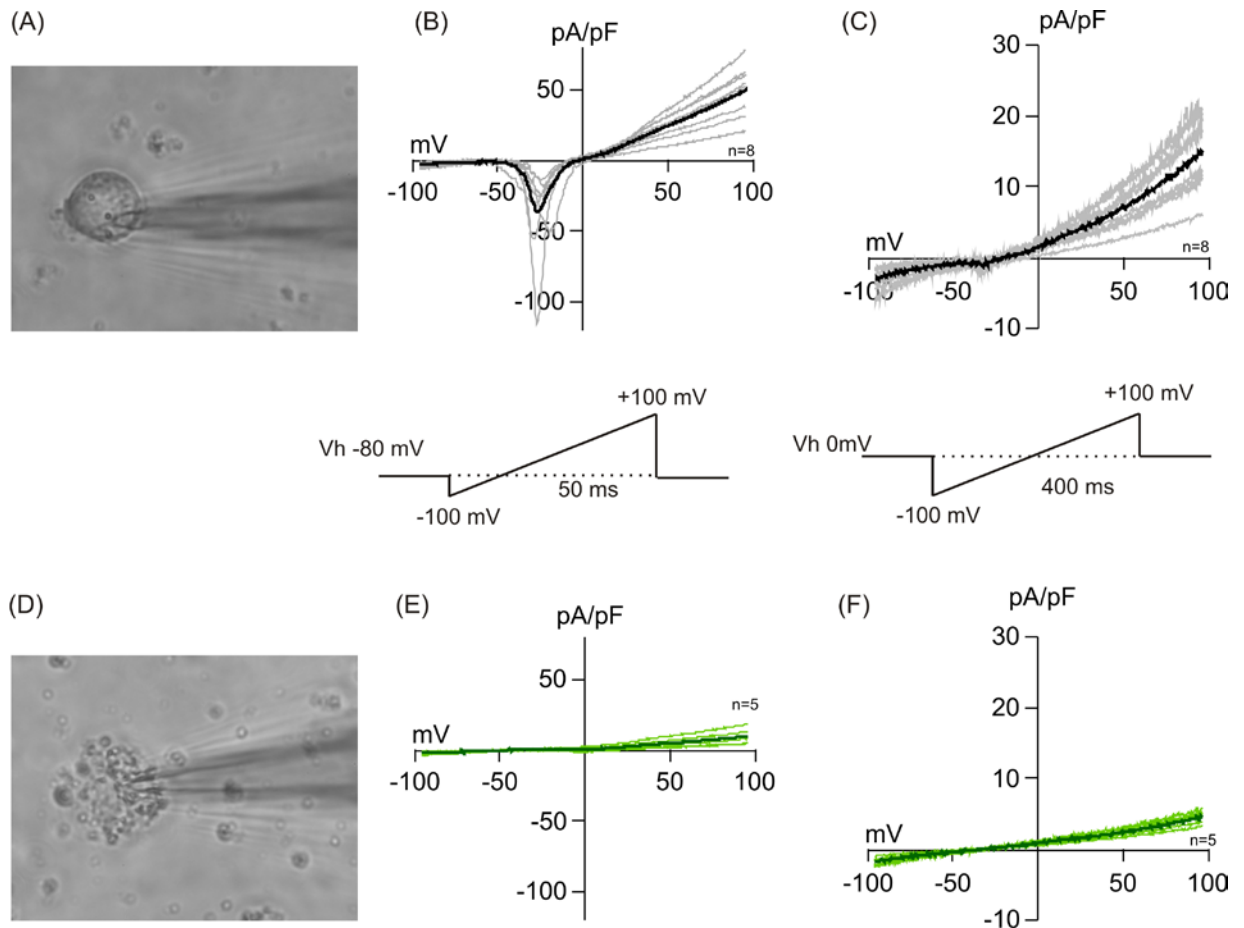
Figure 5-40: Morphological and electrophysiological properties of posterior and intermediate lobe cells.
Round cells (A) and flat, irregular-shaped cells (D) were patched (whole-cell configuration) and currents were measured during the application of voltage ramps from -100 mV to +100 mV within 50 ms starting from a holding potential (Vh) of -80 mV (B,E), or within 400 ms starting from Vh of 0 mV (C,F). Thick traces indicate the mean of the single traces (gray, B, C, and green, E, F). Flat cells neither revealed Na_V currents at a holding potential of -80 mV (E) nor the outward rectifying current, seen in round cells. n indicates the number of measured cells.
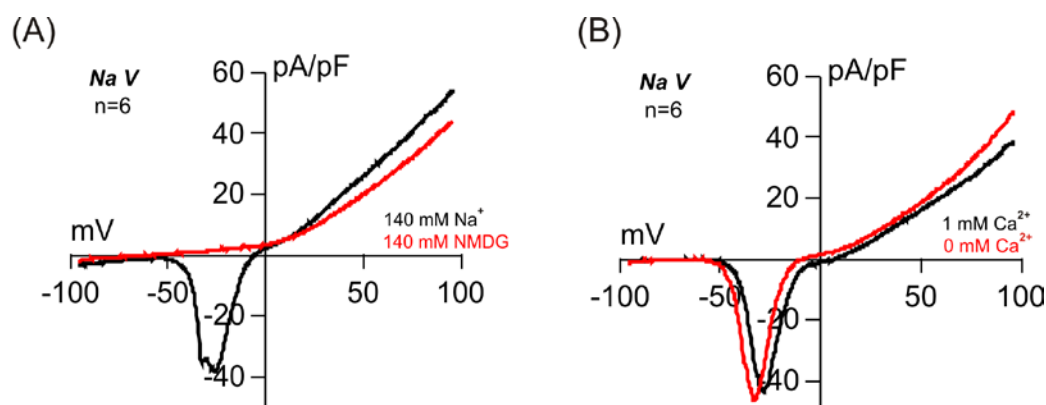
Figure 5-41: Identity of Na$_V$ channels.
(A) Current-voltage relationships (IVs) of whole-cell currents in round cells measured as described before (Figure 5-40, B) in the presence of 140 mM extracellular NaCl (black trace) and after replacement of Na$^+$ by 140 mM NMDG (red trace). (B) Current-voltage relationships (IVs) of Na$_V$ currents in round cells in the presence (black trace) and absence (red trace) of 1 mM extracellular Ca^{2+}, both in the presence of extracellular Na$^+$.

5.5.2 Identification of TRPM3-mediated ionic currents in primary melanotropic cells

Immunohistochemistry (5.3.2.4) and PCR-analysis (5.1.4) as well as Ca^{2+}-imaging experiments of isolated GLAST-negative cells (5.4.2.4), revealed the presence of functional TRPM3 ion channels in melanotrophs. We confirmed this finding and analyzed the biophysiological properties of endogenous TRPM3 channels in the melanotrophs by whole-cell patch-clamp experiments (Figure 5-42). After break-in into round shaped-cells, Na$_V$ currents were measured as described in 5.5.1 to identify the cell as melanotroph. Subsequently, a voltage ramp protocol was applied as described in Figure 5-40, C and ionic currents were challenged by perfusion of 100 µM PregS. As shown in Figure 5-42, strong outward currents and small inward currents appeared upon PregS application resembling the typical current-voltage (IV) relationship described for TRPM3 channels ([103], Figure 5-42, A, B). In addition, the PregS-induced currents were readily inhibited by 10 µM Hesperetin, and thus, displayed the pharmacological fingerprint of recombinant TRPM3α2 channels [115,118]. Current-voltage relationship and inhibition of the PregS-induced currents by Hesperetin strongly indicate the expression of functional TRPM3 channels in these cells. Again, flat and irregular-shaped pituicytes did not show any response to PregS (Figure 5-42, C, D).
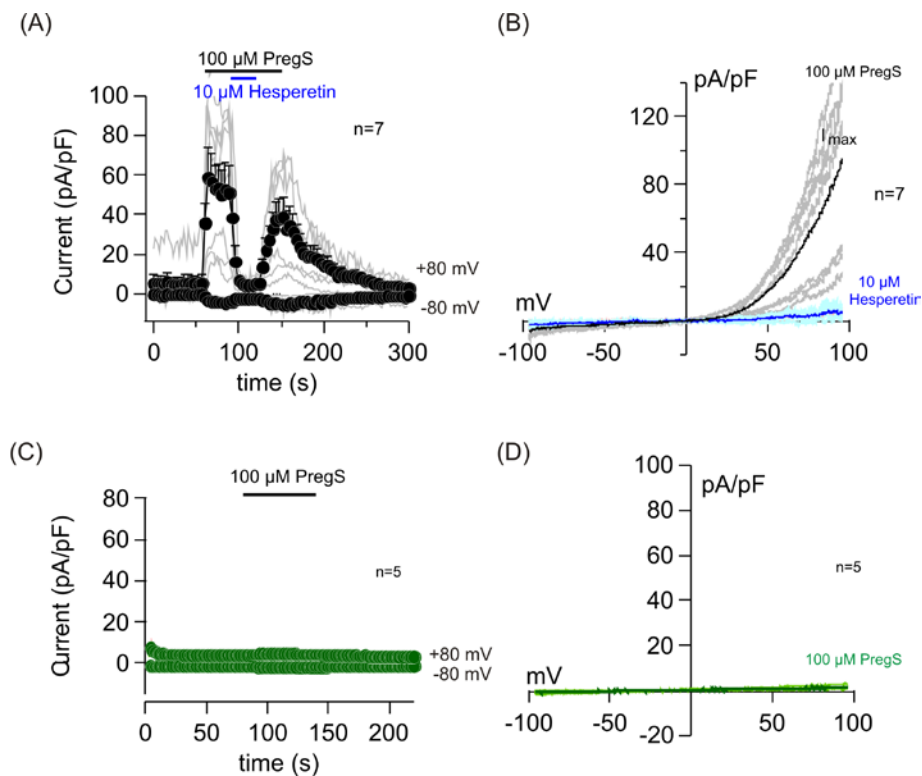
Figure 5-42: PregS-induced currents in primary cells of the intermediate/posterior lobe cells of the pituitary.

(A, C) Inward and outward currents at -80 and +80 mV, respectively, measured in melanotrophs (A) and pituicytes (C) during the application of 100 µM PregS, and in (A), 10 µM Hesperetin. Basic currents right before PregS application were subtracted. B and D depict the respective current-voltage relationships (IVs) of the net current induced by 100 µM PregS in melanotrophs (B, single experiments in gray and mean in black) and pituicytes (C, single experiments in light green and mean in green). Hesperetin inhibited the PregS-induced currents in melanotrophs (A, B). The IVs of the remaining currents in A are shown in B (single experiment in light blue and mean in blue). Data represent means (± SEM) of the indicated number of experiments (n).

TRPM1, the closest relative of TRPM3, may also be activated by PregS [109]. To rule out any contribution of TRPM1 channels to the PregS-induced currents in melanotrophs, we applied 100 µM Zn^{2+}, which has been shown to inhibit TRPM1 but not TRPM3 [109], during the presence of the PregS-induced current. As shown in Figure 5-43, we found almost no change of the PregS-induced currents in melanotrophs when 100 µM Zn^{2+} was added. Furthermore, TRPM1 transcripts were not detectable in these cells (5.1.4).
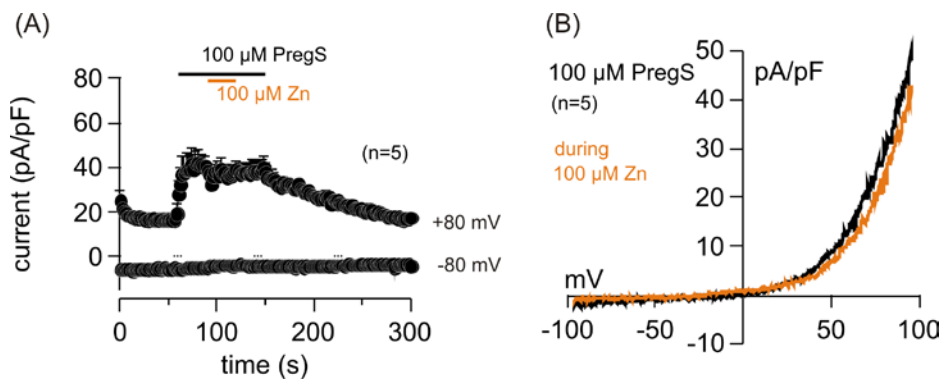
Figure 5-43: PregS-induced currents are not inhibited by zinc ions in melanotropic cells.
(A) Inward and outward currents measured at -80 and +80 mV, respectively, during application of 100 µM PregS and 100 µM Zn^{2+}. (B) Current-voltage relationships of the net PregS-induced current (basic currents subtracted) before (black) and in the presence of 100 µM Zn^{2+} (red). Data represent means (± SEM) of the indicated number of experiments (n).

To further proof the identity of the PregS/Hesperetin-sensitive currents in melanotrophs as TRPM3-dependent, we isolated melanotrophs from TRPM3-deficient mice (KO, Figure 5-44). The whole-cell patch-clamp experiments, revealed no difference in the appearance of the voltage-gated Na^+ currents in melanotrophs from both genotypes (Figure 5-44, A, D). However, in contrast to melanotrophs isolated from wild type mice (Figure 5-44, B, C), melanotrophs isolated from TRPM3-deficient mice (Figure 5-44, E, F) did not reveal any current upon application of 100 µM PregS.

This data prove the presence of functional TRPM3 channels in melanotrophic cells of mouse pituitary.
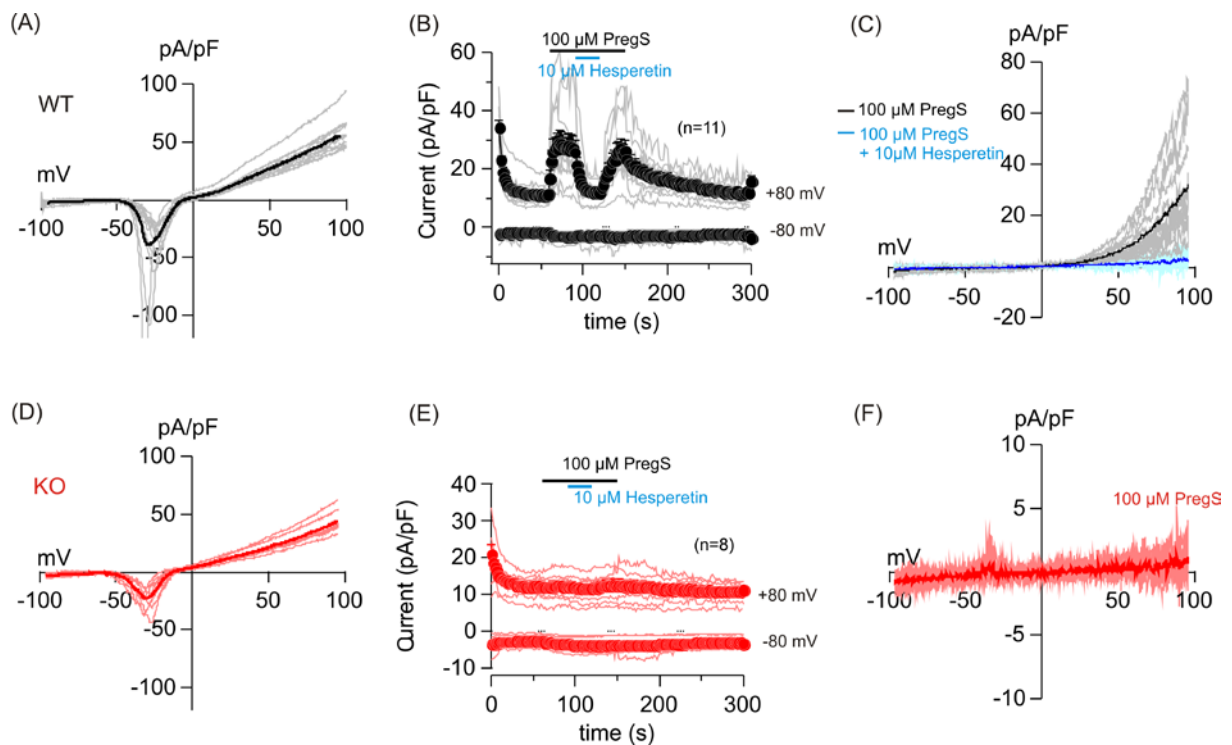
Figure 5-44: PregS-inducible currents are absent in melanotrophs isolated from TRPM3-deficient (KO) mice.

(A, D) Current-voltage relationships (IVs) of Na_V currents measured as described in Figure 5-40, B in melanotrophs from WT (A) and TRPM3-KO mice (D). (B, E) Inward and outward currents at -80 and +80 mV, respectively, measured in WT cells (B) and TRPM3-KO cells (E) during the application of 100 µM PregS, and 10 µM Hesperetin. (C) and (F) depict the respective current-voltage relationships (IVs) of the net measured current (basic currents subtracted) induced by 100 µM PregS in WT cells (B, single experiments in gray and mean in black) and TRPM3-KO cells (single experiments in light red and mean in red). Hesperetin inhibited the PregS-induced currents in WT cells (B, C). The IVs of the remaining current is shown in C (single experiments in light blue and mean in blue). Data represent means (± SEM) of the indicated number of experiments (n). The amplitude of the PregS-induced currents in WT melanotrophs were slightly smaller than in the experiment shown in (Figure 5-42, A, B). This might be due to the different internal solutions used in both experiments. Experiments in Figure 5-42 were done using Cs-glutamate in the patch pipette and in the present experiment Cs-methanosulfonate was used.

6   Discussion

The current work aimed at the identification of TRPM3 proteins in mouse pituitary gland and the definition of pituitary cell types expressing these proteins.

Using GFP-Ki mice and a collection of cell type-specific antibodies, I identified three types of cells that express TRPM3 proteins.

1. Folliculostellate cells of the adenohypophysis which form a signaling network connected by gap junctions and which are considered to be non-secretory cells.
2. Pituicytes, which are glial cells of the neurohypophysis that mainly assist in the storage and release of hypothalamic hormones.
3. Melanotrophs of the intermediate lobe that release α-MSH into the blood.

I also aimed at the determination of TRPM3-mediated Ca^{2+}-signals and TRPM3 currents in pituitary cells in order to elucidate the physiological role of TRPM3 channels in the hypophysis. Using a combination of the TRPM3 agonist PregS and the antagonist Hesperetin, I dissected TRPM3-mediated Ca^{2+} signals in cell preparations of both the anterior lobe and the intermediate/posterior lobe demonstrating the activity of native TRPM3 channels in both regions of the hypophysis and confirming the results of the immunohistochemical experiments. Finally, characterization of PregS/Hesperetin-sensitive currents in primary melanotrophic cells proofed the presence of functional TRPM3 channels.

6.1   Possible roles of TRPM3 channels in folliculostellate (FS) cells of the anterior lobe

Fura-2 measurement of anterior pituitary cells uncovered Ca^{2+}-signals (5.4.1) that were activated by PregS and inhibited by Hesperetin. Thus, these cells displayed the pharmacological fingerprint of recombinant TRPM3 channels and therefore it is reasonable to sugesst that these signals were mediated by TRPM3 channels. 15 % of the cells displayed such a phenotype, which is in good agreement with the number of folliculostellate (FS) cells described in pituitary gland [1]. This functional observation was strongly supported by my immunohistochemical results. First, no hormone secreting cell population within the adenohypophysis matched to the GFP-fluorescence observed in pituitaries of GFP-Ki mice. Vice versa, glutamate aspartate transporter (GLAST) proteins have been described to be expressed on the surface of FS cells [8] and cells stained with anti-GLAST antibodies co-

stained with anti-GFP antibodies in these mice. Thus, it is reasonable to conclude that TRPM3 proteins build Ca^{2+}-permeable ion channels in FS cells.

FS cells are known to form a three dimensional cell network connected by gap junctions [5]. This network was shown to carry Ca^{2+} waves and other small diffusible molecules over long distances in the millimeter range providing a communication system between anterior lobe cells. It has been described that the initiation of this Ca^{2+} waves is dependent on the activity of voltage-activated Na^+ and Ca^{2+} channels expressed in these cells [9]. Na^+ and Ca^{2+} influx through TRPM3 channels might increase the membrane potential and may facilitate the activation of voltage-activated channels. This way TRPM3 channels may contribute to the propagation of Ca^{2+} waves through the FS cell network.

FS cells influence the release of FSH from gonadotrophs [55,184]. Binding of pituitary adenylate cyclase-activating peptide (PACAP) to its receptor on FS cells stimulates transcription of the follistatin gene through cyclic adenosine monophosphate/protein kinase A (PKA) signaling. TRPM3 might be involved in this process in a hitherto undiscovered manner. Since follistatin is known to reduce FSH-release from gonadotrophs of the pituitary, TRPM3 might have an indirect regulatory influence upon ovulation [184].

Vascular endothelial growth factor (VEGF) is a signal protein that stimulates vasculogenesis and angiogenesis and has been implicated as an important factor in tumorigenesis such as in mamma carcinoma [185,186]. Therefore, VEGF has been recognized as a drug target to treat solid tumors and a number of anti-VEGF antibodies such as bevacizumab and ranibizumab have been developed as anti-tumor drugs [186]. The secretion of vascular endothelial growth factor (VEGF) from FS cells has been shown to be Ca^{2+}-dependent [187]. Ca^{2+} influx through TRPM3 might trigger the release of VEGF and contribute this way to disease development. Agonists of TRPM3 such as Hesperetin and isosakuranetin [118,168] may reduce TRPM3-dependent VEGF release from FS cells and may finally represent an alternative approach for the treatment of solid tumors.

6.2 Possible roles of TRPM3 channels in pituicytes of the neurohypophysis

Immunohistochemical analysis of the posterior lobe revealed that neither vasopressin (VP)- nor oxytocin (OXT)-releasing nerve terminals matched to GFP staining of the posterior lobe indicating that TRPM3 proteins are absent in nerve endings of the neuropituitary. Pituicytes, a subtype of astrocytes in the pituitary gland [188], are known to express GLAST, GFAP and

S100B proteins [8,182]. I found that cells stained with anti-GLAST antibodies were co-stained with anti-GFP antibodies indicating that TRPM3 is expressed in the pituicytes. However, the colocalization displayed a spectrum of coloration due to the difference in intensity of each immune reaction. Therefore, the identity of these green cells was confirmed by co-staining of both GFAP and S100B antibodies. I found that all GFP-positive cells were immunoreactive to anti-S100B antibodies. On the other hand, there were cells which were GFP-positive but did not show staining with anti-GFAP antibodies. This finding is in good agreement with the fact that two types of pituicytes including parenchymatous and fibrous pituicytes exist [182]. The parenchymatous pituicytes have been shown to be immunoreactive to both anti-GFAP and anti-S100B antibodies but the fibrous pituicytes are only immunoreactive to anti-S100B antibodies [182]. In contrast to my immunohistochemical results indicating the presence of TRPM3 in pituicytes, these cells did not respond to PregS. This unexpected finding was confirmed by three individual approaches:

1. The posterior/intermediate lobe (PL/IL) and the anterior lobe (AL) could be easily separated from each other under the stereomicroscope [189]. However, the intermediate lobe was always tightly attached to the posterior lobe and could not be removed. Cell preparations of the PL/IL contained mainly two types of cells which could be already distinguished by their shape: round cells and flat star-shaped cells (Figure 5-37, Figure 5-40). Co-staining with anti-α-MSH and anti-GFAP antibodies identified round cells as melanotrophs and flat cells as pituicytes (Figure 5-33). Fura-2 imaging experiments demonstrated that the round-shaped melanotrophs responded to PregS whereas the flat shaped pituicytes did not. The identity of the analyzed cells was reconfirmed by staining of the very same cells on a grided coverslip (Figure 5-36).

2. Patch-clamp recordings of the round cells identified Na^+-currents mediated by voltage-activated Na_V channels (Figure 5-40). These channels have already been described in melanotrophs [3] confirming that the round cells represent melanotrophs and the voltage-gated Na^+ currents were taken as independent functional indicator of the identity of melanotrophs. Without any exception all Na_V-positive cells displayed currents in response to PregS that were absent in the presence of Hesperetin (Figure 5-42). However, measurements of the flat cells within the preparations did never show any response to PregS.

3. I made use of fluorescence-activated cell sorting (FACS) to separate GLAST-positive pituicytes from GLAST-negative cells and analyzed these cells in calcium imaging experiments. GLAST-positive cells did not respond to PregS in contrast to GLAST-

negative cells (Figure 5-37). Thus although pituicytes do express TRPM3, they do not respond to PregS.

The most probable reason for such a behavior was, that the pituicytes did not survive the cell preparation process. However, pituicytes (I) immediately responded to a change of the extracellular Ca^{2+} concentration (not shown); (II) showed reasonable low basal currents after break-in with the patch pipette (Figure 5-40) and (III) could be kept in culture for 8-12 days [48]. In culture, the cells proliferated but still did not respond to PregS (Figure 5-38). Another explanation for the lack of a PregS response could be that the TRPM3 isoforms expressed in pituicytes form non-functional channels or channels that are impermeable for Ca^{2+}. However, PCR analysis of GLAST-positive cells isolated by FACS indicated that the TRPM3 transcripts expressed in these cells encode channels with a Ca^{2+}-permeable pore [103] and which do not lack the ICF-region that is indispensable for channel function [111].

Thus it remains an open question, whether functional TRPM3 channels are present in pituicytes and how they get activated. There is still an ongoing debate, if PregS is really a physiological ligand of TRPM3 channels and additional modulators of TRPM3 activity have been identified recently [163]. Perhaps, additional or other stimuli like D-erythrosphingosine [161], increased temperature [105] and hypoosmotic extracellular conditions [101] are necessary to activate TRPM3 channels in pituicytes and need to be tested in the future.

Indirect evidence supports the idea that TRPM3 may be involved in one of the key functions of pituicytes, which is the regulation of vasopressin and oxytocin release by hypothalamic nerve terminals. Under resting conditions, pituicytes form a physical barrier between axon terminals and blood vessels thereby reducing hormone availability. Under stress such as dehydration or parturition, pituicytes undergo morphological changes and retract from the vessels leading to an increased hormone output from the axons into the blood [10,48]. This process is called "stellation" and has been studied *in vitro* using explant cultures of primary pituicytes. Adenosine has been found to induce stellation of pituicytes after activation of A1 adenosine receptors but this process is independent of the intracellular calcium concentration since it also happens when $[Ca^{2+}]_i$ is buffered with BAPTA [172]. However, released vasopressin acts on V1a-vasopressin receptors present on the surface of pituicytes resulting in an increase of $[Ca^{2+}]_i$ and a subsequent taurine release which acts as a negative feedback inhibitor of VP release from the nerve terminals [46,48]. Taurine release from pituicytes has also been shown to be induced under hypotonic conditions, but hypotonic solutions were not able to evoke calcium signals in the cells [172]. When $[Ca^{2+}]_i$ was buffered with BAPTA, both the vasopressin and the hypotonicity induced taurine release was blocked.

These findings suggest that Ca^{2+} plays an important role in pathways underlying taurine release [48]. TRPM3 channels may coordinate the different stimuli involved in taurine release and may only get active under hypotonic conditions after binding of vasopressin to its receptors.

6.3 TRPM3 is expressed in melanotrophs and may contribute to the release of α-MSH and other hormones

In the intermediate lobe of GFP-Ki mice, immunohistochemical staining using anti-GFP antibodies and anti-α-MSH antibodies indicated the expression of TRPM3 in α-MSH-producing melanotrophs (Figure 5-29). The expression of TRPM3 in melanotrophs was confirmed using anti-TRPM3 antibodies (AK695) which strongly labelled the whole intermediate lobe of the gland similar to anti-α-MSH antibodies (Figure 5-30). Both Fura-2 measurements and patch-clamp recordings confirmed this finding and demonstrated functionally active TRPM3 channels in these cells (5.4.2.4, 5.5):

- Almost all cells which displayed Ca^{2+} signals in response to PregS and Hesperetin were stained with anti-α-MSH antibodies (Figure 5-36).
- PregS inducible Ca^{2+}-signals that were sensitive to Hesperetin were absent in IL/PL cell preparations of TRPM3-deficient mice (Figure 5-34)
- GLAST-negative cells isolated by FACS showed the typical morphology of melanotrophs, responded to both PregS and Hesperetin (Figure 5-37) and contained TRPM3 transcripts (Figure 5-5).
- Round cells prepared from IL/PL showed both voltage-activated Na^+ currents and PregS induced currents which displayed a current/voltage relationship (Figure 5-42) highly similar to currents through recombinant TRPM3 channels [103]. These currents were absent in both the presence of Hesperetin and in cells obtained from TRPM3-deficient mice.

Melanotrophs release α-MSH, which fulfills important physiological functions including melanogenesis, inflammation, energy homeostasis, appetite regulation and inhibition of food intake [35,38,39,190]. POMC precursor peptides undergo proteolytic cleavage resulting in the formation of α-MSH, β-endorphin and other regulatory peptides. It has been described that gene expression of POMC as well as its cleavage by prohormone convertase are Ca^{2+}-dependent [191-193]. Furthermore, hormone peptides are packaged in secretory vesicles and are released by Ca^{2+}-dependent exocytosis [62]. Ca^{2+} influx through TRPM3 might be

important in one or more of the processing steps of POMC as well as in the release of α-MSH.

Outlook

It would be exciting to investigate the influence of TRPM3 upon α-MSH release eg. by enzyme-linked immunosorbent assay (ELISA). One could ask whether the activation of TRPM3 with PregS could increase the release of α-MSH. Furthermore, one could compare α-MSH release or the amount of α-MSH inside the cell between wild type and TRPM3-deficient mice. Preliminary data of ELISAs and bead-based immunoassays (not shown) indeed indicated that TRPM3 participates in the production and/or the release α-MSH from primary melanotrophs. The amount of α-MSH was increased in the supernatant of PregS-treated cells but not in the presence of Hesperetin. Furthermore, the α-MSH concentrations in the supernatant of melanotrophs prepared from TRPM3-deficient mice (KO) was strongly reduced as was the amount of β-endorphin. Thus, TRPM3 may not only be important for the release of α-MSH but also for the release of β-endorphin.

7 References

1. Perez-Castro, C., Renner, U., Haedo, M. R., Stalla, G. K. & Arzt, E. (2012) Cellular and molecular specificity of pituitary gland physiology. *Physiol Rev* 92, 1-38.
2. Cheung, C. C. & Lustig, R. H. (2007) Pituitary development and physiology. *Pituitary* 10, 335-350.
3. Stojilkovic, S. S., Tabak, J. & Bertram, R. (2010) Ion channels and signaling in the pituitary gland. *Endocr Rev* 31, 845-915.
4. Farquhar, M. G. & Rinehart, J. F. (1954) Electron microscopic studies of the anterior pituitary gland of castrate rats. *Endocrinology* 54, 516-541.
5. Soji, T., Mabuchi, Y., Kurono, C. & Herbert, D. C. (1997) Folliculo-stellate cells and intercellular communication within the rat anterior pituitary gland. *Microsc Res Tech* 39, 138-149.
6. Nakajima, T., Yamaguchi, H. & Takahashi, K. (1980) S100 protein in folliculostellate cells of the rat pituitary anterior lobe. *Brain Res* 191, 523-531.
7. Velasco, M. E., Roessmann, U. & Gambetti, P. (1982) The presence of glial fibrillary acidic protein in the human pituitary gland. *J Neuropathol Exp Neurol* 41, 150-163.
8. Berger, U. V. & Hediger, M. A. (2000) Distribution of the glutamate transporters GLAST and GLT-1 in rat circumventricular organs, meninges, and dorsal root ganglia. *J Comp Neurol* 421, 385-399.
9. Fauquier, T., Guerineau, N. C., McKinney, R. A., Bauer, K. & Mollard, P. (2001) Folliculostellate cell network: a route for long-distance communication in the anterior pituitary. *Proc Natl Acad Sci U S A* 98, 8891-8896.
10. Hatton, G. I. (1999) Astroglial modulation of neurotransmitter/peptide release from the neurohypophysis: present status. *J Chem Neuroanat* 16, 203-221.
11. Brown, C. H., Bains, J. S., Ludwig, M. & Stern, J. E. (2013) Physiological regulation of magnocellular neurosecretory cell activity: Integration of intrinsic, local and afferent mechanisms. *J Neuroendocrinol*.
12. Rhoades, R. A. & Tanner, G. A. (Lippincott Williams & Wilkins, 2003) Medical Physiology. Second Edition.
13. Livingstone, C. (2013) Insulin-like growth factor-I (IGF-I) and clinical nutrition. *Clin Sci (Lond)* 125, 265-280.
14. Giustina, A., Mazziotti, G. & Canalis, E. (2008) Growth hormone, insulin-like growth factors, and the skeleton. *Endocr Rev* 29, 535-559.
15. Vijayakumar, A., Novosyadlyy, R., Wu, Y., Yakar, S. & LeRoith, D. (2010) Biological effects of growth hormone on carbohydrate and lipid metabolism. *Growth Horm IGF Res* 20, 1-7.
16. Cunha, S. R. & Mayo, K. E. (2002) Ghrelin and growth hormone (GH) secretagogues potentiate GH-releasing hormone (GHRH)-induced cyclic adenosine 3',5'-monophosphate production in cells expressing transfected GHRH and GH secretagogue receptors. *Endocrinology* 143, 4570-4582.
17. Barinaga, M., Bilezikjian, L. M., Vale, W. W., Rosenfeld, M. G. & Evans, R. M. (1985) Independent effects of growth hormone releasing factor on growth hormone release and gene transcription. *Nature* 314, 279-281.
18. Cohen, L. E., Hashimoto, Y., Zanger, K., Wondisford, F. & Radovick, S. (1999) CREB-independent regulation by CBP is a novel mechanism of human growth hormone gene expression. *J Clin Invest* 104, 1123-1130.
19. Grottoli, S., Gasco, V., Ragazzoni, F. & Ghigo, E. (2003) Hormonal diagnosis of GH hypersecretory states. *J Endocrinol Invest* 26, 27-35.
20. Yang, S. K., Steyn, F. & Chen, C. (2012) Influence of membrane ion channel in pituitary somatotrophs by hypothalamic regulators. *Cell Calcium* 51, 231-239.
21. Howard, A. D. *et al.* (1996) A receptor in pituitary and hypothalamus that functions in growth hormone release. *Science* 273, 974-977.
22. Trott, J. F. *et al.* (2012) Triennial Lactation Symposium: Prolactin: The multifaceted potentiator of mammary growth and function. *J Anim Sci* 90, 1674-1686.
23. De Camilli, P., Macconi, D. & Spada, A. (1979) Dopamine inhibits adenylate cyclase in human prolactin-secreting pituitary adenomas. *Nature* 278, 252-254.

24. Perrone, M. H., Greer, T. L. & Hinkle, P. M. (1980) Relationships between thyroid hormone and glucocorticoid effects in GH3 pituitary cells. *Endocrinology* 106, 600-605.

25. Samson, W. K., Taylor, M. M. & Baker, J. R. (2003) Prolactin-releasing peptides. *Regul Pept* 114, 1-5.

26. McFarland, K. C. *et al.* (1989) Lutropin-choriogonadotropin receptor: an unusual member of the G protein-coupled receptor family. *Science* 245, 494-499.

27. Matsumoto, A. M., Karpas, A. E., Paulsen, C. A. & Bremner, W. J. (1983) Reinitiation of sperm production in gonadotropin-suppressed normal men by administration of follicle-stimulating hormone. *J Clin Invest* 72, 1005-1015.

28. Anderson, L. (1996) Intracellular mechanisms triggering gonadotrophin secretion. *Rev Reprod* 1, 193-202.

29. Damante, G. *et al.* (1989) Thyrotropin regulation of thyroid peroxidase messenger ribonucleic acid levels in cultured rat thyroid cells: evidence for the involvement of a nontranscriptional mechanism. *Endocrinology* 124, 2889-2894.

30. Sun, Y., Lu, X. & Gershengorn, M. C. (2003) Thyrotropin-releasing hormone receptors -- similarities and differences. *Journal of molecular endocrinology* 30, 87-97.

31. Raffin-Sanson, M. L., de Keyzer, Y. & Bertagna, X. (2003) Proopiomelanocortin, a polypeptide precursor with multiple functions: from physiology to pathological conditions. *Eur J Endocrinol* 149, 79-90.

32. D'Agostino, G. & Diano, S. (2010) Alpha-melanocyte stimulating hormone: production and degradation. *J Mol Med (Berl)* 88, 1195-1201.

33. Eves, P. C. & Haycock, J. W. (2010) Melanocortin signalling mechanisms. *Adv Exp Med Biol* 681, 19-28.

34. Yamaguchi, Y. & Hearing, V. J. (2009) Physiological factors that regulate skin pigmentation. *Biofactors* 35, 193-199.

35. Schallreuter, K. U., Kothari, S., Chavan, B. & Spencer, J. D. (2008) Regulation of melanogenesis--controversies and new concepts. *Exp Dermatol* 17, 395-404.

36. Abdel-Malek, Z. *et al.* (1995) Mitogenic and melanogenic stimulation of normal human melanocytes by melanotropic peptides. *Proc Natl Acad Sci U S A* 92, 1789-1793.

37. Eves, P. C., MacNeil, S. & Haycock, J. W. (2006) alpha-Melanocyte stimulating hormone, inflammation and human melanoma. *Peptides* 27, 444-452.

38. Parker, J. A. & Bloom, S. R. (2012) Hypothalamic neuropeptides and the regulation of appetite. *Neuropharmacology* 63, 18-30.

39. Ellacott, K. L. & Cone, R. D. (2004) The central melanocortin system and the integration of short- and long-term regulators of energy homeostasis. *Recent Prog Horm Res* 59, 395-408.

40. Bohm, M. *et al.* (2012) Modulation of basophil activity: a novel function of the neuropeptide alpha-melanocyte-stimulating hormone. *J Allergy Clin Immunol* 129, 1085-1093.

41. Pardy, K., Carter, D. & Murphy, D. (1990) Dopaminergic mediation of physiological changes in proopiomelanocortin messenger ribonucleic acid expression in the neurointermediate lobe of the rat pituitary. *Endocrinology* 126, 2960-2964.

42. Itoh, K. *et al.* (2012) Continuous illumination through larval development suppresses dopamine synthesis in the suprachiasmatic nucleus, causing activation of alpha-MSH synthesis in the pituitary and abnormal metamorphic skin pigmentation in flounder. *Gen Comp Endocrinol* 176, 215-221.

43. Iwanaga, T., Hozumi, Y. & Takahashi-Iwanaga, H. (2011) Immunohistochemical demonstration of dopamine receptor D2R in the primary cilia of the mouse pituitary gland. *Biomed Res* 32, 225-235.

44. Zhao, W. *et al.* (2013) Dopamine receptors modulate cytotoxicity of natural killer cells via cAMP-PKA-CREB signaling pathway. *PLoS One* 8, e65860.

45. Perdona, E., Arban, R. & Griffante, C. (2012) Distinct receptor subtypes mediate arginine vasopressin-dependent ACTH release and intracellular calcium mobilization in rat pituitary cells. *Eur J Pharmacol* 679, 16-23.

46. Rosso, L. & Mienville, J. M. (2009) Pituicyte modulation of neurohormone output. *Glia* 57, 235-243.

47. Hatton, G. I., Bicknell, R. J., Hoyland, J., Bunting, R. & Mason, W. T. (1992) Arginine vasopressin mobilises intracellular calcium via V1-receptor activation in astrocytes (pituicytes) cultured from adult rat neural lobes. *Brain Res* 588, 75-83.

48. Rosso, L., Peteri-Brunback, B., Poujeol, P., Hussy, N. & Mienville, J. M. (2004) Vasopressin-induced taurine efflux from rat pituicytes: a potential negative feedback for hormone secretion. *J Physiol* 554, 731-742.

49. Rosso, L., Peteri-Brunback, B. & Mienville, J. M. (2004) Putative physiological significance of vasopressin V1a receptor activation in rat pituicytes. *J Neuroendocrinol* 16, 313-318.

50. Osuna, M. *et al.* (2012) Differentiation capacity of native pituitary folliculostellate cells and brain astrocytes. *J Endocrinol* 213, 231-237.

51. Drewett, N., Jacobi, J. M., Willgoss, D. A. & Lloyd, H. M. (1993) Apoptosis in the anterior pituitary gland of the rat: studies with estrogen and bromocriptine. *Neuroendocrinology* 57, 89-95.

52. Shirasawa, N. & Yamanouchi, H. (1999) Glucocorticoids induce glutamine synthetase in folliculostellate cells of rat pituitary glands in vivo and in vitro. *J Anat* 194 (Pt 4), 567-577.

53. Johnson, M. D., Gray, M. E., Pepinsky, R. B. & Stahlman, M. T. (1990) Lipocortin-1 immunoreactivity in the human pituitary gland. *J Histochem Cytochem* 38, 1841-1845.

54. Loxley, H. D., Cowell, A. M., Flower, R. J. & Buckingham, J. C. (1993) Effects of lipocortin 1 and dexamethasone on the secretion of corticotrophin-releasing factors in the rat: in vitro and in vivo studies. *J Neuroendocrinol* 5, 51-61.

55. Kaiser, U. B. *et al.* (1992) Follistatin gene expression in the pituitary: localization in gonadotropes and folliculostellate cells in diestrous rats. *Endocrinology* 130, 3048-3056.

56. Hentges, S., Boyadjieva, N. & Sarkar, D. K. (2000) Transforming growth factor-beta3 stimulates lactotrope cell growth by increasing basic fibroblast growth factor from folliculo-stellate cells. *Endocrinology* 141, 859-867.

57. Ceccatelli, S. *et al.* (1993) Nitric oxide synthase in the rat anterior pituitary gland and the role of nitric oxide in regulation of luteinizing hormone secretion. *Proc Natl Acad Sci U S A* 90, 11292-11296.

58. Inoue, K., Couch, E. F., Takano, K. & Ogawa, S. (1999) The structure and function of folliculo-stellate cells in the anterior pituitary gland. *Arch Histol Cytol* 62, 205-218.

59. Clapham, D. E. (2007) Calcium signaling. *Cell* 131, 1047-1058.

60. Berridge, M. J., Bootman, M. D. & Roderick, H. L. (2003) Calcium signalling: dynamics, homeostasis and remodelling. *Nat Rev Mol Cell Biol* 4, 517-529.

61. Zorec, R. (1996) Calcium signaling and secretion in pituitary cells. *Trends Endocrinol Metab* 7, 384-388.

62. Sedej, S., Klemen, M. S., Schluter, O. M. & Rupnik, M. S. (2013) Rab3a is critical for trapping alpha-MSH granules in the high Ca(2)(+)-affinity pool by preventing constitutive exocytosis. *PLoS One* 8, e78883.

63. Fonfria, E. *et al.* (2006) Tissue distribution profiles of the human TRPM cation channel family. *J Recept Signal Transduct Res* 26, 159-178.

64. Riccio, A. *et al.* (2002) mRNA distribution analysis of human TRPC family in CNS and peripheral tissues. *Brain Res Mol Brain Res* 109, 95-104.

65. Zheng, J. (2013) Molecular mechanism of TRP channels. *Compr Physiol* 3, 221-242.

66. Montell, C. (2005) The TRP superfamily of cation channels. *Sci STKE* 2005, re3.

67. Cosens, D. J. & Manning, A. (1969) Abnormal electroretinogram from a Drosophila mutant. *Nature* 224, 285-287.

68. Montell, C. & Rubin, G. M. (1989) Molecular characterization of the Drosophila trp locus: a putative integral membrane protein required for phototransduction. *Neuron* 2, 1313-1323.

69. Minke, B. & Selinger, Z. (1992) The inositol-lipid pathway is necessary for light excitation in fly photoreceptors. *Soc Gen Physiol Ser* 47, 201-217.

70. Hardie, R. C. & Minke, B. (1992) The trp gene is essential for a light-activated Ca2+ channel in Drosophila photoreceptors. *Neuron* 8, 643-651.

71. Venkatachalam, K. & Montell, C. (2007) TRP channels. *Annu Rev Biochem* 76, 387-417.

72. Flockerzi, V. & Nilius, B. (2014) TRPs: truly remarkable proteins. *Handb Exp Pharmacol* 222, 1-12.

73. Wes, P. D. *et al.* (1995) TRPC1, a human homolog of a Drosophila store-operated channel. *Proc Natl Acad Sci U S A* 92, 9652-9656.

74. Caterina, M. J. *et al.* (1997) The capsaicin receptor: a heat-activated ion channel in the pain pathway. *Nature* 389, 816-824.

75. Duncan, L. M. *et al.* (1998) Down-regulation of the novel gene melastatin correlates with potential for melanoma metastasis. *Cancer Res* 58, 1515-1520.

76. Jaquemar, D., Schenker, T. & Trueb, B. (1999) An ankyrin-like protein with transmembrane domains is specifically lost after oncogenic transformation of human fibroblasts. *J Biol Chem* 274, 7325-7333.

77. Mochizuki, T. *et al.* (1996) PKD2, a gene for polycystic kidney disease that encodes an integral membrane protein. *Science* 272, 1339-1342.

78. Li, S. W., Westwick, J. & Poll, C. T. (2002) Receptor-operated Ca2+ influx channels in leukocytes: a therapeutic target? *Trends Pharmacol Sci* 23, 63-70.

79. Mosavi, L. K., Cammett, T. J., Desrosiers, D. C. & Peng, Z. Y. (2004) The ankyrin repeat as molecular architecture for protein recognition. *Protein Sci* 13, 1435-1448.

80. Lishko, P. V., Procko, E., Jin, X., Phelps, C. B. & Gaudet, R. (2007) The ankyrin repeats of TRPV1 bind multiple ligands and modulate channel sensitivity. *Neuron* 54, 905-918.

81. Wu, L. J., Sweet, T. B. & Clapham, D. E. (2010) International Union of Basic and Clinical Pharmacology. LXXVI. Current progress in the mammalian TRP ion channel family. *Pharmacol Rev* 62, 381-404.

82. Voets, T. & Nilius, B. (2007) Modulation of TRPs by PIPs. *J Physiol* 582, 939-944.

83. Mason, J. M. & Arndt, K. M. (2004) Coiled coil domains: stability, specificity, and biological implications. *Chembiochem* 5, 170-176.

84. Delmas, P. (2004) Polycystins: from mechanosensation to gene regulation. *Cell* 118, 145-148.

85. Giamarchi, A. *et al.* (2010) A polycystin-2 (TRPP2) dimerization domain essential for the function of heteromeric polycystin complexes. *Embo J* 29, 1176-1191.

86. Tsuruda, P. R., Julius, D. & Minor, D. L., Jr. (2006) Coiled coils direct assembly of a cold-activated TRP channel. *Neuron* 51, 201-212.

87. Erler, I. *et al.* (2006) Trafficking and assembly of the cold-sensitive TRPM8 channel. *J Biol Chem* 281, 38396-38404.

88. Phelps, C. B. & Gaudet, R. (2007) The role of the N terminus and transmembrane domain of TRPM8 in channel localization and tetramerization. *J Biol Chem* 282, 36474-36480.

89. Runnels, L. W., Yue, L. & Clapham, D. E. (2001) TRP-PLIK, a bifunctional protein with kinase and ion channel activities. *Science* 291, 1043-1047.

90. Schmitz, C. *et al.* (2003) Regulation of vertebrate cellular Mg2+ homeostasis by TRPM7. *Cell* 114, 191-200.

91. Liao, M., Cao, E., Julius, D. & Cheng, Y. (2013) Structure of the TRPV1 ion channel determined by electron cryo-microscopy. *Nature* 504, 107-112.

92. Cao, E., Liao, M., Cheng, Y. & Julius, D. (2013) TRPV1 structures in distinct conformations reveal activation mechanisms. *Nature* 504, 113-118.

93. Clapham, D. E. (2003) TRP channels as cellular sensors. *Nature* 426, 517-524.

94. Owsianik, G., Talavera, K., Voets, T. & Nilius, B. (2006) Permeation and selectivity of TRP channels. *Annu Rev Physiol* 68, 685-717.

95. Gees, M., Colsoul, B. & Nilius, B. (2010) The role of transient receptor potential cation channels in Ca2+ signaling. *Cold Spring Harb Perspect Biol* 2, a003962.

96. Zeilhofer, H. U., Kress, M. & Swandulla, D. (1997) Fractional Ca2+ currents through capsaicin- and proton-activated ion channels in rat dorsal root ganglion neurones. *J Physiol* 503 (Pt 1), 67-78.

97. Drews, A. in *Acta Physiologica* Vol. Volume 198 (2010).

98. Kim, S. H. *et al.* (2007) Nonselective cation channels are essential for maintaining intracellular Ca2+ levels and spontaneous firing activity in the midbrain dopamine neurons. *Pflugers Arch* 455, 309-321.

99. Kiselyov, K. *et al.* (2011) TRPML: transporters of metals in lysosomes essential for cell survival? *Cell Calcium* 50, 288-294.

100. Freichel, M., Almering, J. & Tsvilovskyy, V. (2012) The Role of TRP Proteins in Mast Cells. *Front Immunol* 3, 150.

101. Grimm, C., Kraft, R., Sauerbruch, S., Schultz, G. & Harteneck, C. (2003) Molecular and functional characterization of the melastatin-related cation channel TRPM3. *J Biol Chem* 278, 21493-21501.

102. Lee, N. *et al.* (2003) Expression and characterization of human transient receptor potential melastatin 3 (hTRPM3). *J Biol Chem* 278, 20890-20897.

103. Oberwinkler, J., Lis, A., Giehl, K. M., Flockerzi, V. & Philipp, S. E. (2005) Alternative splicing switches the divalent cation selectivity of TRPM3 channels. *J Biol Chem* 280, 22540-22548.

104. Lis, A. Identifizierung von TRPM3- und TRPM1- Ionenkanälen: Funktionelle Diversität durch alternatives Spleißen der Transkripte und durch heterooligomere Assemblierung der Kanaluntereinheiten, (2005) Doctoral Degree thesis, University of Saarland.

105. Vriens, J. *et al.* (2011) TRPM3 is a nociceptor channel involved in the detection of noxious heat. *Neuron* 70, 482-494.

106. Oberwinkler, J. & Philipp, S. E. (2014) Trpm3. *Handb Exp Pharmacol* 222, 427-459.

107. Hughes, S. *et al.* (2012) Profound defects in pupillary responses to light in TRPM-channel null mice: a role for TRPM channels in non-image-forming photoreception. *Eur J Neurosci* 35, 34-43.

108. Mannebach, S. Untersuchung von TRPM3-Kationenkanälen mit Hilfe von Knock-down- und Knock-out-Methoden, (2008) Doctoral degree thesis, Saarland University.

109. Lambert, S. *et al.* (2011) Transient receptor potential melastatin 1 (TRPM1) is an ion-conducting plasma membrane channel inhibited by zinc ions. *J Biol Chem* 286, 12221-12233.

110. Hoffmann, A. *et al.* (2010) TRPM3 is expressed in sphingosine-responsive myelinating oligodendrocytes. *J Neurochem* 114, 654-665.

111. Frühwald, J. *et al.* (2012) Alternative splicing of a protein domain indispensable for function of transient receptor potential melastatin 3 (TRPM3) ion channels. *J Biol Chem* 287, 36663-36672.

112. Frühwald, J. Identifizierung und Charakterisierung funktionell bedeutender Proteindomänen in TRPM3-Steroidrezeptoren, (2010) Doctoral Degree thesis, Saarland University.

113. Holakovska, B. *et al.* (2012) Calmodulin and S100A1 protein interact with N terminus of TRPM3 channel. *J Biol Chem* 287, 16645-16655.

114. Holendova, B., Grycova, L., Jirku, M. & Teisinger, J. (2012) PtdIns(4,5)P2 interacts with CaM binding domains on TRPM3 N-terminus. *Channels (Austin)* 6, 479-482.

115. Wagner, T. F. *et al.* (2008) Transient receptor potential M3 channels are ionotropic steroid receptors in pancreatic beta cells. *Nat Cell Biol* 10, 1421-1430.

116. Mayer, S. I., Muller, I., Mannebach, S., Endo, T. & Thiel, G. (2011) Signal transduction of pregnenolone sulfate in insulinoma cells: activation of Egr-1 expression involving TRPM3, voltage-gated calcium channels, ERK, and ternary complex factors. *J Biol Chem* 286, 10084-10096.

117. Thiel, G., Mueller, I. & Roessler, O. G. (2013) Signal transduction via TRPM3 channels in pancreatic beta-cells. *Journal of Molecular Endocrinology* 50, R75-R83.

118. Straub, I. *et al.* (2013) Flavanones that selectively inhibit TRPM3 attenuate thermal nociception in vivo. *Mol Pharmacol* 84, 736-750.

119. Naylor, J. *et al.* (2010) Pregnenolone sulphate- and cholesterol-regulated TRPM3 channels coupled to vascular smooth muscle secretion and contraction. *Circ Res* 106, 1507-1515.

120. Millar, I. D., Bruce, J. & Brown, P. D. (2007) Ion channel diversity, channel expression and function in the choroid plexuses. *Cerebrospinal Fluid Res* 4, 8.

121. Harteneck, C. (2005) Function and pharmacology of TRPM cation channels. *Naunyn Schmiedebergs Arch Pharmacol* 371, 307-314.

122. Fantozzi, I. *et al.* (2003) Hypoxia increases AP-1 binding activity by enhancing capacitative Ca2+ entry in human pulmonary artery endothelial cells. *Am J Physiol Lung Cell Mol Physiol* 285, L1233-1245.

123. Inoue, R. *et al.* (2006) Transient receptor potential channels in cardiovascular function and disease. *Circ Res* 99, 119-131.

124. Jang, Y. *et al.* (2012) Quantitative analysis of TRP channel genes in mouse organs. *Arch Pharm Res* 35, 1823-1830.

125. Gilliam, J. C. & Wensel, T. G. (2011) TRP channel gene expression in the mouse retina. *Vision Res* 51, 2440-2452.

126. Kunert-Keil, C., Bisping, F., Kruger, J. & Brinkmeier, H. (2006) Tissue-specific expression of TRP channel genes in the mouse and its variation in three different mouse strains. *BMC Genomics* 7, 159.

127. Deo, M., Yu, J. Y., Chung, K. H., Tippens, M. & Turner, D. L. (2006) Detection of mammalian microRNA expression by in situ hybridization with RNA oligonucleotides. *Dev Dyn* 235, 2538-2548.

128. Karali, M., Peluso, I., Marigo, V. & Banfi, S. (2007) Identification and characterization of microRNAs expressed in the mouse eye. *Invest Ophthalmol Vis Sci* 48, 509-515.

129. Kastenhuber, E., Gesemann, M., Mickoleit, M. & Neuhauss, S. C. (2013) Phylogenetic analysis and expression of zebrafish transient receptor potential melastatin family genes. *Dev Dyn* 242, 1236-1249.

130. Zamudio-Bulcock, P. A., Everett, J., Harteneck, C. & Valenzuela, C. F. (2011) Activation of steroid-sensitive TRPM3 channels potentiates glutamatergic transmission at cerebellar Purkinje neurons from developing rats. *J Neurochem* 119, 474-485.

131. Staaf, S., Franck, M. C., Marmigere, F., Mattsson, J. P. & Ernfors, P. (2010) Dynamic expression of the TRPM subgroup of ion channels in developing mouse sensory neurons. *Gene Expr Patterns* 10, 65-74.

132. Vandewauw, I., Owsianik, G. & Voets, T. (2013) Systematic and quantitative mRNA expression analysis of TRP channel genes at the single trigeminal and dorsal root ganglion level in mouse. *BMC Neurosci* 14, 21.

133. Straub, I. *et al.* (2013) Citrus fruit and fabacea secondary metabolites potently and selectively block TRPM3. *Br J Pharmacol* 168, 1835-1850.

134. Nealen, M. L., Gold, M. S., Thut, P. D. & Caterina, M. J. (2003) TRPM8 mRNA is expressed in a subset of cold-responsive trigeminal neurons from rat. *J Neurophysiol* 90, 515-520.

135. Hackler, L., Jr., Wan, J., Swaroop, A., Qian, J. & Zack, D. J. (2010) MicroRNA profile of the developing mouse retina. *Invest Ophthalmol Vis Sci* 51, 1823-1831.

136. Krol, J. *et al.* (2010) Characterizing light-regulated retinal microRNAs reveals rapid turnover as a common property of neuronal microRNAs. *Cell* 141, 618-631.

137. Wistow, G. *et al.* (2008) NEIBank: genomics and bioinformatics resources for vision research. *Mol Vis* 14, 1327-1337.

138. Wistow, G. *et al.* (2002) Expressed sequence tag analysis of adult human iris for the NEIBank Project: steroid-response factors and similarities with retinal pigment epithelium. *Mol Vis* 8, 185-195.

139. Xie, Q. *et al.* (2013) Pax6 interactions with chromatin and identification of its novel direct target genes in lens and forebrain. *PLoS One* 8, e54507.

140. Shaham, O. *et al.* (2013) Pax6 regulates gene expression in the vertebrate lens through miR-204. *PLoS Genet* 9, e1003357.

141. Adijanto, J. *et al.* (2012) Microphthalmia-associated transcription factor (MITF) promotes differentiation of human retinal pigment epithelium (RPE) by regulating microRNAs-204/211 expression. *J Biol Chem* 287, 20491-20503.

142. Wang, F. E. *et al.* (2010) MicroRNA-204/211 alters epithelial physiology. *Faseb J* 24, 1552-1571.

143. Cuajungco, M. P., Grimm, C. & Heller, S. (2007) TRP channels as candidates for hearing and balance abnormalities in vertebrates. *Biochim Biophys Acta* 1772, 1022-1027.

144. Gabashvili, I. S., Sokolowski, B. H., Morton, C. C. & Giersch, A. B. (2007) Ion channel gene expression in the inner ear. *J Assoc Res Otolaryngol* 8, 305-328.

145. Kuster, D. W. *et al.* (2013) MicroRNA transcriptome profiling in cardiac tissue of hypertrophic cardiomyopathy patients with MYBPC3 mutations. *J Mol Cell Cardiol* 65, 59-66.

146. Yang, X. R., Lin, M. J., McIntosh, L. S. & Sham, J. S. (2006) Functional expression of transient receptor potential melastatin- and vanilloid-related channels in pulmonary arterial and aortic smooth muscle. *Am J Physiol Lung Cell Mol Physiol* 290, L1267-1276.

147. Courboulin, A. *et al.* (2011) Role for miR-204 in human pulmonary arterial hypertension. *J Exp Med* 208, 535-548.

148. Müller, I., Rossler, O. G. & Thiel, G. (2011) Pregnenolone sulfate activates basic region leucine zipper transcription factors in insulinoma cells: role of voltage-gated Ca2+ channels and transient receptor potential melastatin 3 channels. *Mol Pharmacol* 80, 1179-1189.

149. Wagner, T. F. *et al.* (2010) TRPM3 channels provide a regulated influx pathway for zinc in pancreatic beta cells. *Pflugers Arch* 460, 755-765.

150. Xu, G., Chen, J., Jing, G. & Shalev, A. (2013) Thioredoxin-interacting protein regulates insulin transcription through microRNA-204. *Nat Med* 19, 1141-1146.

151. Klose, C. *et al.* (2011) Fenamates as TRP channel blockers: mefenamic acid selectively blocks TRPM3. *Br J Pharmacol* 162, 1757-1769.

152. Langford, P. R., Keyes, L. & Hansen, M. D. (2012) Plasma membrane ion fluxes and NFAT-dependent gene transcription contribute to c-met-induced epithelial scattering. *J Cell Sci* 125, 4001-4013.

153. Mikhaylova, O. *et al.* (2012) VHL-regulated MiR-204 suppresses tumor growth through inhibition of LC3B-mediated autophagy in renal clear cell carcinoma. *Cancer Cell* 21, 532-546.

154. Li, S. L. *et al.* (2008) [Expression of TRPM and TRPV channel family mRNA in rat spermatogenic cells]. *Nan Fang Yi Ke Da Xue Xue Bao* 28, 2150-2153.

155. Wang, H. P., Pu, X. Y. & Wang, X. H. (2007) Distribution profiles of transient receptor potential melastatin-related and vanilloid-related channels in prostatic tissue in rat. *Asian J Androl* 9, 634-640.

156. Abed, E., Labelle, D., Martineau, C., Loghin, A. & Moreau, R. (2009) Expression of transient receptor potential (TRP) channels in human and murine osteoblast-like cells. *Mol Membr Biol* 26, 146-158.

157. Son, A. R. *et al.* (2009) Odontoblast TRP channels and thermo/mechanical transmission. *J Dent Res* 88, 1014-1019.

158. Lee, Y. *et al.* (2010) Network modeling identifies molecular functions targeted by miR-204 to suppress head and neck tumor metastasis. *PLoS Comput Biol* 6, e1000730.

159. Ciurtin, C. *et al.* (2010) TRPM3 channel stimulated by pregnenolone sulphate in synovial fibroblasts and negatively coupled to hyaluronan. *BMC Musculoskelet Disord* 11, 111.

160. Ying, Z. *et al.* (2013) Loss of miR-204 expression enhances glioma migration and stem cell-like phenotype. *Cancer Res* 73, 990-999.

161. Grimm, C., Kraft, R., Schultz, G. & Harteneck, C. (2005) Activation of the melastatin-related cation channel TRPM3 by D-erythro-sphingosine [corrected]. *Mol Pharmacol* 67, 798-805.

162. Harteneck, C. (2013) Pregnenolone sulfate: from steroid metabolite to TRP channel ligand. *Molecules* 18, 12012-12028.

163. Vriens, J. *et al.* (2014) Opening of an alternative ion permeation pathway in a nociceptor TRP channel. *Nat Chem Biol* 10, 188-195.

164. Drews, A. *et al.* (2014) Structural requirements of steroidal agonists of transient receptor potential melastatin 3 (TRPM3) cation channels. *Br J Pharmacol* 171, 1019-1032.

165. Xu, S. Z. *et al.* (2005) Block of TRPC5 channels by 2-aminoethoxydiphenyl borate: a differential, extracellular and voltage-dependent effect. *Br J Pharmacol* 145, 405-414.

166. Majeed, Y. *et al.* (2011) Rapid and contrasting effects of rosiglitazone on transient receptor potential TRPM3 and TRPC5 channels. *Mol Pharmacol* 79, 1023-1030.

167. Majeed, Y. *et al.* (2012) Pregnenolone sulphate-independent inhibition of TRPM3 channels by progesterone. *Cell Calcium* 51, 1-11.

168. Straub, I. *et al.* (2012) Citrus fruit and fabacea secondary metabolites potently and selectively block TRPM3. *Br J Pharmacol*.

169. Warnat, J., Philipp, S., Zimmer, S., Flockerzi, V. & Cavalie, A. (1999) Phenotype of a recombinant store-operated channel: highly selective permeation of Ca2+. *J Physiol* 518 (Pt 3), 631-638.

170. Niwa, H., Yamamura, K. & Miyazaki, J. (1991) Efficient selection for high-expression transfectants with a novel eukaryotic vector. *Gene* 108, 193-199.

171. Bullock, W. O., Fernandez, J. M. & Short, J. M. (1987) XL1-blue: a high efficiency plasmid transforming recA Escherichia coli strain with beta-galactosidase selection. . *Biotechniques* 5, 376-&.

172. Rosso, L. *et al.* (2002) RhoA inhibition is a key step in pituicyte stellation induced by A(1)-type adenosine receptor activation. *Glia* 38, 351-362.

173. Sambrook, J. & Russell, D. W. (2000) Molecular Cloning: A Laboratory Manual. *Cold Spring Harbor Laboratory*.

174. Sambrook, J.   (Cold Spring Harbor Laboratory, 2000).

175. Schroeder, A. *et al.* (2006) The RIN: an RNA integrity number for assigning integrity values to RNA measurements. *BMC Mol Biol* 7, 3.

176. Smith, P. K. *et al.* (1985) Measurement of protein using bicinchoninic acid. *Anal Biochem* 150, 76-85.

177. Laemmli, U. K. (1970) Cleavage of structural proteins during the assembly of the head of bacteriophage T4. *Nature* 227, 680-685.

178. Grynkiewicz, G., Poenie, M. & Tsien, R. Y. (1985) A new generation of Ca2+ indicators with greatly improved fluorescence properties. *J Biol Chem* 260, 3440-3450.

179. Becker, A. Identifizierung von aminoterminalen TRPM3-Varianten in der Hypophyse der Maus, (2013), Saarland University.

180. Brazelton, T. R. & Blau, H. M. (2005) Optimizing techniques for tracking transplanted stem cells in vivo. *Stem Cells* 23, 1251-1265.

181. Wang, D., Yan, B., Rajapaksha, W. R. & Fisher, T. E. (2009) The expression of voltage-gated ca2+ channels in pituicytes and the up-regulation of L-type ca2+ channels during water deprivation. *J Neuroendocrinol* 21, 858-866.

182. Wei, X. Y., Zhao, C. H., Liu, Y. Y., Wang, Y. Z. & Ju, G. (2009) Immuohistochemical markers for pituicyte. *Neurosci Lett* 465, 27-30.

183. Dembla, S. Identification and characterization of TRPM3 and TRPA1 ion channels in epithelial cells, (2013) Doctoral degree thesis, Uneversity of Saarland.

184. Winters, S. J. & Moore, J. P. (2007) Paracrine control of gonadotrophs. *Semin Reprod Med* 25, 379-387.

185. Adams, J. *et al.* (2000) Vascular endothelial growth factor (VEGF) in breast cancer: comparison of plasma, serum, and tissue VEGF and microvessel density and effects of tamoxifen. *Cancer Res* 60, 2898-2905.

186. Schneider, B. P. & Sledge, G. W., Jr. (2011) Anti-vascular endothelial growth factor therapy for breast cancer: can we pick the winners? *J Clin Oncol* 29, 2444-2447.

187. Morris, J. a. C., H. (2011) Folliculo-stellate Cells: Paracrine Communicators in the Anterior Pituitary. *The Open Neuroendocrinology Journal*, 77-89.

188. Parpura, V. & Verkhratsky, A. (2012) Homeostatic function of astrocytes: Ca(2+) and Na(+) signalling. *Transl Neurosci* 3, 334-344.

189. Rosso, L. *et al.* (2002) Vasopressin and oxytocin reverse adenosine-induced pituicyte stellation via calcium-dependent activation of Cdc42. *Eur J Neurosci* 16, 2324-2332.

190. Sobrino Crespo, C., Perianes Cachero, A., Puebla Jimenez, L., Barrios, V. & Arilla Ferreiro, E. (2014) Peptides and food intake. *Front Endocrinol (Lausanne)* 5, 58.

191. Loh, Y. P. (1992) Molecular Mechanisms of Beta-Endorphin Biosynthesis. *Biochem Pharmacol* 44, 843-849.

192. Spencer, J. D., Gibbons, N. C., Bohm, M. & Schallreuter, K. U. (2008) The Ca2+-binding capacity of epidermal furin is disrupted by H2O2-mediated oxidation in vitiligo. *Endocrinology* 149, 1638-1645.

193. Murakami, I., Takeuchi, S., Kudo, T., Sutou, S. & Takahashi, S. (2007) Corticotropin-releasing hormone or dexamethasone regulates rat proopiomelanocortin transcription through Tpit/Pitx-responsive element in its promoter. *J Endocrinol* 193, 279-290.

Curriculum Vitae

Personal data

Name   Nouma Kamel Hasan

Date of birth   08.03.1983 in Latakia, Syria

E-mail address   nouma.hasan@googlemail.com

Education and scientific work experience

2010-present   PhD student at the Experimental and Clinical Pharmacology and
                  Toxicology Institute, University of Saarland, Germany.

2009-2010   Master of science in Pharmacology and Toxicology
                  (Master Equivalent), University of Saarland, Germany.

2006-2009   Scientific assistant, faculty of Pharmacy, Tishreen University, Latakia,
                  Syria.

2001-2006   Bachelor of Science in Pharmacy and Pharmaceutical Chemistry,
                  Tishreen University, Latakia, Syria.

Scientific Publication

- Meiser, J., Hasan, N., Frühwald, J., , Mannebach, S., Weißgerber, P., Dembla, S. and Stephan E. Philipp (2012). Frequency of Transient Receptor Potential Melastatin 3 channel (TRPM3) isoforms in mouse tissues. Naunyn-Schmiedeberg's Archives of Pharmacology, 385 (Suppl 1): 558

- Hasan, N., Beck, A., Mannebach, S., Weißgerber, P. and Stephan E. Philipp (2014). Expression and function of TRPM3 proteins in mouse pituitary gland. Naunyn-Schmiedeberg's Archives of Pharmacology 387 (Suppl 1): 510.

Poster Presentation

- Nouma Hasan, Julia Meiser, Sandeep Dembla, Stefanie Mannebach, Petra Weißgerber & Stephan E. Philipp. "Identification and frequency of TRPM3 isoforms in different mouse tissues". May 2012, Alpbach, Austria, First European Calcium Channel Conference.

- Ilka Mathar, Nouma Hasan, Volodymyr Tsvilovskyy & Marc Freichel. "The role of TRPM and TRPC channels in vascular contractility and blood pressure regulation". January 2010. Homburg, Germany. Kolloquium of the Graduate Research School GK1326.